UNIVERSIDADE FEDERAL DE PERNAMBUCO

CENTRO DE CIÊNCIAS DA SAÚDE

PROGRAMA DE PÓS-GRADUAÇÃO EM NANOTECNOLOGIA FARMACÊUTICA

SARAH BRANDÃO PALÁCIO

DEVELOPMENT AND CHARACTERIZATION OF TARGETED MART-1-NANOPARTICLES FOR MELANOMA TREATMENT AND β-LAPACHONE-LOADED LIPOSOMES IN HYDROGEL FOR WOUND HEALING.

Supervisor: Profa. Dra. Nereide Stela Santos Magalhães

Co-supervisor: Prof. Dr. Gilles Ponchel

Recife – PE

2017

SARAH BRANDÃO PALÁCIO

DEVELOPMENT AND CHARACTERIZATION OF TARGETED MART-1-NANOPARTICLES FOR MELANOMA TREATMENT AND β-LAPACHONE-LOADED LIPOSOMES IN HYDROGEL FOR WOUND HEALING.

Thesis in Cotutela between the Federal University of Pernambuco and the University of Paris-Saclay presented to the Graduate Program in Pharmaceutical Nanotechnology of the Federal University of Pernambuco and to L'école de Innovation Thérapeutique: du fondamental à l'appliqué de Université Paris-Saclay, as a partial requisite for obtaining the title of PhD in Pharmaceutical Nanotechnology and PhD in Innovation Thérapeutique, doctoral specialty: Pharmacotechnie et Biopharmacie.

Supervisor: **Profa. Dra. Nereide Stela Santos Magalhães**
Pharmaceutical Sciences Departament, CCS/UFPE;
Laboratory of Immunopathology Keizo-Asami – LIKA.
Co-supervisor: **Prof. Dr. Gilles Ponchel**
Institut Galien, Université Paris-Sud.

Recife – PE

2017

SARAH BRANDÃO PALÁCIO

DEVELOPMENT AND CHARACTERIZATION OF TARGETED MART-1-NANOPARTICLES FOR MELANOMA TREATMENT AND β-LAPACHONE-LOADED LIPOSOMES IN HYDROGEL FOR WOUND HEALING

Tese em cotutela com a Universidade de Paris-Sud/Paris –Saclay apresentada ao Programa de Pós Graduação em Nanotecnologia Farmacêutica da Universidade Federal de Pernambuco como requisito parcial para obtenção do grau de Doutor em Nanotecnologia Farmacêutica.

Trabalho aprovado em: 1 de dezembro de 2017.

_____
Profa. Dra. Nereide Stela Santos Magalhães (Orientadora no Brasil)
Universidade Federal de Pernambuco

_____
Prof. Dr. Gilles Ponchel – Orientador na França-
Université Paris Sud/Université Paris-Saclay- CNRS UMR 8612

_____
Profa. Dra. Adriana Fontes – Examinadora (Titular)
Universidade Federal de Pernambuco -UFPE

_____
Profa. Dra. Mariane Cajubá de Britto Lira Nogueira – Examinador (Titular)
Universidade Federal de Pernambuco – UFPE

_____
Prof. Dr. Eryvaldo Sócrates Tabosa do Egito– Examinador (Titular)
Universidade Federal do Rio Grande do Norte (UFRN)

ACKNOWLEDGEMENTS

There are many things to be grateful at this moment and the conclusion of my PhD certainly will be a big landmark in my life. When I was a child I had the willness to be a scientist, discovery new things and travel the world changing experiences and knownlegde. Nevertheless, the reality was not that simple as seemed to be. During my graduation, master's degree and PhD, many difficult tasks have come into my way, impelling me to be strong, resilient and hardworking. On the other hand, great moments of joy, reciprocity and passion also accompanied me on this journey. Naturally, there is still a long path to go towards the construction of scientific knowledge.

I would like to thank the wonderful people who crossed my path and who have helped me to achieve my goals and and always encouraging me to be the best version of me. First, I will be eternally grateful to my family, my parents and brothers, for supporting me in all moments. We are a very close-knit family, full of love and compasion. An specially thank for my father who is my mentor and main supporter.

What would life be without friends as well? So, my special thank will be to my childhood friends that knows me more than myself: Elisa, Duda, Tatiane, Rivanda, Pinelli, Renata Lima, Camila Farias and Marcela. Thank you also to my college friends: Amanda, Larissa Morgana, Giovanna, Dea, Rebecca, Vinicius e Fernanda. Still talking about great friends, but now the new ones, I really have to thanks to my colleagues from Maison du Brésil for all the friendship and support during my stay in Paris: Taty, Bárbara, Priscila, Rodrigo, Igor, Júlia, Gustavo, Fabiano etc. Thank you very much for being part of one of the great moments of my life.

I would like to greatly thanks to my supervisors and co-superviors: Nereide Stela Santos Magalhães, Gilles Ponchel and Christine Vauthier for provide amazing opportunities of knowledge and for supporting me in all my needs and requirements. You are for me the biggest examples of competence, intelligence and resilience. I would like to express my huge gratitude for my teammates from Brasil and France, that make this journey less labored and more joyful. Any Taylor (my mexican sister) and Mariane Lira (my roomate), I have no words to thank you girls for all your support and friendship, you were a key part of my development as a person and professional. Isabella Macário, Rafaela Ferraz, Marília Evelynn, Jean Baptist, Francisco Junior, thank you for all the priceless contribuitions in this work and for trusted and believed in me. Finally, but not least, thanks for all my SLC's and Institut Galien- Paris-sud teammates and professor that helped me enormously with all knowledge and friendship.

"If you are distressed by anything external, the pain is not due to the thing itself but to your own estimate of it; and this you have the power to revoke at any moment."

Marcus Aurelius Antoninus
Emperor of Rome and stoic philosopher (121 to 180).

ABSTRACT

The main aim of this work was the development, characterization and in vitro and in vivo evaluation of different nanocarriers with specific nanoparticles for the treatment of melanoma and β-lapachone liposomes incorporated in biopolymer hydrogels for the healing of topical wounds. The first part of this thesis presents a review of the literature and recent advances in the field of targeting mesenchymal circulating cells derived from melanomas. The main biomarkers of these cells have been reviewed to define the suitable characteristics of this nanocarriers. The experimental part of the work consisted of development of nanoparticles (non-spherical) by nanoprecipitation of copolymers derived from poly (γ-benzyl-L-glutamate). These nanoparticles, size between 20 and 100 nm and carrying a negative charge (-3 to -30 mV) were then combined with the MART-1 antibody, specific for the melanoma cell membrane, by biotin-streptavidin binding. The binding of the antibody on the surface of nanoparticles was evaluated by Western blot. The affinity of immuno-nanoparticles for melanoma cells (B16-GFP line) and for endothelial cells of human umbilical vein (HUVECs) was then evaluated in vitro by flow cytometry and, being intended for intravenous injection, it was important to evaluate the degree of activation of the complement system induced by the nanoparticles. The 2D immunoelectrophoresis technique used made it possible to conclude that the activation was limited and favourable to increase the blood circulation time of nanoparticles, after intravenous injection. The nanoparticles exhibited low cytotoxicity (MTT assay) against melanoma cells or endothelial cells. In terms of cellular uptake, the immuno-nanoparticles functionalized with MART1, a specific antibody for the recognition of the overexpressed antigen in melanoma cells, was increased by 40 to 50% compared to control. The second part of this thesis was dedicated to the development, characterization and in vivo evaluation of the wound healing activity of β-lapachone encapsulated in multilamellar liposomes and incorporated in a hydrogel of a biopolymer produced by the bacterium Zoogloea sp. These original formulations (β-lap-Lipo/ ZBP/HEC) had a pH and rheological behavior suitable for topical application, as well as the ability to slow the release of β-lapachone from the hydrogel. A detailed histopathological study of the wound healing activity was conducted in an in vivo model and showed that the biopolymer hydrogel was able to stimulate tissue repair, increasing the local cellularity, fibroblasts, cells inflammatory, blood vessels and the production of collagen fibrils during the proliferative phase of healing. In addition, the β-lap-Lipo/ZBP/HEC formulation promoted local angiogenesis and reduced inflammation of the wound, demonstrating the potential of this original formulation of β-lap-Lipo/ZBP/HEC in cutaneous lesions therapy. To conclude, the developed nanocarriers are interesting approachs for intercepting the circulating melanoma cells, while liposomal formulations combining with original biopolymers have an interesting potential for wound healing applications.

Keywords: Nanoparticles. Melanoma. Biopolymer. Liposomes. Wound healing.

RESUMO

O objetivo principal deste trabalho foi o desenvolvimento, caracterização e avaliação in vitro e in vivo de diferentes nanocarreadores: nanopartículas específicas para o tratamento de melanoma e lipossomas contendo β-lapachona incorporados em hidrogéis de biopolímero para a cicatrização de feridas tópicas. A primeira parte desta tese apresenta uma revisão da literatura e avanços recentes no campo do direcionamento de fármacos através do uso de nanocarreadores para a células circulantes mesenquimatosas derivadas de melanomas. Os principais biomarcadores presentes nestas células foram descritos com o objetivo de definir as características adequadas para o desenvolvimento de nanocarreadores. A parte experimental do trabalho consistiu no desenvolvimento de nanopartículas (não esféricas) por nanoprecipitação de copolímeros derivados de poli (γ-benzil-L-glutamato). Essas nanopartículas, tamanho entre 20 e 100 nm e carga negativa (-3 a -30 mV) foram então combinadas com o anticorpo MART-1, específico para a membrana das células do melanoma, pela ligação biotina-estreptavidina. A ligação do anticorpo na superfície das nanopartículas foi avaliada por Western blot. A afinidade das imuno-nanopartículas para células de melanoma (linha B16-GFP) e para células endoteliais de veia umbilical humana (HUVECs) foi então avaliada in vitro por citometria de fluxo e, sendo destinada a injeção intravenosa, era importante avaliar o grau de ativação do sistema complemento induzido pelas nanopartículas. A técnica utilizada de imunoeletroforese 2D permitiu concluir que a ativação foi limitada e favorável para aumentar o tempo de circulação sanguínea das nanopartículas, após a injeção intravenosa. As nanopartículas apresentaram baixa citotoxicidade (teste MTT) contra células de melanoma ou células endoteliais. Em termos de absorção celular, as imuno-nanopartículas funcionalizadas com MART1, um anticorpo específico para o reconhecimento do antígeno super-expresso em células de melanoma, foi aumentada em 40 a 50% em comparação com o controle. A segunda parte desta tese foi dedicada ao desenvolvimento, caracterização e avaliação in vivo da atividade de cicatrização da β-lapachona encapsulada em lipossomas multilamelares e incorporada em um hidrogel de um biopolímero produzido pela bactéria Zoogloea sp. Estas formulações originais (β-lap-Lipo/ZBP/HEC) apresentaram um pH e comportamento reológico adequados para aplicação tópica, bem como a capacidade de retardar a liberação de β-lapachona do hidrogel. Um estudo histopatológico detalhado da atividade de cicatrização de feridas foi conduzido em um modelo in vivo e mostrou que o hidrogel de biopolímero foi capaz de estimular o reparo tecidual, aumentando a celularidade local, fibroblastos, células inflamatórias, vasos sanguíneos e a produção de fibrilas de colágeno durante a fase proliferativa. Além disso, a formulação β-lap-Lipo/ZBP/HEC promoveu angiogênese local e reduziu a inflamação da ferida, demonstrando o potencial desta formulação original de β-lap-Lipo/ZBP/HEC na terapia de lesões cutâneas. Para concluir, os nanocarreadores desenvolvidos demonstraram ser abordagens interessantes para interceptar as células de melanoma circulantes, enquanto as formulações lipossomais combinada com biopolímero têm um potencial interessante para aplicações de cicatrização de feridas.

Palavras-chave: Nanopartículas. Melanoma. Biopolímero. Lipossomas. Cicatrização.

RÉSUMÉ

Résumé: L'objectif principal de cette travail a été le développement, la caractérisation et l'évaluation in vitro et in vivo de différents nanovecteurs avec, d'une part, des nanoparticules spécifiques pour le traitement de la mélanome et des liposomes de β-lapachone- incorporés dans des hydrogels de biopolymère pour la cicatrisation de blessures topiques. La première partie de cette thèse présente une revue de la littérature et les récentes avancées dans le domaine du ciblage des cellules circulantes mésenchymateuses issues des mélanomes. Les principaux biomarqueurs de ces cellules ont été passes en revue afin de définir les caractéristiques qu'il est souhaitable de conférer aux nanovecteurs. La partie expérimentale du travail a consisté à preparer des nanoparticules (non sphériques) par nanoprécipitation de copolymères dérivés du poly(γ-benzyl-L-glutamate). Ces nanoparticules (taille comprise entre 20 et 100 nm et porteuses d'une charge négative (-3 à -30 mV). Elles ont ensuite été combinées avec l'anticorps MART-1 spécifique de la membrane des cellules de mélanome, en mettant en oeuvre des liaisons de type biotine-streptavidine. La combinaison de l'anticorps en surface des nanoparticules a été évaluée par western blot. L'affinité des immune-nanoparticules pour des cellules modèles du mélanome (lignée B16-GFP) et pour des cellules endothéliales de la veine ombilicale humaine (HUVECs) a ensuite été évaluée in vitro par cytométrie de flux. Par ailleurs, étant destinées à une injection intra-veineuse, il était important d'évaluer le degré d'activation du système du complément induit par les nanoparticules. La technique d'immunoélectrophorèse 2D mise en oeuvre a permis de conclure à une activation limitée, favorable à une augmentation du temps de circulation sanguine après injection intra-veineuse. Par ailleurs, les nanoparticules présentaient une faible cytotoxicité (test au MTT) vis à vis des cellules de mélanome ou des cellules endothéliales. En terme de capture cellulaire, les immuno-nanoparticules fonctionnalisées par MART1, anticorps spécifique pour la reconnaissance de l'antigène surexprimé dans des cellules de mélanome, a été augmentée de 40 à 50% par rapport au contrôle. La deuxième partie de cette thèse a été consacrée au développement, à la caractérisation et l'évaluation in vivo de l'activité cicatrisante de la β-lapachone encapsulée dans des liposomes multilamellaires, eux-mêmes incorporés dans un hydrogel d'un biopolymère produit par la bactérie Zoogloea sp. Ces formulations originales (β-lap-Lipo/ZBP/HEC) présentaient un pH et un comportement rhéologique approprié pour l'application topique, ainsi que la capacité de ralentir la liberation de la β-lapachone à partir de l'hydrogel. Une étude hystopathologique détaillée de l'activité cicatrisante a été conduite dans un modèle *in vivo* et a permis de montrer que l' hydrogel de biopolymère était capable de stimuler la reparation tissulaire, d'augmenter la cellularité locale, de favoriser les fibroblastes, les cellules inflamatoires, les vaisseaux sanguins et la production de fibrilles de collagène pendant la phase proliférative de la cicatrisation. De plus, la formulation β-lap-Lipo/ZBP/HEC a favorisé l'angiogenèse locale et a permis de diminuer l'inflammation de la blessure, démontrant le potentiel de cette formulation originale de β-lap-Lipo/ZBP/HEC dans la thérapie des lesions cutanées. Pour conclure, les nanovecteurs développés constituent des outils intéressants en vue d'intercepter les cellules circulantes du mélanome, tandis que les formulations liposomales associant des biopolymers originaux présentent un potential intéressant dans la cicatrisation des blessures.

Mots Clés: Nanoparticules. Mélanome. Biopolymère. Liposomes. Cicatrisation.

LIST OF FIGURES

2 DEVELOPMENT AND IN VITRO EVALUATION OF NANOPARTICLES FOR TARGETING MELANOMA CANCER CELLS

2.1 Advances in polymeric nanoparticles for metastatic melanoma treatment: therapeutic targeting of cancer stem cells and circulating tumor cells

3 RATIONAL DESIGN OF IMMUNONANOPARTICLES CONCEIVED FOR INTERCEPTING MELANOMA CTCS WITHIN THE BLOOD STREAM

4 TOPICAL LIPOSOMAL-HYDROGELS FOR WOUND CARE APPROACH

4.1 Wound healing properties of β-lapachone-loaded liposomes incorporated in a biopolymer hydrogel

Figure 1. Viscosity *versus* shear rate graphs of the liposomal gels at different lipid concentrations. The upper graphs correspond to the liposomal gel stability followed for a 90-day period: β-lap-Lipo/ZBP/HEC15 (2.5 mg/g) (a), β-lap-Lipo/ZBP/HEC30 (5.1 mg/g) (b) and β-lap-Lipo/ZBP/HEC60 (10.2 mg/g) (c). The lower graphs depict the liposomal gels in three different lipid concentrations on day 1(d) and day 90(e). The last graph (f) shows the effect of lipid concentration in the gels and the storage time on the zero shear rate viscosity values

LIST OF ACRONYMS

µC-IE	Multi-crossed electrophoresis
^{1}H NMR	Proton Nuclear Magnetic Resonance
Bt	Biotin
B16-GFP	Green fluorescent protein-labeled B16 melanoma cells
CAF	Complement activation factor
CMCs	Circulating melanoma cells
CSCs	Cancer stem cells
CTCs	Circulating tumor cells
DLS	Dynamic light scattering
FT-IR	Fourier transform infrared spectroscopy
HABA	4'-hydroxyazobenzene-2-carboxylic acid
HEC	Hydroxyethylcellulose
HUVECs	Human Umbilical Vascular Endothelial cells
IC$_{50}$	Average 50% growth inhibitory concentration
IgG	Immunoglobulin G
MALDI-TOF MS	Matrix-assisted laser desorption/ionization time-of-flight mass spectrometry
MART-1/Melan-A	Melanoma antigen recognized by T-cells
m-CSCs	Melanoma cancer stem cells
MEK	Mitogen-activated protein kinase kinase
PBLG	Poly(γ-benzyl-L-glutamate)
PEG	Poly (ethylene glycol)
Rhod	Rhodamine
TEM	Transmission Electron Microscopy

ZBP	*Zoogloea* sp. polymer
ZBP/HEC	Polymeric blend hydrogel of ZBP and HEC
BRAF	v-raf murine sarcoma viral oncogene homolog B1
β-lap	β-lapachone
β-lap/ZBP/HEC	β-lapachone incorporated in ZBP/HEC hydrogel
β-lap-Lipo	β-lapachone-loaded liposomes
β-lap-Lipo/ZBP/HEC	β-lapachone-loaded liposomes incorporated in ZBP/HEC hydrogel
EMT	Epidermal to Mesenchymal Transition

SUMMARY

1 INTRODUCTION

The nanotechnology have been widely applied in diagnosis and treatment of several diseases (ANGELI *et al.*, 2008). Nanotechnology applications in biomedical field, including vaccination, diagnostics and drug-delivery (BOULAIZ *et al.*, 2011; CHOWDHURY *et al.*, 2016; REED *et al.*, 2015). In pharmaceutical field, the nanocarriers has been used to improve the efficacy of therapeutic and/or diagnosis agents and to overcome biopharmaceutical, pharmacokinetics and toxicological drawbacks related to the conventional therapies (BAO; MITRAGOTRI; TONG, 2013; DEVALAPALLY; CHAKILAM; AMIJI, 2007; PIKTEL *et al.*, 2016). In general, this nanocarrier can be classified as lipidic or polymeric. Liposomes and nanoemulsions are examples of nanocarriers based on lipid components, whereas nanospheres and nanocapsules are examples of polymer-based nanoparticles (ALLEN; CULLEN et al., 2004; MORA-HUERTAS; FESSI; ELAISSARI, 2010).

Nanotechnology applications in cancer based on drug delivery systems have been extensively evaluated over last decade and demonstrated to be a promising approach to improve the efficacy of anti-cancer therapy (BRYS *et al.*, 2016; SUTRADHAR; AMIN, 2014). However, the cellular heterogeneity and plasticity presented in tumors sites represent one of the main causes of metastasis and can be considered as one of the most challenge subjects for the improvement of cancer therapeutics (BROOKS; BURNESS; WICHA, 2015).

Precisely, two types of cancer cells are directly involved in tumor heterogeneity and metastasis: the cancer stem cells (CSCs) and circulating tumor cells (CTCs). The CSCs represents a minority cell population in tumor environment with pluripotent characteristics and high metastatic ability (BROOKS; BURNESS; WICHA, 2015; CSERMELY *et al.*, 2014). On the other side, the CTCs are tumor cells spread in blood and/or lymphatic vessels from solid tumors (XU; ZHONG, 2010). High levels of CSCs and CTCs has been associated with tumor

progression, chemoresistence and metastatic spread (LA PORTA; ZAPPERI, 2013; PORE *et al.*, 2016).

In this context, one of the cancer types with greatest metastatic potential and chemotherapeutic resistance is the melanoma. This tumor is characterized as the malignant transformation of melanocytes of neural crest origin and it is considered the deadliest skin cancer, with a 5-year-survival rate for distant melanoma metastasis of less than 20% (ALBINO *et al.*, 1992; CHEN, *et al.*, 2013). Owing to the clinical relevance of this skin cancer, the melanoma treatment has been widely explored for nanotechnology applications, including the use of polymeric nanoparticles (ANTÔNIO *et al.*, 2017; JAIN; THANKI; JAIN, 2013; LI *et al.*, 2015).

The first section of this thesis was dedicated to the nanotechnological approaches for metastatic melanoma treatment. The first chapter consisted in a literature review about the role of CSCs and CTCs in the development of metastatic melanoma; the current biomarkers of these distinct population of melanoma cells and the advances in polymer based nanoparticles for the metastatic melanoma treatment. In this perspective, the influence of architectural properties of polymeric nanoparticles in the effectiveness of passive and active-melanoma targeting were widely discussed. Thus, the goal of this review was to present and discuss the up-to-date status of melanoma biomarkers and to evaluate the advances in polymeric nanoparticles strategies in order to develop effective drug delivery systems for the treatment of metastatic melanoma.

Thereafter, the second chapter comprised of the development and *in vitro* evaluation of polymeric nanoparticles for targeting melanoma cells. In this study, the melanoma antigen recognized by T-cells (MART-1) was selected as a target, due to this overexpression in melanoma cell lines (TAZZARI *et al.*, 2015). Immunonanoparticles, based on poly (γ-benzyl-L-glutamate) (PBLG) and coupled with antibody against MART-1, were developed, characterized and tested *in vitro* on melanoma and endothelial lineages.

The use of nanotechnology for wound healing treatment also offers a number of advantages when compared to the conventional cutaneous therapies, such as occlusive dressings (JACKSON; KOPECKI; COWIN, 2013). These advantages comprise on the protection of active principles, enhanced drug penetration, promotion of localized drug effects and reduced unwanted systemic absorption (CARNEIRO *et al.*, 2010). In this context, nanoemulsions and liposomes are the most utilized nanocarriers for cutaneous applications (WU; GUY, 2009).

Liposomes are spherical vesicles formed by one or more concentric phospholipid bilayers with an aqueous core. The main advantage of this nanocarrier is the ability to encapsulate lipophilic, amphiphilic and hydrophilic substances, due to their biphasic character (TORCHILIN, 2005). Lipophilic substances, such as β-lapachone, a naphthoquinone that presents important biological properties including wound healing, can be encapsulated into liposomes with high drug loads (CAVALCANTI *et al.*, 2015; FU *et al.*, 2011; KUNG *et al.*, 2008). Nevertheless, the application of liposomal dispersion directly to the skin is limited specially due to their low viscosity characteristic (MOURTAS *et al.*, 2008). In this way, the use of thickening agents, including hydrogels, can improve the liposomes rheological properties for topical drug-delivery and also exhibit biological properties (CIOBANU *et al.*, 2014; MOURTAS *et al.*, 2007).

Thus, the second section of this thesis aimed to develop a liposomal-hydrogel containing β-lapachone for wound healing applications. The liposomal-hydrogel formulation consisted of β-lapachone-loaded multilamellar liposomes incorporated in a polymeric blend, containing a bacterial cellulose hydrogel produced by *Zoogloea* sp. Both bacterial cellulose and β-lapachone are expected to have wound healing properties. This study evaluated the *in vitro* kinetics and rheological properties of the liposomal-hydrogels containing β-lapachone, as well as their *in vivo* wound healing activity.

In general, this thesis aimed to contribute for the development of polymeric and lipidic nanocarriers with different biological applications and administration routes, for instance systemic treatment of melanoma and topical action in wound healing.

2 DEVELOPMENT AND *IN VITRO* EVALUATION OF NANOPARTICLES FOR TARGETING MELANOMA CANCER CELLS

2.1 Advances in polymeric nanoparticles for metastatic melanoma treatment: therapeutic targeting of cancer stem cells and circulating tumor cells

Autores: Sarah Brandão Palácio [a,b]; An Young Taylor Sarahi[b] ; Francisco Humberto Xavier Junior [a,b]; Isabella Macário Ferro Cavalcanti [a,c]; Nereide Stela Santos Magalhães [a]; Gilles Ponchel [b*]

[a] Laboratory of Imunopatology Keizo-Asami, Federal University of Pernambuco, Recife, PE-Brazil

[b] University Paris Sud, Institut Galien Paris-Sud - UMR CNRS 8612 – Faculty of Pharmacy, 92296 Chatenay-Malabry Cedex – France.

[c] Academic Center of Vitória de Santo Antão, Federal University of Pernambuco, Vitória de Santo Antão- PE, Brazil

Corresponding Author*

Prof. Gilles Ponchel, University Paris Sud, Institut Galien Paris-Sud UMR CNRS 8612 - Faculty of Pharmacy, 5 Rue J.B. Clément, 92296 Chatenay-Malabry Cedex – France. Tel.: +33 01 46 83 59 19 fax: +33 01 46 61 93 34. E-mail address: gilles.ponchel@u-psud.fr

2.2 Abstract

Melanoma is a skin cancer characterized by malignant transformation of melanocytes of neural crest origin. Cellular heterogeneity and plasticity involving cancer stem (CSCs) and circulating tumor cells (CTCs) represents one of the most challenge subjects for improvement of metastatic melanoma therapy. Polymeric nanoparticles are a promising technology to improve the efficacy of cancer treatment. These systems can be designed to enhance drug delivery across biological barriers and also to identify specific tumor markers at surface of melanoma cells. However, the optimal architectural properties of polymeric nanoparticles remain a challenge to passive and active-tumor targeting to reach CSCs and CTCs. Thus, the goal of this review was to evaluate the innovative advances in polymeric nanoparticles strategies for metastatic melanoma cell therapies. In this perspective, an overview of the current therapy regarding biological characteristics, resistance mechanisms and clinical relevance to potential biomarkers of the CSCs and CTCs involved in melanoma metastasis were carried out. Furthermore, the potential application of polymeric nanoparticles taking into account its intrinsic physicochemical and modification of surface properties for passive and active tumor targeting were extensively discussed in order to design an effective drug delivery system to CSCs and CTCs for the treatment of metastatic melanoma.

Keywords: Melanoma; cancer stem cells; circulating tumor cells; polymeric nanoparticle; passive tumor targeting; active tumor targeting.

2.3 Introduction

Melanoma is a skin cancer characterized by the malignant transformations of melanocytes of neural crest origin, different from non-melanoma skin cancers, which are originating from the basal and squamous cell layers in the epidermis. Melanoma is the most aggressive skin cancer and exhibits resistance to current treatments (Cichorek et al., 2013; Slominski & Carlson, 2015). Although melanoma accounts for only 1% of all skin cancers, it is the major cause of poor prognostics and deaths due to its markedly metastatic potential. Extensive research efforts have been made over the past years to better understand the melanoma metastasis mechanisms/pathogenesis and which factors, environmental and genetics, are involved in disease progression (Landow et al., 2016; Pietila et al., 2016).

In general, different types of cancer cells are found within the same tumor site and these phenotypic and functional heterogeneity can be a result of an extensive genetic and epigenetic instability, cell plasticity and tumor microenvironmental characteristics (Meacham & Morrison, 2013; Sun & Yu, 2015). These intratumor heterogeneity are closely related to metastatic disease and represents the main cause of anti-cancer therapy resistance, therefore it is a challenging subject for the improvement of cancer patient's survival (Brooks et al., 2015; Gay et al., 2016). Two main concepts have been proposed to explain these intratumor heterogeneity and cancer progression: stochastic model and cancer stem cells (CSCs) model. The stochastic or clonal evolution preconizes that differences between tumorigenic cancer cells are generated through genetic and epigenetic mechanisms and lack hierarchical organization. On the other hand, the CSC model hypothesizes that cancer is hierarchically organized into nontumorigenic and tumorigenic fractions. These mesenchymal cancer cells with tumorigenic potential represents the minority population in tumor environment and has capacity of self-renewing and generate heritable phenotypic variation (Csermely et al., 2014; Brooks et al., 2015). The pluripotent characteristics of the CSCs have been considered the driving force of tumor progression and

these cells are involved in metastatic dissemination due to their ability to initiate and sustain the cancer disease (La Porta & Zapperi, 2013). Studies suggested the existence of these tumor cells subpopulation in *in vivo* melanoma models (Dou et al., 2007; Sigalotti et al., 2008; Shakhova & Sommer, 2013).

Another type of cancer cells, directly related to tumor heterogeneity and involved in melanoma metastasis development, are the circulating tumor cells (CTCs). This cancer cells are shed in peripheral blood from a primary or metastatic tumor (Xu & Zhong, 2010). Epithelial CTCs were first reported over 100 years ago and since then, the isolation and identification of these cells by specific biomarkers displayed at their surface or intracellularly are used to evaluate cancer prognostics, have been correlated with metastatic disease and poor patient outcome (Ashworth, 1869; Lianidou et al., 2015).

In recent years, the biological understanding of invasive and metastatic capability of CSCs and CTCs have attracted increasing attention in target these cells for diagnosis, prognostics and clinical treatment of melanoma cancer. Nowadays, besides the prognostics properties, the identification of CSCs and CTCs biomarkers have been described as a potent clinical approach to optimize the chemotherapeutic scheme and to develop personalized targeted systems for cancer therapy, improving the survival in patients with a variety of solid tumors, such as melanoma (La Porta & Zapperi, 2013; Li et al., 2015; Zhang et al., 2016).

The conventional anti-cancer monotherapy based on systemic administration of cytotoxic agents, such as paclitaxel, cisplatin and doxorubicin, are commonly ineffective in metastatic diseases, presenting poor pharmacokinetics properties, dose-limiting toxicities and induction of drug resistant cancer cells (Grundy et al., 2016). Recent studies have been suggested that combination therapies of cytotoxic agents, as dacarbazine, with newer molecularly targeted inhibitors, as vemurafenib and trametinib, or immunotherapy agents, as ipilimumab, are the most promising strategy to achieving long-term sustained response,

decrease the relapse rate and increase the overall survival rate for patients with metastatic melanoma (Davey et al., 2016; Tran et al., 2016). Despite of the increasing effort in propose new therapeutic schemas for metastatic melanoma, these treatments have limited effectiveness and serious health-threatening effects (Eroglu & Ribas, 2016).

In last decade, the nanotechnology approach, based on the versatile and modifiable drug delivery nanocarriers systems, as polymeric nanoparticles, has been an extensively explored strategy to overcome the hazards related to conventional anti-cancer therapy (Drewes et al., 2016; Silva et al., 2016). Nanotechnology applications based on passive and active targeted drug delivery systems demonstrated to be a promising technology to improve the efficacy of melanoma diagnostic and therapy (Bombelli et al., 2014; Silva et al., 2015; Kumari & Kondapi, 2016). The passive targeting is based on the nonspecific accumulation of nanocarriers on tumor microenvironment by the enhanced permeability and retention effect (EPR effect), whereas the active targeting is based on the affinity of target moieties attached at nanocarrier surface to specifically recognize biomarkers on the tumor cells (Upponi et al., 2014). Researchers are being carried out using polymeric nanoparticles in order to enhance the transport of active or/and imaging agents across biological barriers and also to recognize specific tumor markers at the surface of melanoma cells (Drewes et al., 2016). Nevertheless, the use of nanotechnology to target CSCs and CTCs, in order to impair tumor progression and prevent metastasis, is still emerging and being purposed in current research (Li et al., 2015; Garcia-Mazas et al., 2016). The intrinsic physicochemical characteristics of polymeric nanoparticles, such as the large surface area, modifiable surface properties and long circulation half-life, represent a promising path to develop drug delivery systems to reach the heterogeneous cancer cell population, including the CSCs and CTCs that have a high metastatic potential and are not easily targeted (Li et al., 2015; Zuo et al., 2016).

In these perspectives, the first part of this review provided an overview of the current research regarding biological mechanisms of CSCs and CTCs in metastatic development and their related biomarkers detected in melanoma patients. On the second part, the recent advances in polymeric nanoparticles for passive and active targeting to advanced melanoma treatment are presented and discussed. This section focused on CSCs and CTCs targeting strategies and on the influence of architectural properties of nanoparticles in their *in vivo* performance. In summary, this review aims to shed light on the potential biomarkers for nanotechnology applications, specially in polymeric nanoparticles, to target CSCs and CTCs and to improve metastatic melanoma treatment.

2.4 Cancer stem cells (CSCs) and circulating tumor cells (CTCs) role in melanoma tumor

2.4.1 CSCs

Since Briggs & Robert (1952) challenged the unidirectional development model of embryonic stem cells that differentiates into somatic cells, several studies also demonstrated that normal cells and tumor cells could go back in time through the dedifferentiation process. This process is defined as the reversion of cells from a differentiated state to an embryonic state with less specialized characteristics and functions (Jopling et al., 2011).

The dedifferentiation process and genetic mutation of normal stem/progenitor cells, somatic cells and cancer cells, leading by pro-oncogenes, may result in a transformation into a self-renewing and multipotent type of tumorigenic cells called cancer stem cells (CSCs) (Borovski et al., 2011; Friedmann-Morvinski & Verma, 2014). The CSCs have been demonstrated to play an important role in tumor progression, including melanoma (Herreros-Villanueva et al., 2013; Shakhova & Sommer, 2013). These cells are considered to be a rare subpopulation of tumor niche and they have a long-term proliferative ability and capacity for

asymmetrical division, besides are involved in angiogenic induction and apoptotic resistance, including resistance to chemo-radiation therapy. Numerous researches appointed that the CSCs characteristics are intimately involved in metastasis development and cancer relapse (Shiozawa et al., 2013; Allegra et al., 2014). Thanks to these features, the CSCs becomes a new therapeutic target for cancer treatment, specially for tumor progression impairment, as well as, a valuable biological marker for cancer prognostics, since they could be detected in majority of malignant tumors (Vinogradov & Wei, 2012; Bao et al., 2013).

The mechanisms that may originate the CSCs are not fully understood yet. One of the key mechanism for generation of CSC phenotype cells in tumor site is the epidermal to mesenchymal transition (EMT) (Figure 1). Briefly, this mechanism consists in an activation of the embryogenic state of cancer cells located at the primary tumor (Borovski et al., 2011). Studies demonstrated that cell fusion, horizontal gene transfer and microenvironment conditions such as hypoxia and induction factors as transforming growth factor-β (TGF-β), could promote CSC formation, proliferation and clonal selection of CSCs (Lobo et al., 2007; Borovski et al., 2011).

Owing to the concept that tumors are characterized by their cell heterogeneity, CSCs can be considered a side cell population of tumor that have unlimited proliferation capability, potential to differentiate, accumulate genetic mutations and consequently may presented a strong tumorigenicity, giving rise to various population of tumor cells. Nevertheless, depending on the type of cancer, CSCs concept was not completely accepted yet, specially due to the controversial results of current research that identify these cells in tumor sites (Kelly et al., 2007; Visvader & Lindeman, 2012; Shiozawa et al., 2013).

The evidences suggest a controversy regarding the existence of CSCs in tumor microenvironment. Bonnet & Dick (1997) demonstrated one of the first evidences of CSCs hypothesis thought the acute myeloid leukemia model. In this research was observed that the

leukemogenic event was originate by primitive cells that expressed the specific markers on their surface, as the $CD34^+$ and $CD38^-$, and had the capability to prevent the normal differentiation occurrence. Challenging the CSCs concept, Kelly and colleges (2007) injected mouse lymphoma cells into nonirradiated congenic animals and demonstrated that all animals developed fatal lymphoma, suggesting that the CSCs were not the only tumor initiating cells. In the same way, Quintana and collegues (2010) investigated the tumorigenic capacity of melanoma cells. This study demonstrated that cancer cells with different biomarkers and phenotypes had the potential to form tumors and that melanoma exhibited a phenotypic plasticity, which contrasts with CSCs model that hypothesizes irreversible genetic changes by tumorigenic cells.

Despite these controversial studies, most of the evidence indicate the existence of CSCs in melanoma tumor models and indicate that these cells can constitute a small fraction (0.0001 to 1%) of heterogeneous cells population in tumor microenvironment (Dou et al., 2007; Schatton et al., 2008). Meanwhile, other researchers suggest that the frequency of tumorigenic cells in primary tumors could be underestimated by the xenograft transplantation model, the most applied *in vivo* model to demonstrate the CSCs existence (Kelly et al., 2007; Zhong et al., 2010; Jandl et al., 2013). Furthermore, Kelly and collegues (2007) hypothesize that the presence and frequency of CSCs strongly depend of the tumor type, specially due to the variable degrees of functional heterogeneity as consequence of the specific oncogenic pathways. Researches have been proposed new methods to improve the detectable frequency of CSCs applying more severely immunocompromised mice. Quintana and coworkers (2008) modified xenotransplantation assay conditions, using non-obese diabetic combined immunodeficiency (NOD/SCID) interleukin-2 receptor gamma chain null (Il2rg2/2) mice and observed an increase, by several orders of magnitude, of detectable melanoma tumorigenic cells. Similarly,

Zhong and coworkers (2010) also found a substantial population of CSCs (> 10%) in B16-F10 melanoma cells in syngeneic mice.

In view of to shed light on definition, origin, identification and frequency of CSCs *in vivo*, it is essential to identify the expression of appropriate surface markers, which could be able to distinguish tumorigenic melanoma CSCs by their distinct functions from the tumor cells that are non-tumorigenic.

2.4.2 CTCs

The 'seed and soil theory' proposed by Paget (1889) preconizes that the metastasis' formation is a nonrandom process where the CTCs (seeds) target specific organs that presents a desirable microenvironment (soil) for tumor cells growth. It is already well established that CTCs are cells located in peripheral blood directly involved in the spread of tumor cells from an organ-confined site to distant sites, resulting in metastases to multiple organs. However, the transition of cancer cells, derivate from primary tumors, to blood circulation can be very drastic for the cells and they need to acquire a special phenotype to survive to the harsh conditions of an anchorage-independent environment. One of the most critical mechanisms involved in CTCs production is epidermal to mesenchymal transition (EMT). This epithelial cancer cell transition to mesenchymal state helps to maintain the invasive phenotype and metastatic potential of CTCs (Borovski et al., 2011). Evidences indicates that cancer cells loss their cell-cell junctions after EMT, becoming more motile and aggressive, allowing more efficient cancer cell metastasis (Zhang et al., 2016). EMT process occurs specially as a result of combined epigenetic mutations and changes in tumor microenvironment and directly influences the regulation of tumor development (Pietila et al., 2016).

CTCs are part of tumor cellular heterogeneity and the mainly difficult in obtain a suitable molecular definition for these cells is their rarity in blood. It is estimated to exist 1 among 10^6 to 10^7 normal white blood cells (Ross et al., 1993) or 1 to 10 CTCs for each 4 mL of

blood of metastatic melanoma patients (Freeman et al., 2012). A recent mini-review exalted the importance of CTCs detection and characterization in the blood of cancerous patients as an alternative to invasive tissue biopsies and to improve the cancer prognostics (Zhang et al., 2016). This new prognostic strategy has been called liquid biopsy and could be very helpful to elucidate how the CTCs gain resistance against anti-cancer treatments. Therefore, CTCs isolated from blood flow through non-invasive method could allow various clinical advantages: monitoring phenotypic changes in cancer cells of metastatic patients; detection of this markers as an indicative of tumor progression; discovered future targets to individualized cancer therapies, apart lead to a better understand of cancer cell biology and metastasis mechanisms (Lianidou et al., 2015). The available methods to CTCs isolation and detection in blood flow can include antibody-based capture assays, size-based filtration or nucleic acid-based assays (Pore et al., 2016). Unluckily, these methods are very technically limited, specially due to the sparse number of CTCs in circulating blood of cancer patients (Adams et al., 2015). Xu & Zhong (2010) reinforce the necessity to discovery miniaturized methods, specially using the nanotechnology, that allows fully characterized CTCs in a single-cell level. Due to this expressively role of CTCs in metastases pathogenesis, these cells have become a very promising target to evaluate the patient's prognostics and to develop new treatment strategies to prevent cancer dissemination (Hayes & Paoletti, 2013).

2.4.3 Clinical relevance of melanoma cancer stem cells (m-CSCs) and circulating melanoma cells (CMCs) and their biomarkers for diagnosis, prognosis and treatment of melanoma cancer

Biomarkers are molecules that can be measured and evaluated as indicative of normal biological processes or pathological conditions, such as cancer. There is a wide variety of biomarkers including transmembrane proteins (e.g., receptors), glycoproteins (e.g., integrins),

nucleic acids (e.g., microRNAs), transcription factors, carbohydrates, hormones and antibodies (Schwarzenbach et al., 2011; Sethi et al., 2013). In recent years, significant efforts have been made to better characterize biomarkers in oncology which play a critical role in initiation, progression and maintenance of tumors. In melanoma skin cancers, a large number of biomarkers, mainly proteins, have been identified in melanoma cells and their expression have been correlated with different stages of melanocytic tumor progression (Marconi et al., 2015). In this context, the identification and recognition of biomarkers expressed in two particular types of metastatic melanoma cells, melanoma cancer stem cells (m-CSCs) and circulating melanoma cells (CMCs), have been reported as an important strategy to provide an accurate diagnosis and improve the therapy of this skin cancer (Freeman et al., 2012; Schlaak et al., 2012; La Porta & Zapperi, 2013).

The biomarkers can be non-invasively assessed and detected in body fluids as blood, urine, feces and sputum, or invasively assessed by a tissue biopsy (Henry & Hayes, 2012; Xiao et al., 2013). High throughput technologies have been adopted to identify and characterize potential biomarkers include positron emission tomography, protein microarray, exome sequencing, flow/mass cytometry, multicolor immunohistochemistry and capillary electrophoresis (Sethi et al., 2013; Yuan et al., 2016).

The detection and characterization of m-CSCs and CMCs by accurate techniques could allow to clinicians establishes more effective prognostics and infers the melanoma metastatic risk of current patients as well as the relapse disease potential of patients that were submitted by curative resections (Huang & Hoon, 2016). Despite the clinical relevance of these cells, the most challenge drawbacks to clinical applications of m-CSCs and CMCs is their heterogeneity of biomarker expression and the isolation of these cells from tumor sites and blood circulation (La Porta & Zapperi, 2013; Gray et al., 2015; Zand et al., 2016).

In the next two sections of this review we describe the main biomarkers reported in literature for m-CSC and CMCs (Figure 1 and Table 1), their role in metastasis and their current clinical applications in diagnosis and treatment of melanoma.

2.4.4 Biomarkers for m-CSCs

A novel and promising clinical approach to improve the prognostics of patients with metastatic melanoma is the targeting of m-CSCs, specially through immunotherapy in both tumor site and blood flow. Unfortunately, despite of the increase research efforts to understand the antigenic profile of these cells, little is known about the expression of specific tumor-associated antigens and which are the triggers and microenvironmental conditions that regulates these antigens expressions in m-CSCs (Sigalotti et al., 2008). Nevertheless, it is well-known that normal and tumor pluripotent cells generally displays cluster differentiation markers at the cell surface and that m-CSCs also overexpressed specific cluster differentiation antigens, such as CD133, CD44, CD20 and CD271 (Shmelkov et al., 2008; Singh & Settleman, 2010; Morath et al., 2016).

In this context, CD133 is one of the most well characterized antigen presented in the surface of normal stem cells and CSCs derivate from a wide range of tissue types and its epitope AC133 has also been highly used as an important biomarker to detected and isolated CSCs (Mak et al., 2014). The CD133 is a 120-kDa transmembrane glycoprotein, expressed in plasma membrane and their expression have been associated with chemoresistance and radioresistance in various cancer types (Ferrandina et al., 2009; Wu & Wu, 2009). Recent evidences support that CD133 plays an essential role in establishing the vascular niche through the cell differentiation into tumor endothelium, however the mechanisms that govern its function require further elucidation (Mak et al., 2014). CSCs expressing CD133 (CD133+) have also been demonstrated to have an important signaling function, attracting and activating cells from

the tumor microenvironment (Borovski et al., 2011). Another study suggested that CD133^{+} melanoma cells have an enhanced ability to initiate primary tumors compared to melanoma cells that not expressed CD133 (CD133^{−}) (Monzani et al., 2007).

Furthermore, CD44, a very well described m-CSCs surface marker, has been a topic of an intense research interest, specially due to the increased evidences of their role in tumor progression and metastasis (Negi et al., 2012; Thapa & Wilson, 2016). The CD44 is a cell molecule adhesion overexpressed in several types of cancers, including melanoma, and might promote the ability of cancer cells to self-renew and differentiate by interacting with tumor microenvironment (Morath et al., 2016). Overall years, various studies have been correlated the level of CD44 in malignant melanoma cells lines with a higher metastatic risk (Dietrich et al., 1997; Ahrens et al., 2001). In addition, it was demonstrated that the stimulation of CD44 by hyaluronic acid on melanoma cells mainly induced an increase in proliferative capacity of these cells (Ahrens et al., 2001) . Dou and coworkers (2007) demonstrated that the co-expression of the markers CD44 and CD133 in B16F10 melanoma cells are associated with stronger tumorigenic potential in mice and the identification of these two markers provide an important method for further CSCs target therapy.

Another important marker of mature B cells associated with m-CSCs is the CD20. Fang and collegues (2005) suggested a correlation between CD20 expression in melanoma sphere cultures and preferential clonogenicity capacity. Due to this property, the monoclonal antibody against CD20 (Rituximab[®]) has been tested aiming m-CSC elimination. Schmidt and collegues (2011) demonstrated that CD20 was an effective target to eradicate estabilished melanoma lesions in immunodeficient mice. Furthermore, clinical studies evaluating metastatic melanoma patients treated with Rituximab[®] resulted in a regression of metastatic lesions and prevention of disease recurrence (Pinc et al., 2012; Schlaak et al., 2012).

The CD271, a neurotrophin receptor, has been related with m-CSCs profile (Valyi-nagy et al., 2012). This receptor is widely expressed in human normal and neoplastic tissues of neural crest origin, specially melanoma (Kruger et al., 2002). Recently, it was suggested an inversely correlation between the CD271 expression in melanoma cells and tumor progression. The expression of CD271 exhibited a significantly decrease in metastatic melanoma cells when compared with primary tumor using *in vitro* zebrafish melanoma model of three-dimensional multicellular spheroids (Saltari et al., 2016).

One of the suggested explanations for these results was that CD271 negative profiles promoted the down regulation of β_1-integrin, decreasing the cell-cell adhesion which improved the cells ability to invade and causes the melanoma progression. Another cluster differentiation molecule that also has been correlated with poor prognosis in malignant melanoma patients is the activated leukocyte cell adhesion molecule (ALCAM/CD166). This m-CSC marker is involved in cell growth, migration and adhesion. The regulation of cell adhesion in tumor tissue is a key process for metastatic development through the cell evasion from primary tumor to surrounding tissue (Swart, 2002; Weidle et al., 2014).

2.4.5 Biomarkers for CMCs

Van der Bruggen (1991) discovered the first Melanoma Differentiation Antigens (MDA), proteins that are only expressed on melanocyte lineage, whether normal or tumor cells. Since then, more than 55 proteins with a homolog domain of 200 amino acids (MAGE Homology Domain, MHC) were identified and characterized. These proteins represent the melanoma differentiated cells and are associated with tumorigenic phenotypes (Sang et al., 2011). MAGE proteins are rather expressed in normal cells but is overexpressed in various forms of cancers as bladder, breast, squamous carcinoma and more frequently in melanoma and lung cancer (Roeder et al., 2005). The recent literature showed that these proteins play a major

role in cell cycle progression and apoptosis as also on immune response against cancer. However, their biological functions and mechanisms are not yet well understood (Sang et al., 2011).

A well-characterized biomarker of this family is the MAGE-A3, a tumor-specific antigen expressed in a variety of cancers and presented in 57% to 76% of metastatic melanoma. It has been utilized as a diagnosis and prognosis biomarker for CMC and has also been studied as a target for cancer immunotherapy (Sigalotti et al., 2002; Roeder et al., 2005). Despite of MAGE-A3 has been considered an attractive target for immunotherapy, this antigen recently failed in two different phase 3 trials for melanoma and non-small-cell lung cancer (NSCLC). The adjuvant treatment with the MAGE-A3 immunotherapeutic did not increase disease-free survival and any other clinical outcome measure compared with placebo (Vansteenkiste et al., 2016). These results reinforce the problematic of cancer vaccination technology to improve the prognostics in patients and overcome the immunosuppressive environment of aggressive cancer types as NSCLC.

Apart MAGE antigens, another three MDA can be highlighted, specially due to the application in melanoma diagnosis and cancer immunology: melanoma antigen recognized by T-cells (MART-1/Melan-A); glycoprotein 100 (gp100) and tyrosinase (TYR). These melanocyte antigens are responsible for melanoma differentiation, biosynthesis of melanin and T-cells recognition of antigens presented at cells surface. In recent years, a new approach for cancer prevention and immunotherapy are the development of vaccines using these antigens, specially MART-1 (Gibney et al., 2015; Reed et al., 2015; Tazzari et al., 2015).

The melanocyte differentiation marker MART-1 is found in the membranes of the Golgi apparatus, endoplasmic reticulum, as well as the plasma membrane itself (Chen et al., 1996; De Mazière et al., 2002). It is homogenously expressed in 75 to 100% of human melanomas, but not in other cancer types, and in normal melanocytes from skin and retina (Meng et al., 2015).

Mockey and collegues (2007) developed histidylated lipopolyplexes containing MART-1 mRNA and demonstrated that this system was effective on protected against B16F10 melanoma tumor progression, drastically reducing by 75% the total number of lung metastases. A pilot phase I-II trial designed by Pucchio and collegues (2006) evaluated the effects of a co-therapy using IFN-α; Melan-A/MART-1 and gp100 peptides in stage IV melanoma patients. It was demonstrated an enhancement in CD8+ T cells recognizing MART-1+gp100+ melanoma cells.

TYR, a protein expressed in melanocytes, is another important CMC biomarker utilized in cancer immunotherapy. The technique of real time reverse transcription polymerase chain (RT-PCR) can detect marker RNA expression in the peripheral blood and was used for the first time by Smith, Lattman & Carter (1991) for detection of TYR. Cancer vaccines based on injection of xenogeneic TYR DNA peptide have been tested and demonstrated to induce humoral and cytotoxic lymphocyte immune responses against human melanoma cells that express TYR, resulting in tumor growth inhibition (Yuan et al., 2013). On the other side, the most relevant achievement for xenogeneic TYR DNA vaccine have been the effectiveness of this tumor associated antigen to improve survival in dogs with metastatic melanoma (Bergman et al., 2006; Aurisicchio et al., 2015). Based on these positive results, xenogeneic TYR DNA vaccine (Oncept®) was commercially approved in USA (Bergman et al., 2006).

In the context of MDA, various researches have been observed an upregulation of gp100, MART-1 and TYR antigens in melanoma cell lines treated with (v-raf murine sarcoma viral oncogene homolog B1) (BRAF) and mitogen-activated protein kinase kinase (MEK) inhibitors, resulting in improvement of antigen-specific recognition by gp100 and MART-1 specific T-cells (Boni et al., 2010; Ott et al., 2013). It has been suggested that the oncogenic BRAF suppressed the MDA expression by Microphthalmia Associated Transcription Factor' (MITF). This transcriptional factor is also considered a class of human melanoma marker that regulates the transcription of multiple MDAs. MITF is consider the master regulator of

melanocyte development and melanoma oncogene. It is also involved with the plasticity of melanoma cells (Hartman et al., 2014). The overexpression of this oncogene MITF was shown high sensitivity for metastatic melanoma (88-100%) and could be associated with a reduced survival in melanoma patients (Prieto & Shea, 2011). MITF can also support the diagnosis of metastatic tumors that are suspicious for melanoma but negative for common melanoma markers as MART-1 and TYR (Guo et al., 2013).

Melanocortin-1 receptor (MC1R) is an important member of G-protein-couple receptor family that regulates the amount and type of melanin (eumelanin and pheomelanin) produced from melanocytes, which determine the melanoma phenotype and risk factor. On the other hand, the expression and function of MC1R in amelanotic and nonmelanocytic tumors remains unclear (Ghiorzo et al., 2009; Ordóñez, 2014). This receptor is highly expressed in melanoma but lower expressed on normal cells and other cancer types (López et al., 2007) . Kennedy and collegues (2001) described that numerous MC1R variants predispose to cutaneous melanoma and this predisposition is largely independent of skin type. It is also suggested that the risk for malignant melanoma, associated with MC1R variants, was confined only to BRAF-mutant melanomas (Fargnoli et al., 2008).

Despite of above discussed evidences, the recent literature about the feasibility of CMCs clinical applications demonstrated to be controversial. Although there was a general agreement that correlated the abundance of CMCs tumor biomarkers in blood flow with a poor prognostic and decrease of patients overall survive another researches suggested that the use of melanocytic markers to detect CMCs could lead to false-negatives results, specially with the cells that presents anmelanotic and phenotypes associated with lack of pigmentation production (Notani et al., 2002).

One of the most used methods for CMCs isolation is based on the immunocytochemical identification of surface markers (Liu et al., 2011). The CellSearch® system is a recent platform

commercially approved by FDA for CTCs isolation. This technique is based on targeting cell markers in metastatic cancers, such as epithelial cell adhesion molecule (EpCAM) and melanoma cell adhesion molecule (MCAM/CD146/MUC18) (Farace et al., 2011). MCAM, generally expressed in lymphoid tissues as a receptor for laminin alpha 4, is strongly expressed on the surface of CSCs derived from human bone marrow (Covas et al., 2008; Russell et al., 2013). In addition, this receptor is also largely expressed by endothelium cells and their function has been associated with support of endothelial integrity (Schrage et al., 2008). Besides, the MCAM is up-regulated in inflammatory diseases and is also involved in lymphocyte recruitment by endothelium (Guezguez et al., 2007; Duan et al., 2013). Despite the lack of specificity for melanoma, studies have been explored MCAM as a promising target in melanoma diagnosis and cancer therapy, particularly in cases where the histology is suggestive but other melanoma markers are negative (Koch et al., 2001; Staquicini et al., 2008). Besides, recent studies associated the detection of MCAM/MUC18 in melanoma patients as a molecular warning of melanoma metastatic potential, with higher incidence of disease relapse, poor prognosis and death (Elshal et al., 2005; Rapanotti et al., 2014).

Biomarkers also associated with general tumorigenic phenotypes have been used for target melanoma diagnosis and treatment. Two examples of these types of general makers are the Ganglioside GD2 and HMW-MAA/CSPG4. The Ganglioside GD2 is a membrane receptor, highly expressed on tumors of neuroectodermal origin as melanoma, neuroblastoma, brain tumors and osteosarcomas, and have restricted expression in normal tissues, specially in peripheral nerves, melanocytes and brain cells (Longee et al., 1991; Yu et al., 2016). This ganglioside receptor is also highly expressed in human mesenchymal stem cells and has been reported as a useful cancer stem cells biomarker, specially for neuroblastomas, breast cancers and melanoma (Battula et al., 2012; Senses et al., 2017). Studies suggested that the anti-GD2 antibodies can have a direct cytotoxic activity, inducing a rapid cell death when incubated with

GD2-positive tumor cells (Kowalczyk et al., 2009; Doronin et al., 2014). Multiple clinical trials have been performed using different types of anti-GD2 monoclonal antibodies classes in different cancer types, including melanoma (Albertini et al., 1997; King et al., 2004; Choi et al., 2006). Generally, the positive results of these studies were prominent to neuroblastoma cases, improving patients survival (Handgretinger et al., 1995; Cheung et al., 1998; Navid et al., 2014). However, the treatment with anti-GD2 antibodies have been related with peripheral nerves fibers toxicity resulting in acute pain during the treatment (Roth et al., 2014). Phase I trial using humanized Anti-GD2 is ongoing in children and adolescents with neuroblastoma, osteosarcoma, ewing sarcoma and melanoma (ClinicalTrials.gov identifier: NCT00743496). Recently, FDA has approved the antibody GD2, dinutuximab[®], for the treatment of pediatric patients with high-risk neuroblastoma, based on findings from a phase III clinical trial conducted by the Children's Oncology Group (Yu et al., 2010).

Another well-characterized melanoma surface antigen is the melanoma-associated chondroitin sulfate proteoglycan or high molecular weight-melanoma-associated antigen (CSPG4/HMW-MAA/NG2). This transmembrane proteoglycan is frequently expressed on normal tissues throughout development and in various types of cancers, including glioma, squamous cell carcinoma, breast carcinoma and melanoma. In addition, CSPG4 is expressed by cancer stem cells in squamous cell carcinoma, glioblastoma, breast carcinoma and melanoma (Major et al., 2013; Beard et al., 2014). In fact, studies have been demonstrated that CSPG4 plays an important role in controlling tumor microenvironment signals, specially through the activation of integrins promoting adhesion, motility and survival of cancer cells (Bluemel et al., 2010). CSPG4 protein is expressed in all melanoma stages, probably due to their multifunctional mechanisms that regulates multiple oncogenic pathways which leads the melanoma progression, enhancing the metastatic properties (Burg et al., 1998). Therefore, the

CSPG4 has been considered as a promising immunotherapeutic target to delaying progression and/or recurrence in melanoma patients (Wang et al., 2011).

2.5 Current Therapy for Metastatic Melanoma

Over 30 years, one of the most used biochemotherapic approaches for treatment of metastatic malignant melanoma consisted in the administration of classical chemotherapeutic agents such as dacarbazine, vinblastine and cisplatin in combination with the immunotherapeutic agents such as interferon-alfa-2b and interleukin-2 (Legha et al., 1998; Rosenberg et al., 1999). However, several studies demonstrated that only a small part, below 20%, of advanced metastatic melanoma patients treated with these agents, separately or in combination, had a relevant impact on five-year survival rates or clinical regression (Maio et al., 2015). In addition, serious side effects have been associated with conventional chemotherapeutic agents specially due to high toxicity to normal cells, low bioavailability, non-specific distribution and multidrug resistance (Gao et al., 2014).

Many efforts have been made, over the past decade, to overcome these drawbacks, improving the efficacy of classical chemotherapeutic agents and introducing single targeted therapies and immunotherapies (Amann et al., 2016; Kakavand et al., 2016). These pharmacotherapeutic options in melanoma treatment, as second-generation BRAF and MEK inhibitors and new immunotherapeutic agents, represented a great medical breakthrough, leading to better prognostics to advanced melanoma patients. A significant increase in progression free survival on order of 5-7 months has been observed on patients treated with targeted therapies as vemurafenib and trametinib and a 2-year survival for most patients (79%) treated in combination with the two immunotherapeutic agents, nivolumab and ipilimumab (Weber et al., 2016). Regardless of survival improvement, most patients with advanced melanoma rapidly acquire drug resistance and present severe toxicities. The most relevant

toxicities related with these treatments can be exemplified as immune-mediated diarrhea and colitis; keratoacanthomas; squamous cell carcinoma; respiratory toxicity and hypotension, which leads to a therapies discontinuation of approximately 30% of patients or to multiorgan failure and death (Ma & Armstrong, 2014).

2.6 Resistance Mechanisms of m-CSCs and CMCs

As already discussed in previous sessions, the subpopulation of m-CSCs and CMCs play a key role in development of distant metastasis and their presence are correlated with poor prognostics. The multidrug resistance of m-CSCs to currently chemotherapy agents is until one of the major therapeutic challenge in advanced melanoma treatment and can explain the high incidence of disease relapse, giving rise to new tumors and metastases (Vinogradov & Wei, 2012). In general, CSCs demonstrated an enhanced capacity to develop specific drug resistance mechanisms to chemotherapy, such as the overexpression of different drug efflux transporters (Abdullah & Chow, 2013). Various drug efflux transporters involved in chemoresistance of m-CSCs have been identified, including P-glycoprotein (P-gp), DNMT3B, EPAS1, JARID1B, TERT and ABC multidrug transporters, specifically ABCB5, ABCB1 and ABCG2 glycoproteins (Wouters et al., 2013; Wilson et al., 2014).

Other factors as the presence of antiapoptotic signaling pathways, specific protective microenvironment and hypoxia are responsible for the multiple resistance mechanisms of CSCs in tumor site and in blood flow. The most extensively characterized growth and survival pathway involved in melanoma resistance to apoptosis is the phosphatidylinositol-3-kinase (PI3K) pathway (Paluncic et al., 2016). The activation of PI3K results in phosphorylation of ERK and protein kinase B (AKT) leading to an activation of the mammalian target of rapamycin (mTOR) and GSK3β inhibition, respectively. In turn, the inhibition of GSK3β protein results in an upregulation of oncogenic genes, such as c-MYC and cyclin D1, that leads to a strong

anti-apoptotic effect and cancer progression (Brachmann et al., 2009). Studies demonstrated that inhibition of survival mechanisms as PI3K/m-TOR pathway could overcome melanoma acquired resistance to MAPK inhibitors (Kolev et al., 2014; Vaidhyanathan et al., 2016). In addition, another known CSCs antiapoptotic resistance mechanism in melanoma is the dysregulation of BCL-2 family members. Combination strategies to BCL-2 targeting have been demonstrated to be efficient in eliminating both wild-type and mutant BRAF melanoma cells and m-CSCs (Mukherjee et al., 2015).

Still in this context, one of the major characteristics that contributes for m-CSCs multidrug resistance is the existence of a protective microenvironment with specific properties that helps to maintain the m-CSC in a quiescent state and consequently minimizing the chemotherapy effects (Vinogradov & Wei, 2012). The phenotypic plasticity of melanoma cells explains how the cells respond to microenvironmental signals that downregulates the melanocytic proliferation activity and activates a mesenchymal cell state which conduce to a more metastatic potential (Widmer et al., 2015). The niche-associated vasculature supports, protects and maintain the CSCs and the heterogeneous microenvironment composed by different cell types and cytokines (Vinogradov & Wei, 2012). Considering these characteristics, the combination of antiangiogenic therapies and chemotherapies can reduce the number of CSCs and increase the tolerance to chemotherapy toxicity (Spitler et al., 2015; Haase et al., 2016). On the other hand, besides the preclinical studies and clinical trials demonstrated that antiangiogenic agents have a potential efficacy to suppress tumor growth, several studies have been suggested a limited survival benefit, high relapse rates, acquired drug resistance and toxicity (Pàez-Ribes et al., 2009; Gacche & Meshram, 2014). These drawbacks are specially related to the fact that the anti-angiogenic agents can target indiscriminately both physiological and pathological angiogenesis resulting in toxicity and limiting efficacy due to compensatory angiogenesis pathways/revascularization (Wang et al., 2016).

Hypoxia has been considered one of the most important triggers to induce phenotype switch of proliferative melanoma cells to cancer mesenchymal cells with more invasive characteristics, capable to survive and proliferate in low oxygen ratio conditions. A well-known protein that mediates the hypoxic response is the HIF1alpha, more expressed in aggressive melanoma subtypes (Marconi et al., 2015; Rhee et al., 2016). In response to the hypoxia, this protein regulates the expression of transcriptional genes that codify proangiogenic factors involved in angiogenesis induction and apoptosis regulation, sustaining the tumor progression due to physiological adaptation to a low oxygen tension (Jour et al., 2016).

Other important reported consequences after treatment with angiogenesis inhibitors described in clinical assessments is the development of more invasive-metastatic phenotypes (Haase et al., 2016; Jayson et al., 2016). *In vivo* studies demonstrated the approved antiangiogenic agents, sunitinib and sorafenib, can facilitate metastatic dissemination of syngeneic melanoma in mice (Ebos et al., 2009; Pàez-Ribes et al., 2009). The researchers suggested that the typical plasticity phenotype of CSCs and the capacity to survive to hypoxia conditions makes the cells resistant to angiogenesis inhibitors, which also can explain the aggressive recurrence of tumors and adaptive resistance after treatment (Gacche & Meshram, 2014).

To overcome these consequences, studies suggest that the combination therapies associated to the nanotechnology could reduce the stem cell-associated drug resistance and enhance the chemotherapeutic efficacy (Mukherjee & Ranjan, 2016).

2.7 Nanotechnology approach to m-CSCs and CMCs targeting

In general, nanotechnology is a multidisciplinary field and can be defined as the engineering and manufacturing of materials at the atomic and molecular scales with the aim to produce materials with specific and unique characteristics (Maynard, 2006). In biomedical

field, specially in oncology, the application of nanotechnology in drug delivery systems has been extensively explored through the development of nanoscale-sized structures for local drug delivery (Xie et al., 2015; Piktel et al., 2016). Among the different types of nanoscale drug delivery systems, the most studied for anticancer applications are the lipid-based or polymer-based nanoparticles (Prabhu et al., 2015; Arranja et al., 2017).

The nanotechnology has been considered one of the most important strategies to overcome the hazards related to the current cancer therapies, such as toxicity, limited efficacy and/or drug resistance. In this way, nanotechnology approach aim to improve the efficacy of existing cancer therapies, promote the site specificity on tumor cells and minimizing the several adverse effects arising from off-target toxicities. Besides anti-cancer drug delivery applications, nanocarriers have been extensively utilized to incorporate imaging agents in multi-functional nanoparticles and improve their biodistribution to cancer sites allowing the monitoring of disease progression in real-time (Daga et al., 2016; Parvanian et al., 2016). Furthermore, the integration, in a single formulation, of therapeutic drug delivery and diagnostic agents, characterizing a theranostic nanomedicine, has been considered a promising strategy to personalize the cancer treatment and to avoid the metastasis through early diagnosis and continuously monitoring of therapeutic response (Sharma et al., 2016; Shi et al., 2016).

In a review of Brys and collegues (2016), they emphasize how the nanotechnology-based strategies provides an opportunity to vanquish drug resistance and toxicity associated with current advanced melanoma therapies and improving pharmacokinetics, targeting, or other features of anti-cancer pharmaceuticals. It is already well established that the most efficient strategy to prevent the multidrug resistance in advanced melanoma patients is the combination therapy. The combination of different pharmacotherapies for metastatic melanoma as kinase inhibitors, immunomodulators and conventional chemotherapeutic agents as paclitaxel (PTX), could reach a greater number of potential targets involved in melanoma development and

consequently result in a higher overall response and progression free survival (Bombelli et al., 2014; Brys et al., 2016).

Several studies have been demonstrated that the vehiculation of antiangiogenic agents in nanoparticles can surpass the drug resistance, toxicity and low efficacy relative to the pure drug (Guan et al., 2014a; Guan et al., 2014b; Mukherjee et al., 2015; Haase et al., 2016). It is already well established that the tumor vascularity is critical to regulate tumor microenvironment functions and consequently ensure CSCs survival. A strong correlation was observed between enhanced tumor growth and metastasis in human malignant melanoma and vascular endothelial growth factor (VEGF) overexpression (Spitler et al., 2015). Strategies to indirectly eradicate CSCs by encapsulation of cytotoxic and antiangiogenic agents in nanoparticles, including VEGF antibody (bevacizumab), have been reported (Guan et al., 2014a; Guan et al., 2014b). The antibodies encapsulation into nanoparticulated delivery systems can decrease the dosage, toxicity and treatment cost, besides enhanced efficacy.

Other promising anti-cancer molecules candidates to nanotechnology applications are efflux pump and/or antiapoptotic inhibitors. Drug delivery systems encapsulating these inhibitors have been a promising approach to increase the bioavailability and consequently the therapeutic efficacy of wide range of anti-cancer drugs, specially their target to CSCs (Chen et al., 2014; Wu et al., 2017). Related to antiapoptotic effect, the nanotechnology can be applicated to improve the inhibition of PI3K/AKT pathway by using iron and zinc oxide nanoparticles that demonstrated to induce cytotoxicity and apoptotic death in hepatocytes and macrophages (Sarkar & Sil, 2014). In a recent research, the co-encapsulation of two drug resistance inhibitors, celecoxib to down-regulate P-gp efflux pump and buthionine sulfoximine that inhibit glutathione synthesis, into polymer/inorganic hybrid nanoparticles demonstrated to be promising strategy to reverse drug resistance in tumor treatments. In this study, was observed a significant improve in tumor cell inhibition after resistant cancer cells were treated by

doxorubicin-loaded nanoparticles, indicate that the dual-inhibitor co-delivery system can effectively reverse drug resistance (Wu et al., 2017).

Nanotechnology applications for detection and treatment of the small population of circulating cancer cells, including melanoma cells, continuous to be an enormous challenge. Less than 1 in 10000 circulating tumor cells can survive to blood system, however merely one cell is enough to metastasize other tissues, decreasing the patient's overall survival. The rarity of these cells in circulation make their early blood detection a great weapon to improve the patient's prognostics, assessing tumor progression or even avoid metastasis and cure cancers (Wang, 2016). Examples of recent developments in nanotechnology to detect and/or intercept CMCs in blood flow for diagnosis purposes include: Raman scattering (SERS) nanoparticles (Wu et al., 2016); MCR1 antibody immobilized in amino-functionalized silica nanoparticles (Seenivasan et al., 2015); Cross-linked iron oxide nanoparticles conjugated with melanocyte markers, such as MART-1 (Gee et al., 2016) and also a poly(lactic-co-glycolic acid) (PLGA)-nanofiber nanovelcro chip conjugated with melanoma-specific antibody as anti-CD146 (Hou et al., 2013).

In view of the discussion above, the use of nanotechnology can be a useful tool to combat the chemotherapy resistance mechanisms developed by m-CSCs/CMC and the inherent disadvantages of currently available treatments options, improving the effectiveness of anti-cancer drugs (Banerjee et al., 2011; Burke et al., 2012). The hypothesis that supports the nanomedicine therapeutic approach to specifically targeted m-CSCs/CMC is based on the harness potential of nanotechnology to create modifiable drug-delivery platforms, capable to carry high payloads of anti-cancer drugs and increase their uptake by specific cells. Among the wide range of nanomaterials used for this aim, the polymeric nanoparticles are suitable structures for drug transport (Garcia-Mazas et al., 2016; Silva et al., 2016).

2.7.1 Polymeric nanoparticles in melanoma treatment

Biocompatible and resorbable polymers were first introduced in biomedical field as an alternative to metal surgical devices and implants (Ramakrishna et al., 2001). Since then, several types of polymeric nanomedicines have been largely studied for anti-cancer therapy and diagnosis, including polymer–lipid hybrid systems (Rao & Prestidge, 2016), micelle-polymeric nanoparticles (Li et al., 2015) and polymeric nanoparticles (Li et al., 2016; Antônio et al., 2017). Nanoparticles formulated with biocompatible and biodegradable polymers are one of the most investigated vectors for cancer therapy, mainly due to these potentially modifiable physicochemical properties and large variety of anti-cancer compounds that can be delivered into tumors in a more specific and homogeneous way (Prabhu et al., 2015; Li et al., 2016; Vauthier & Ponchel, 2016).

Generally, polymers used to develop nanoparticles are based on polyesters, such as poly (lactic acid) (PLA), poly (glycolic acid) (PGA), polycaprolactone (PCL) and their copolymers poly (alkyl cyanoacrylate) polycarbonates, poly (aminoacids) and polyphosphoesters, and also naturally occurring biodegradable polymers as chitosan and hyaluronic acid-based polymers (Jin et al., 2012; Abruzzo et al., 2016; Vauthier & Ponchel, 2016).

Among the several advantages of polymeric nanoparticles in cancer therapy and diagnosis the most representatives are: improve solubility and stability of anti-cancer drugs, delivery large doses of chemotherapy agents, promote the accumulation of drugs in tumor site by passive and active targeting, prevents drug leakage and reduce nonspecific biodistribution, reduce toxicity and systemic side effects related to off-target distribution, reduce cancer cell drug resistance, control the drug pharmacokinetics by sustained release, increasing drug circulation time in blood, reduce dose regimens, combinate therapy and imaging agents in a single carrier, targeting multiple pathways in cancer, protect the active principals from

enzymatic degradation and rapid clearance *in vivo* (Couvreur & Vauthier, 2006; Prabhu et al., 2015).

In the scope of nanoparticles targeting, passive targeting and active targeting are the two main strategies currently used (Liu et al., 2014; Kamaly et al., 2016), as represented in Figure 2. Each approach takes in account nanoparticle's size, shape and surface charge, tumor microenvironment and cells characteristics (Bazak et al., 2014). Among these nanoparticles, different types have been studied for diagnostic and treatment of advanced melanoma including conventional surface nonmodified; stealth; targeted; pH sensitive and core-shell nanoparticles (Table 2).

However, experimental studies of nanoparticles designed to specifically target the m-CSCs and CMCs are still sparse and incipient. The recent literature involving polymer-based nanoparticles for melanoma diagnosis and treatment will be reviewed with focus on passive and active targeting to melanoma cells. We also analyzed the fundamentals and challenges behind the development of polymeric nanoparticles to target the m-CSCs/CMC, according with new insights about their biological mechanisms and biomarkers.

2.8 Passive tumor-targeting of drug loaded nanoparticles

In the early stages of tumor progression, it is demonstrated that solid tumors cannot grow further than 2 mm in diameters without angiogenesis (Folkman, 1971). To support the tumor growth, a high oxygen and nutrients are demanded and these factors stimulate the uncontrolled angiogenesis. That phenomenon leads to leaky and intricate blood vessels, that are constantly under inflammatory state and it is associated with metastasis, tumor recurrence and poor survival rates (Banerjee et al., 2011; Bertrand et al., 2013). First described by Matsumura and colleges (1987), enhanced permeability and retention (EPR) phenomenon is based on these anatomical and pathophysiological properties of tumor microenvironment which can promote an accumulation of large molecules, such as proteins, through leaky vasculature and poor

lymphatic drainage in the tumor (Bazak et al., 2014). Passive targeting of drugs is based on non-specific accumulation of drug-loaded nanoparticles in the tumor site, as a consequence of EPR effect (Danhier et al., 2010).

Structurally simple polymeric nanoparticles based on polyesters, as PCL and PLA, or cellulose polymers, such as carboxymethylcellulose, have been recently developed to improve the passive drug accumulation by EPR effect in melanoma tumor niche. Nanoparticles consisted of PEGylated carboxymethylcellulose conjugate with docetaxel (DTX) improved the specificity of delivery increasing 203-fold the tumor accumulation compared to the FDA approved Abraxane® in B16F10 melanoma models (Ernsting et al., 2012). Lipid-core nanocapsules, composed of PCL shell and caprylic triglyceride oil core, encapsulating acetyleugenol (AcE-LNC), were administered orally in B16F10 mice melanoma model. The treatment with empty LNC induced a higher reduction in the tumor volume when compared to the AcE-LNC and free AcE at the same dose. The authors explained these interesting results by the possible interactions between AcE and PCL altering the crystallinity of the polymer and the LNC supramolecular structure, decreasing the anti-tumor activity of AcE-LNC. These results imply the relevance of nanocapsule supramolecular structure to improve the passive targeting and cancer cells endocytosis, increasing the anti-melanoma therapeutic effect (Drewes et al., 2016). In another study, PLA nanoparticles containing ursolic acid (UA) were able to maintain the drug anti-melanoma activity in B16F10 cells, reducing the cell viability in 70%, and decrease the drug toxicity effects over normal cells (Antônio et al., 2017).

Another example of structurally simple and biocompatible polymeric nanocarriers are micellar nanoparticles, nanoscopic core/shell structures formed by amphiphilic block copolymers that can carrier both hydrophobic and hydrophilic drugs (Croy & Kwon, 2006). Micellar nanoparticles were tested in B16 melanoma tumor models to enhanced drug accumulation by EPR effect. Self-crosslinkable and intracellularly decrosslinkable micellar

nanoparticles containing doxorubicin (DOX-SCID-Ms) showed low systemic toxicity and ability to suppress tumor growth and prolong survival in malignant B16 melanoma-bearing C57BL/6 mice, in a dose-dependent manner when compared to free DOX·HCl (Zou et al., 2016). On the other hand, polymeric hybrid micelles (PHMs) and their potential to co-deliver small anti-cancer molecules and nucleic acid has recently been reported. PHMs with different surface charges, varying from neutral to cationic, containing micro-RNA-34a (miR-34a), a well-defined tumor suppressor, and Hedgehog (Hh) pathway inhibitor vismodegib (VIS), were evaluated as target therapeutic agent for CSCs elimination. This study observed that neutral PHMs compared to cationic ones have the capability to overcome systemic biological barriers and improve the stability in blood circulation. Besides, the co-encapsulation of miR-34a and VIS into neutral PHMs showed a synergistic anti-cancer efficacy in *in vivo* B16F10-CD44$^+$ melanoma model, presenting a higher tumor inhibition rate (80%) compared to PHM containing VIS (51.5%) or miR-34a (65%). These cells displayed CSC characteristics and tumorigenic ability compared to B16F10-CD44$^-$ cells (Shi et al., 2014; Li et al., 2015).

Among the molecules that act as positive regulators of angiogenesis, the VEGF and TGF-β are the most investigated targets to anti-cancer therapy, in general (Otrock et al., 2007; Luo et al., 2016). Pittella and collegues (2012) demonstrated through the administration of VEGF siRNA in calcium phosphate/charge-conversional polymer hybrid nanoparticles *in vivo* that silencing of VEGF gene expression could importantly inhibit tumor growth up to 68% in subcutaneous pancreatic tumor models. In an advanced *in vivo* melanoma model, Xu and collegues (2014) demonstrated that a nanoparticle-delivered TGF-β can augment the efficacy of a vaccine based in lipid nanoparticles functionalized with mannose loaded with tumor antigens and inhibited tumor growth by 52% compared with vaccine treatment alone.

The use of PI3K inhibitors as antiangiogenic agents is has also been explored as a promising strategy to induce cancer cell apoptosis and inhibit cell proliferation. Harfouche and

collegues (2009) reported that PLGA nanoparticles containing a selective PI3K inhibitor can inhibit both melanoma and breast cancer cells induced angiogenesis in zebrafish tumor xenograft model. These approaches provide promising platforms for anti-angiogenesis therapy and indirectly eradicate m-CSCs.

2.8.1 Stimuli responsive nanoparticles for melanoma targeting

A promising targeting strategy for theranostic approach to melanoma is the development of nanoparticles that can be activated by different external stimuli, such as magnetism, photo-irradiation and temperature, or internal stimuli from the tumor microenvironment, such as extracellular and endosomal pH (Navarro et al., 2013; Cyphert et al., 2017). The fast activity, poor lymphatic drainage and their inefficient blood irrigation, tumor growth is carried out through hypoxia, anaerobic metabolism and acidosis conditions (Alimoradi et al., 2016). Therefore, tumor microenvironment can be significantly acid, with pH values ranged from 6.0 to 7.0 compared with normal pH tissue of 7.4 (Danhier et al., 2010). Throw the spotlight of tumor pH, nanoparticles with pH-sensitive biomaterials are currently formulated for drug delivery therapy. Those stimuli-responsive nanoparticles after passive accumulation at tumor site by EPR effect can release the drug near or *in-situ* to the target by either the degradation of the nanoparticle itself or degradation of nanoparticle's shell. The drug can be loaded either by covalent bonds to the bio-sensitive material or encapsulated into the nanoparticle's core (Ding, et al., 2013).

The development of pH-sensitive polymeric nanoparticles has been intensively studied in recent years, specially to improve DOX intracellular and nuclei delivery. An ideal nano-delivery system for DOX require a dual pH-sensitivity nanoparticle, firstly to overcome the extracellular barrier of pH gradients in tumor microenvironment and secondly to overcome the increased acidity in intracellular compartments, such as endosomes (pH~5.0) and subsequently

release DOX from nanocarriers (Xiong et al., 2010). The design of new optimized pH-sensitive drug delivery system for DOX can be a promising strategy to surpass the m-CSCs multidrug resistance mechanisms since the major chemotherapy obstacle is the inefficient and unspecific cellular uptake. Talelli and collegues (2010) developed a DOX-loaded core-crosslinked polymeric micelles, composed by thermosensitive block copolymer covalently bounded to DOX. In the *in vitro* cytotoxicity assay in melanoma cells the DOX micelles were less effective than free DOX, probably due to slower uptake of the polymeric micelles. However, in mice bearing B16F10 melanoma model this polymeric nanocarrier showed a significant decrease in the tumor growth rate than free DOX. These results indicate a better tumor accumulation, through the EPR effect, of polymeric micelles instead free drug. In the same way, Du and collegues (2011) developed a dual pH-sensitive polymeric nanoparticle and reported an enhanced anti-cancer efficiency and intracellular delivery in *in vitro* model of SK-3rd drug-resistant CSCs. These pH-sensitive nanoparticles demonstrated a higher internalization rate and cytoplasmic distribution at pH 6.8 than at pH 7.4 and a higher release rate at pH 5 (75%) than at pH 6.8 (25.5%). In most recent study, a pH-responsive polymeric nanoparticle based-amphiphilic copolymer of low molecular weight heparin conjugated with doxorubicin (LH-DOX) significantly increased tumor growth inhibition (1.5-fold) compared to free DOX-treated group in mice bearing a B16F10 tumors (Mei et al., 2016).

Another type of stimuli responsive multifunctional nanoparticles for theranostic of malignant melanoma are based on photothermal therapy (PTT) and photodynamic therapy (PDT). These methods to intercept and kill skin cancer cells are based on nanoparticle light-heat conversion ability or singlet oxygen generation using the near-infrared (NIR) as the light source (Lv et al., 2015). As demonstrated by Navarro and collegues (2013), gold nanoparticles functionalized with luminescent block copolymers, labeled with dibromobenzene based chromophore, are efficient nanocarries for fluorescent imaging and PDT. These nanoparticles

increased the local concentration of photosensitizer molecules, improving photoinduced cell death in B16F10 melanoma cells. In another study, PTT using PEGylated gold nanorods and NIR showed a significant reduction in tumor volume of approximately 80% compared to the control (saline + NIR light) and increase animal survival in a mouse melanoma model when compared to control groups (Popp et al., 2014). Another theranostic nanoparticle, made by surface attachment of a new indocyanine green dye (IR820) to magnetic iron oxide nanoparticles coated with chitosan, showing an excellent magnetic resonance imaging (MRI) capability when compared to IR820 and functioned as a PDT against A375 melanoma cells with the increase of nanoparticles concentration (16µg/mL) (Hou et al., 2016). The PDT was also recently employed by Ogawara and collegues (2016). In this research, polymeric nanoparticles composed by poly (ethylene glycol) (PEG) and PLA block copolymer, encapsulating hydrophobic porphyrin derivative, showed a significant *in vitro* phototoxicity in B16BL6 melanoma cells.

2.8.2 Architectural properties of nanoparticles in passive targeting

In order to take benefit of tumor microenvironment and the EPR effect, certain characteristics of nanoparticles should be evaluated, specifically the size, surface charge, shape and stealth. As explained by Matsumura and collegues (1987), small molecules or particles are not influenced by EPR effect. Among their results, the authors described that small molecules under 30 kDa do not exhibit EPR effect (Maeda, 2012; Upponi et al., 2014). Therefore, macromolecules above 40 kDa or 10-200 nm in size tend to accumulated more effectively in the tumor site rather than small molecules of 3 to 12 kDa or 2 to 3 nm in size (Upponi et al., 2014; Zhong et al., 2014).

Nevertheless, recently researches also emphasizes that nanoparticles ranged between 10 to 40 nm present a better pharmacokinetic and immunological profile when compared to larger

nanoparticles, specially because they are larger enough to prevent quickly renal excretion and sufficiently small to allow the EPR effect and penetrate through the dense cellular extracellular matrix (Kunjachan et al., 2014; Hou et al., 2016).

The EPR-mediate passive effect of a ~ 10 nm prototypic polymeric nanocarrier based on poly(N-(2-hydroxypropyl) methacrylamide) (p-HPMA) were evaluated in highly and poorly leaky tumor models and also compared with Arg-Gly-Asp (RGD) and (Asn-Gly-Arg) NGR-mediated active targeting. Study findings lead to conclude that for the tested ~ 10 nm prototypic nanocarriers the passive targeting was significantly more effective than active tumor targeting utilizing integrin-ligand peptides in both mice bearing tumor models (Kunjachan et al., 2014).

Regarding to surface charge of nanoparticles to anti-cancer drug delivery, neutral nanocarriers could exhibit a better tumor accumulation and consequently a favorable *in vivo* behavior (Gabizon & Papahadjopoulos, 1992; Ogawara et al., 2016). Considering the factors described above, the modulation of nanoparticle's geometry can also enhance their tumor accumulation by passive targeting and consequently their applications as drug delivery (Ponchel & Cauchois, 2016). Van De Ven and collegues (2012) evaluated the tumor accumulation of silicon nanoparticles with different shapes and sizes, plateloid (600 x 200nm and 1000×400 nm) and cylindroid (1500×200 nm). They observed that larger plateloid nano-sized particles had the higher accumulation efficiency (5% of the dose per gram organ) in tumors in a melanoma mice model, probably because of the large surface area of the nanoparticle that favors their interaction and adherence to tumoral microvasculature.

Another critical parameter in nanoparticle's properties is their capacity to avoid immune elimination. The formation of protein corona or the recognition by the complement complex, lead to a rapid clearance by the kupffer cells in the liver and macrophages in the spleen as a part of the reticuloendothelial (RES) system, limiting the circulation half-life (Bazak et al., 2014; Upponi et al., 2014; Fornaguera et al., 2015). Thus, the longevity of nanoparticles in the blood

circulation is a critical parameter for passive targeting. Grafted polymers on nanoparticle's surface can enhance this property and the most world-wide polymer used to this aim is the PEG. In addition, this polymer exhibit a steric stabilization effect by its protective hydrophilic layer once its exhibit in nanoparticle's surface (Veronese & Pasut, 2005; Romberg et al., 2008).

2.9 Active tumor-targeting of drug loaded nanoparticles

The passive EPR-mediated targeting presents some drawbacks to nanotechnology applications specially related to the large differences between the tumors types and the inter- and intra-individual variability of the pathophysiological states (Kunjachan et al., 2014). On the other hand, the active targeting is based on specific cancer cells molecules exclusively or overexpressed on the cell surface or subcellular compartments, as well as on the other cells of tumor microenvironment, such as the endothelial cells of microvasculature (Bazak et al., 2014). Generally, the targeting moieties most utilized to build site-specific nanoparticles for cancer treatment are the antibodies, antibodies fragments, aptamers, peptides, nucleic acid-based ligands, carbohydrates and small molecules as folic acid (Bertrand et al., 2013; Zhong et al., 2014). The ligand-modified tumor-targeted nanoparticles aims to increase the receptor-mediated endocytosis improving the specificity, retention and accumulation of drug nanocarriers into tumor site, leading to an increase in therapeutic efficacy and a decrease in off-target effects (Arranja et al., 2017).

2.9.1 Active targeting of melanoma cancer cells

Regarding cancer cells active targeting, a largely described and well explored molecule to target hyaluronan receptors (CD44), also overexpressed in m-CSC lineages, is the polysaccharide hyaluronic acid (HA). This polysaccharide, biocompatible and biodegradable, has a wide potential to be utilized to construct multifunctional nanoparticles to cancer diagnosis

and therapy. DOX loaded HA-ceramide based nanoparticles were investigated for *in vitro* cellular uptake ability and antitumor effect into B16F10 tumor-bearing mouse model and demonstrated a receptor-mediated endocytosis and significant tumor growth inhibition (Jin et al., 2012).

Gene-specific therapeutic approach based on polymeric nanoparticle for delivery of siRNA, has been tested in clinical trials for advanced melanoma treatment. A cyclodextrin-based polymeric nanoparticles, displaying target transferrin protein on their surface, were evaluated in phase I clinical trial according to the specificity and capacity to improve the intracellular delivery of siRNA to melanoma tissue. This study observed a significant reduction in the expression of the enzyme ribonucleotide reductase, as well as a dose-dependent accumulation of targeted nanoparticles in melanoma tumors (Davis et al., 2010). Nevertheless, the same research group reported that after one year treatment, severe adverse effects occurred and 21% of the patients discontinued the treatment. These adverse events were attributed to the instabilities in the nanoparticles formulation (Zuckerman & Davis, 2015). Recently, an innovative pH-responsive nanocarrier using a lactoferrin as a matrix for the preparation of nanoparticles containing 5-fluorouracil was evaluated in B16 melanoma cells. The intracellular delivery of fluorouracil demonstrated to be pH dependent and the *in vitro* tests showed a receptor-mediated endocytosis and consequently a higher cytotoxic activity related to free fluorouracil (Kumari & Kondapi, 2016).

Otherwise, the development of active targeting nanoparticulate vaccines for melanoma prophylactic and therapeutic purposes was demonstrated for Silva and collegues (2015). In this study, PLGA polymeric nanoparticles coated with mannose for co-delivery of melanoma-associated antigens (Mart-1 and gp100) and toll-like receptor ligands (immunopotentiators) were developed. These nanoparticles, tested *in vivo* in murine B16F10 melanoma tumors, demonstrated a synergistic effect of immunopotentiators to induce a long lasting Th1 immune

response; and the combination of toll-like receptor ligands with melanoma antigens potentiate the anti-tumor immune response, activating both $CD4^+$ and $CD8^+$ T-cells in the efficacy of the anti-tumor immune response.

The active targeting of CTCs/CMCs by functionalized nanoparticles for diagnosis, treatment and post-therapeutic follow-up, is until an under-exploited strategy and remains a great challenge in nanotechnology. The main challenges involved in CTCs/CMCs targeting by nanomedicines are the rarity of these cells in peripheral blood, their short circulation time and their heterogeneous subpopulation, that can present different phenotypes and could express epithelial (non-CSCs) or/and CSCs biomarkers (Li et al., 2015). Nevertheless, some alternatives can be used to surpass these drawbacks and intercept the CTCs/CMCs in blood flow, such as the design of multifunctional nanoparticles with different ligands to target both epithelial and mesenchymal biomarkers on the CMCs surface. However, until this present study, CellSearch® system is the only platform approved by FDA for CTCs screening/diagnostics. However, as this technique is based on EpCAM expression on the surface of cancer cells, their application to other EpCAM negative cancers, as melanoma, is limited. In view of methodologic limitations for CMCs detection in blood, Seenivasan and collegues (2015) developed an electrochemical immunosensing system composed by silica nanoparticles functionalized with MCR1 antibody. The detection limit of this nanocarrier was 20 cells/mL for melanoma cells in peripheral blood of patients.

The assessment of cancer signaling pathways to perform molecular tumor profile is also very important for appropriate treatment choices and post-therapy follow-up. The micro-nuclear magnetic resonance (µNMR) is one of the methods available for this approach. The CMCs expression of melanocyte biomarkers, such as MART-1, and MAP kinase signaling molecules were assessed by µNMR through an iron oxide nanoparticle conjugation with

specific antibodies. The results of this research appointed a correlation between the CMCs biomarkers expression levels and metastatic burden (Gee et al., 2016).

2.9.2 Active targeting of tumor endothelium

The synthetic peptide Arg–Gly–Asp (RGD) sequence is one of the most common targeting ligand used in nanoparticles for active targeting of tumor endothelium (Park et al., 2004; Singh et al., 2009; Choi et al., 2017). This target moiety can strongly bind to $\alpha_v\beta_3$ and $\alpha_v\beta_5$ integrin receptors, generally overexpressed in different cancer types, such as prostate carcinoma, breast cancer and melanoma, as well as in endothelial cells of tumor vasculature, specially during tumor progression and metastasis (Contois et al., 2015; Guan et al., 2014a; Guan et al., 2014b; Amin et al., 2015; He et al., 2015). The vasculature tumor targeting has been employed as a promising approach to complement the EPR effect-mediated passive targeting, directly facilitating the nanoparticle internalization into tumor cells, after their extravasation through the microvasculature (Bertrand et al., 2013; Amin et al., 2015).

The development of active targeting nanoparticles to overcome chemotherapy resistance of melanoma cancers has been widely investigated in last decade. As previously discussed, the use of nanotechnology can improve the therapeutic efficacy of classic chemotherapeutic agents that have a limited clinical application due to their poor pharmacokinetic properties, high toxicity to normal cells and acquired drug resistance. In a study conducted in B16F10 melanoma cell line, pH sensitive and site-specific nanoparticles composed of RGD-linked copolymer, encapsulating epirubicin, demonstrated a pH sensitive drug controlled release and a selective cellular uptake. This nanoparticle presented a significant increased anti-tumor activity *in vivo* and a lower systemic toxicity compared with free drug (Guan et al., 2014c). Zou and collegues (2016) developed self crosslinkable and intracellularly decrosslinkable biodegradable micellar nanoparticles containing DOX (DOX-SCID-Ms) for passive targeting and active targeting. In active targeting purpose, they compared RGD-decorated DOX-SCID-Ms with pegylated

liposomal doxorubicin (DOX-LPs). The *in vivo* results performed in malignant B16 melanoma model demonstrated a 3-fold higher drug tumor accumulation, low systemic toxicity and a markedly improved survival rate for RGD-decorated DOX-SCID-Ms.

Another example of ligand for tumor vasculature is the anti-VEGF (bevacizumab) that can be conjugated on nanoparticle's surface to promote active targeting. A phase II clinical assessment of nanoparticle albumin-bound paclitaxel (Nab-PTX) combinated with bevacizumab treatment, concluded that this combination therapy significantly improved the clinical efficacy of PTX and increased the progression-free survival rate and the overall survival rate of patients with unresectable metastatic melanoma (Spitler et al., 2015). Most recently, Nab-PTX non-covalently conjugated with bevacizumab significantly improve the biodistribution of paclitaxel into tumor tissue and enhanced tumor regression compared to Nab-PTX in *in vivo* human melanoma xenograft model (A375) (Nevala et al., 2016).

Despite of promising results of targeting tumor microvasculature through receptor-ligand interaction, care should be taken to nonspecific targeting drug delivery, once integrin and VEGF receptors are widespread in normal or inflamed tissues (Sun et al., 2015). Paradoxically, the use of RGD-based peptides can accelerate tumor progression in mouse B16F0 melanoma and in Lewis lung carcinoma tumor grafts by inducing endothelial migration (Reynolds et al., 2009). To overcome this problem, Redko and collegues (2016) recently developed non-RGD cyclic $\alpha_v\beta_3$ peptide conjugated with Camptothecin for targeted drug delivery and reported a specific and strong binding affinity both *in vitro* and *in vivo* in a xenograft human metastatic melanoma model, improving the anti-tumor activity and reducing the off-targeted toxicity.

Besides integrins and VEGF receptors, melanoma-associated chondroitin sulfate proteoglycan (NG2), also strongly expressed in tumor vascular pericytes, have been emerging as a new target for antiangiogenic therapy. The efficacy of nanoparticles for DTX delivery

conjugated with TH10 peptide to target NG2 receptors in tumor vasculature were investigated in mice bearing B16F10-luc-G5 melanoma experimental lung metastasis. The NG2-binding peptide TH10 promoted a specific mediated endocytosis of nanoparticles in tumor pericytes and significantly increased the mice survival, with low toxicity related (Guan et al., 2014a).

2.9.3 Architectural properties of nanoparticles in active targeting

The surface modification of nanoparticles through the conjugation of target ligands, such as peptides and antibodies, could directly affect the *in vivo* performance of these surface modified nanocarriers. The main nanoparticle characteristics that can influence the targeted cancer chemotherapy are the size, shape, surface charge and ligands density (Bertrand et al., 2013).

The architectural properties of nanoparticles can determine their biodistribution, bioavailability, endocytosis pathway and diffusion mobility within the cytoplasm (Chou et al., 2011; Elsabahy & Wooley, 2012). Generally, according to the biological application of nanoparticle, the size could vary from 4 to 250 nm (Zhong et al., 2014). The varied sizes can strongly dictate the pharmacokinetics and pharmacological behavior of the nanoparticles. All biological barriers have an average pore size range that delimits the diffusion of macromolecules and nanocarriers. In the vasculature of the mammalians, for example, particles with size below 5 nm can across the healthy endothelium to extracellular space; in case of tumor vasculature, leakier then normal endothelium, the pore size can be until 200 nm. At a cellular level, the size of endosomes can range from 60 to 120 nm, depending on the pathophysiological conditions, the endocytosis mechanisms and the nanoparticle physicochemical characteristics (Elsabahy & Wooley, 2012). The size influence of copolymeric nanoparticles consisted of natural polysaccharide hyaluronan (target CD44 receptors) and poly(γ-benzyl-L-glutamate) (PBLG) in active targeting were studied in *in vivo* lung cancer models. Nanoparticles with two

different sizes were tested and the 30 nm nanoparticles demonstrated a more efficiently cellular uptake and a preferential active targeting of CD44$^+$ tumors when compared with the 300 nm nanoparticles after intravenous administration (Jeannot et al., 2016).

Another important characteristic that must be considered during nanoparticle design is the shape. Modifications in this parameter can modulate the drug solubilization capacity, immunogenicity, blood circulation time, toxicity and cell uptake (Elsabahy & Wooley, 2012; Bertrand et al., 2013; Zhong et al., 2014). Gratton et al., (2008), studied the shape effect of nanoparticles upper to 100 nm on cellular internalization by using HeLa cells. In this study, the rod-like particles, with high aspect ratios (ARs= 3; diameter = 150 nm, height = 450 nm), presented a higher uptake and consequently a higher *in vitro* cytotoxicity compared to more symmetric nanoparticles, such as spheres (diameter = 200 nm, height = 200 nm), in nonphagocytic cells. In the same way, Huang and collaborators (2010) studied the influence of various shaped mesoporous silica nanoparticles with different aspect ratios (ARs 1, 2, 4) in cell uptake of melanoma cell lineage A375 and concluded that the more elongated particles had higher non-specific uptake and faster internalization rates.

Regarding to CTCs/CMCs targeting, the nanoparticles shape can influence on their blood trafficking and the hemodynamic forces can affect the nanoparticle interactions with CTCs/CMCs and endothelial cells. It has been demonstrated that rod-like nanoparticles could improve the margination onto the endothelium and the circulation time, potentiating the assessment of CTCs/CMCs into blood flow. These results can be explained probably due to larger surface areas of elongated nanoparticles which facilitates particle-cell and particle-vessel wall collisions and interactions. It is hypothesized that ligands coupled to the oblong nanoparticles can interact more efficiently with cell surface receptors, enhancing the number of specific bindings when compared with ligands attached to spherical particles, mainly due to the

different surface areas in x and y axes (Albanese et al., 2012; Toy et al., 2014; Ponchel & Cauchois, 2016).

The number of ligands attached to the nanoparticle surface over a specific shape can directly affect their affinity and avidity by the bind target receptors at cell surface, as well as the membrane wrapping around the nanoparticle. The strength of ligand-coated nanoparticles and target cells interactions is analyzed as the avidity of the entire nanocarrier (Albanese et al., 2012). In general, an increase in ligands density on the surface of nanoparticles can lead to an increase in the target avidity and cellular internalization, nevertheless this correlation is not always linear and could have negative effects on cells interactions (Bertrand et al., 2014). Related to the nanoparticles surface charge, it has been demonstrated that higher positively particles tend to be more internalized when compared to more negatively ones in a non-specific way (Gratton et al., 2008; Albanese et al., 2012). This effect can be explained by the slightly negative charge of cells membrane which can attract by electrostatic force the positively nanoparticles, improving the cellular uptake. Nonetheless, an excess of positively charges is not recommended due to possible toxic and immunological effects (Elsabahy & Wooley, 2012). The surface charge can be optimized by changing nanoparticle materials and ligands density. For more reliable results, the effect of surface charge should be considering the tumor type and treatment arrangements, as well as the nanoparticles interactions with plasma and extracellular matrix. The plasma proteins could bind to nanoparticles surface and form a protein corona that can affect the particle-cell interactions (Monopoli et al., 2011).

In summary, it is essential to counterbalance the multiple physicochemical characteristics of nanoparticles, specially the size, shape, surface charge and ligands density, to improve the efficacy of these nanocarriers *in vivo*, according to the desired targets, for example, CMCs or m-CSCs. Besides, an ideal nanomedicine could also be design to reach distinct types of tumorigenic cells at the same time using specific ligands that could target multiple cell types.

2.10 Conclusions and perspectives

The melanoma treatment with cytotoxic agents is doomed to fail, specially due to the lack of drug specificity and multiple resistance mechanisms of cancer cells. Moreover, an ideal approach to prevent melanoma metastasis progression is the eradication of m-CSCs and CMCs presented in tumor site or in blood circulation. In this way, nanomedicines for specific recognition of these cells are still sparse and demand more attention from the scientific community. For targeting purpose, more accurately researches should be performed to detect and characterize more specific biomarkers present in m-CSCs and CMCs and to elucidate the signaling pathways involved in their maintenance and survival. Several studies point out that the polymeric nanoparticles are ideal platforms for the future tailoring and optimization of their surface physicochemical properties according to the pathophysiological peculiarities of each cancer. It is clear how architectural properties of nanoparticles can influence passive and active targeting of melanoma cells *in vitro* and *in vivo*. This review presented and discussed the current status of m-CSCs and CMCs biomarkers as potential targets for melanoma treatment using nanotechnological approaches. In conclusion, this review highlighted the challenging aspects of metastatic melanoma treatment and could guide future research to design polymeric nanoparticles that aiming to improve the clinical prognosis of this skin cancer.

Acknowledgments

References

Abdullah, L.N. & Chow, E.K.-H., 2013. Mechanisms of chemoresistance in cancer stem cells. *Clinical and translational medicine*, 2(1), pp.1–9. Available at: http://www.ncbi.nlm.nih.gov/pubmed/23369605%5Cnhttp://www.pubmedcentral.nih.gov/articlerender.fcgi?artid=PMC3565873.

Abruzzo, A. et al., 2016. Chitosan nanoparticles for lipophilic anticancer drug delivery: Development, characterization and in vitro studies on HT29 cancer cells. *Colloids and Surfaces B: Biointerfaces*, 145, pp.362–372. Available at: http://dx.doi.org/10.1016/j.colsurfb.2016.05.023.

Adams, D.L. et al., 2015. Cytometric characterization of Circulating Tumor Cells Captured by microfiltration and their correlation to the cellsearch?? CTC test. *Cytometry Part A*, 87(2), pp.137–144.

Ahrens, T. et al., 2001. CD44 is the principal mediator of hyaluronic-acid-induced melanoma cell proliferation. *Journal of Investigative Dermatology*, 116(1), pp.93–101. Available at: http://dx.doi.org/10.1046/j.1523-1747.2001.00236.x.

Albanese, A., Tang, P.S. & Chan, W.C.W., 2012. [Review] The Effect of Nanoparticle Size, Shape, and Surface Chemistry on Biological Systems. *Annual Review of Biomedical Engineering*, 14(1), pp.1–16.

Albertini, M.R. et al., 1997. Phase IB trial of chimeric antidisialoganglioside antibody plus interleukin 2 for melanoma patients . *Clinical Cancer Research*, 3(August), pp.1277–1288.

Alimoradi, Houman; S. Matikonda, Siddharth; B. Gamble, Allan; I. Giles, Gregory; Greish, K., 2016. Hypoxia Responsive Drug Delivery Systems in Tumor Therapy. *Current Pharmaceutical Design*, 22, p.2808–2820(13).

Allegra, A. et al., 2014. The Cancer Stem Cell Hypothesis: A Guide to Potential Molecular Targets. *Cancer investigation*, 7907(July 2013), pp.470–495. Available at: http://www.ncbi.nlm.nih.gov/pubmed/25254602.

Amann, V.C. et al., 2016. Developments in targeted therapy in melanoma. *European Journal of Surgical Oncology*. Available at: http://dx.doi.org/10.1016/j.ejso.2016.10.014.

Amin, M. et al., 2015. Development of a novel cyclic RGD peptide for multiple targeting approaches of liposomes to tumor region. *Journal of Controlled Release*, 220, pp.308–315. Available at: http://dx.doi.org/10.1016/j.jconrel.2015.10.039.

Antônio, E. et al., 2017. Poly(lactic acid) nanoparticles loaded with ursolic acid: Characterization and in vitro evaluation of radical scavenging activity and cytotoxicity. *Materials Science and Engineering: C*, 71, pp.156–166.

Arranja, A.G. et al., 2017. Tumor-targeted nanomedicines for cancer theranostics. *Pharmacological Research*, 115, pp.87–95. Available at: http://dx.doi.org/10.1016/j.phrs.2016.11.014.

Ashworth, T.R., 1869. "A case of cancer in which cells similar to those in the tumours were seen in the blood after death." *Aust Med J*, 14.3, pp.146–149.

Aurisicchio, L. et al., 2015. Superior Immunologic and Therapeutic Efficacy of a Xenogeneic Genetic Cancer Vaccine Targeting Carcinoembryonic Human Antigen. *Human Gene Therapy*, 398(June), pp.386–398.

Banerjee, D., Harfouche, R. & Sengupta, S., 2011. Nanotechnology-mediated targeting of tumor angiogenesis. *Vasc Cell*, 3(1), p.3. Available at: http://www.ncbi.nlm.nih.gov/pubmed/21349160.

Bao, G., Mitragotri, S. & Tong, S., 2013. Multifunctional nanoparticles for drug delivery and molecular imaging. *Annual review of biomedical engineering*, 15(April), pp.253–82. Available at: http://www.ncbi.nlm.nih.gov/pubmed/23642243.

Battula, V.L. et al., 2012. Ganglioside GD2 identifies breast cancer stem cells and promotes tumorigenesis. *The Journal of clinical investigation*, 122(6), pp.2066–78. Available at: http://www.pubmedcentral.nih.gov/articlerender.fcgi?artid=3591166&tool=pmcentrez&rendertype=abstract.

Bazak, R. et al., 2014. Cancer active targeting by nanoparticles: a comprehensive review of literature. *Journal of Cancer Research and Clinical Oncology*, 141(Greish 2007), pp.769–784.

Bazylińska, U. et al., 2014. Polymeric nanocapsules and nanospheres for encapsulation and long sustained release of hydrophobic cyanine-type photosensitizer. *Colloids and Surfaces A: Physicochemical and Engineering Aspects*, 442, pp.42–49.

Beard, R.E. et al., 2014. Multiple chimeric antigen receptors successfully target chondroitin sulfate proteoglycan 4 in several different cancer histologies and cancer stem cells. *Journal for immunotherapy of cancer*, 2(1), p.25. Available at: http://www.pubmedcentral.nih.gov/articlerender.fcgi?artid=4155770&tool=pmcentrez&rendertype=abstract.

Bergman, P.J. et al., 2006. Development of a xenogeneic DNA vaccine program for canine malignant melanoma at the Animal Medical Center. , 24, pp.4582–4585.

Bertrand, N. et al., 2013. Cancer nanotechnology: The impact of passive and active targeting in the era of modern cancer biology. *Advanced drug delivery reviews*. Available at: http://www.ncbi.nlm.nih.gov/pubmed/24270007 [Accessed January 24, 2014].

Bioley, G. et al., 2016. Specific T Cells by MHC Class II Tetramers 1.

Bluemel, C., Hausmann, S. & Fluhr, P., 2010. Epitope distance to the target cell membrane and antigen size determine the potency of T cell-mediated lysis by BiTE antibodies specific for a large melanoma surface antigen. , pp.1197–1209.

Bombelli, F.B. et al., 2014. The scope of nanoparticle therapies for future metastatic melanoma treatment. *The Lancet Oncology*, 15(1), pp.22–32.

Boni, A. et al., Selective BRAF V600E Inhibition Enhances T-Cell Recognition of Melanoma without Affecting Lymphocyte Function. , (9), pp.5213–5219.

Bonnet, D. & Dick, J.E., 1997. Human acute myeloid leukemia is organized as a hierarchy that originates from a primitive hematopoietic cell. *Nature medicine*, 3(7), pp.730–737.

Borovski, T. et al., 2011. Cancer stem cell niche: The place to be. *Cancer Research*, 71(3), pp.634–639.

Brachmann, S.M. et al., 2009. Specific apoptosis induction by the dual PI3K/mTor inhibitor NVP-BEZ235 in HER2 amplified and PIK3CA mutant breast cancer cells. *Proceedings of the National Academy of Sciences of the United States of America*, 106(52), pp.22299–304. Available at: http://www.pubmedcentral.nih.gov/articlerender.fcgi?artid=2799764&tool=pmcentrez&rendertype=abstract.

Briggs, Robert, and T.J.K., 1952. "Transplantation of living nuclei from blastula cells into enucleated frogs' eggs." *Proceedings of the National Academy of Sciences*, 38.5, pp.455–463.

Brooks, M.D., Burness, M.L. & Wicha, M.S., 2015. Therapeutic Implications of Cellular Heterogeneity and Plasticity in Breast Cancer. *Cell Stem Cell*, 17(3), pp.260–271.

Van der Bruggen, P. et al., 1991. A gene encoding an antigen recognized by cytolytic T lymphocytes on a human melanoma. *Science*, 254(5038), p.1643.

Brys, A.K. et al., 2016. Nanotechnology-based strategies for combating toxicity and resistance in melanoma therapy. *Biotechnology Advances*, 34(5), pp.565–577.

Burg, M.A., Grako, K.A. & Stallcup, W.B., 1998. Expression of the NG2 proteoglycan enhances the growth and metastatic properties of melanoma cells. *Journal of Cellular Physiology*, 177(2), pp.299–312.

Burke, A.R. et al., 2012. Molecular Biomarkers & Diagnosis Targeting Cancer Stem Cells with Nanoparticle-Enabled Therapies. *Molecular Biomarkers & Diagnosis*, pp.8–11.

Chen, M. et al., 2014. PLGA-nanoparticle mediated delivery of anti-OX40 monoclonal antibody enhances anti-tumor cytotoxic T cell responses. *Cellular Immunology*, 287(2), pp.91–99. Available at: http://dx.doi.org/10.1016/j.cellimm.2014.01.003.

Chen, Y. et al., 2013. Resveratrol Inhibits Alpha-Melanocyte-Stimulating Hormone Signaling , Viability , and Invasiveness in Melanoma Cells. *Evidence-Based Complementary and AlternativeMedicine*, 2013, pp.1–8.

Chen, Y. et al., 1996. Serological analysis of Melan-A (MART-l), a melanocyte-specific. , 93(June), pp.5915–5919.

Cheung, N.-K. V et al., 1998. 3F8 monoclonal antibody treatment of patients with stage 4 neuroblastoma : a phase II study. *international journal of oncology*, 12, pp.1299–1306.

Choi, B.S. et al., 2006. Phase I trial of combined treatment with ch14 . 18 and R24 monoclonal antibodies and interleukin-2 for patients with melanoma or sarcoma. , pp.761–774.

Choi, J. et al., 2017. Targeting tumors with cyclic RGD-conjugated lipid nanoparticles loaded with an IR780 NIR dye: In vitro and in vivo evaluation. *International Journal of Pharmaceutics*. Available at: http://linkinghub.elsevier.com/retrieve/pii/S0378517317301758.

Chou, L.Y.T., Ming, K. & Chan, W.C.W., 2011. Strategies for the intracellular delivery of nanoparticles. *Chemical Society reviews*, 40(1), pp.233–245.

Cichorek, M. et al., 2013. Skin melanocytes: Biology and development. *Postepy Dermatologii i Alergologii*, 30(1), pp.30–41.

Contois, L.W. et al., 2015. Inhibition of tumor-associated avb3 integrin regulates the angiogenic switch by enhancing expression of IGFBP-4 leading to reduced melanoma growth and angiogenesis in vivo. *Angiogenesis*, 18(1), pp.31–46.

Couvreur, P. & Vauthier, C., 2006. *Expert Review Nanotechnology : Intelligent Design to Treat Complex Disease*,

Covas, D.T. et al., 2008. Multipotent mesenchymal stromal cells obtained from diverse human tissues share functional properties and gene-expression profile with CD146+ perivascular cells and fibroblasts. *Experimental Hematology*, 36(5), pp.642–654.

Croy, S.R. & Kwon, G.S., 2006. Polymeric micelles for drug delivery. *Expert opinion on drug delivery*, 3(1), pp.139–162.

Csermely, P. et al., 2014. Cancer stem cells display extremely large evolvability: alternating plastic and rigid networks as a potential Mechanism: Network models, novel therapeutic target strategies, and the contributions of hypoxia, inflammation and cellular senescence. *Seminars in cancer biology*, pp.1–10. Available at: http://www.ncbi.nlm.nih.gov/pubmed/24412105 [Accessed September 22, 2014].

Cyphert, E. L., Fu, A. S., & von Recum, H.A., 2017. Chemotherapeutic delivery using pH-responsive, affinity-based release. *Experimental Biology and Medicine*, p.1535370217693115.

Daga, M. et al., 2016. Latest News on Nanotechnology for Melanoma Therapy and Diagnosis SM Gr up Latest News on Nanotechnology for SM Journal of Nanotechnology Melanoma Therapy and Diagnosis. *SM Journal of Nanotechnology and Nanomedicine*, 1(May), pp.1–13.

Danhier, F., Feron, O. & Préat, V., 2010. To exploit the tumor microenvironment: Passive and active tumor targeting of nanocarriers for anti-cancer drug delivery. *Journal of Controlled Release*, 148(2), pp.135–146. Available at: http://dx.doi.org/10.1016/j.jconrel.2010.08.027.

Davey, R.J., Westhuizen, A. van der & Bowden, N.A., 2016. Metastatic melanoma treatment:

Combining old and new therapies. *Critical Reviews in Oncology/Hematology*, 98, pp.242–253.

Davis, M.E. et al., 2010. Evidence of RNAi in humans from systemically administered siRNA via targeted nanoparticles. *Nature*, 464(7291), pp.1067–1070. Available at: http://www.pubmedcentral.nih.gov/articlerender.fcgi?artid=2855406&tool=pmcentrez&rendertype=abstract.

Dietrich, A., Tanczos, E. & Vanscheidt, W., 1997. Original Paper High CD44 Surface Expression on Primary Tumours of Malignant Melanoma Correlates with Increased Metastatic Risk and Reduced Survival. , 33(6), pp.926–930.

Ding, H.-M.; Ma, Y.-Q., 2013. Controlling Cellular Uptake of Nanoparticles with pH-Sensitive Polymers. *Scientific Reports*, 3, p.2804.

Doronin, I.I. et al., 2014. Ganglioside GD2 in reception and transduction of cell death signal in tumor cells. *BMC Cancer*, 14, pp.1–17.

Dou, J. et al., 2007. Isolation and identification of cancer stem-like cells from murine melanoma cell lines. *Cell Mol Immunol*, 4(6), pp.467–472.

Drewes, C.C. et al., 2016. Novel therapeutic mechanisms determine the effectiveness of lipid-core nanocapsules on melanoma models. *International Journal of Nanomedicine*, 11, pp.1261–1279.

Du, J.Z. et al., 2011. Tailor-Made dual pH-sensitive polymer-doxorubicin nanoparticles for efficient anticancer drug delivery. *Journal of the American Chemical Society*, 133(44), pp.17560–17563.

Duan, H. et al., 2013. Targeting endothelial CD146 attenuates neuroinflammation by limiting lymphocyte extravasation to the CNS. *Scientific reports*, 3, p.1687. Available at: http://www.nature.com/srep/2013/130418/srep01687/full/srep01687.html.

Ebos, J.M.L. et al., 2009. Accelerated Metastasis after Short-Term Treatment with a Potent Inhibitor of Tumor Angiogenesis. *Cancer Cell*, 15(3), pp.232–239. Available at: http://dx.doi.org/10.1016/j.ccr.2009.01.021.

Ehrlich, P., 1891. Experimentelle untersuchungen über immunität. I. Ueber ricin. *DMW-Deutsche Medizinische Wochenschrift*, 17(32), pp.976–979.

Elsabahy, M. & Wooley, K.L., 2012. Design of polymeric nanoparticles for biomedical delivery applications. *Chemical Society reviews*, 41(7), pp.2545–2561.

Elshal, M. et al., 2005. CD146 (Mel-CAM), an adhesion marker of endothelial cells , is a novel marker of lymphocyte. *Blood*, 106(8), pp.2923–2924.

Eroglu, Z. & Ribas, A., 2016. Combination therapy with BRAF and MEK inhibitors for melanoma: latest evidence and place in therapy. *Therapeutic advances in medical oncology*, 8(1), pp.48–56. Available at: http://www.ncbi.nlm.nih.gov/pubmed/26753005%5Cnhttp://www.pubmedcentral.nih.gov/articlerender.fcgi?artid=PMC4699264.

Fang, D. et al., 2005. A Tumorigenic Subpopulation with Stem Cell Properties in Melanomas A Tumorigenic Subpopulation with Stem Cell Properties in Melanomas. , pp.9328–9337.

Farace, F. et al., 2011. A direct comparison of CellSearch and ISET for circulating tumour-cell detection in patients with metastatic carcinomas. , (August), pp.847–853.

Fargnoli, M.C. et al., 2008. MC1R variants increase risk of melanomas harboring BRAF mutations. *The Journal of investigative dermatology*, 128(10), pp.2485–90. Available at: http://www.ncbi.nlm.nih.gov/pubmed/18368129%5Cnhttp://www.pubmedcentral.nih.gov/articlerender.fcgi?artid=PMC2835495.

Ferrandina, G. et al., 2009. CD133 antigen expression in ovarian cancer. *BMC Cancer*, 9, p.221. Available at: http://www.ncbi.nlm.nih.gov/entrez/query.fcgi?cmd=Retrieve&db=PubMed&dopt=Citation&list_uids=19583859.

Folkman, J., 1971. Tumor Angiogenesis: therapeutic implications. *The New England journal of medicine*, 18(Nov), pp.1182–1186.

Fornaguera, C.; Caldero, G.; Mitjans, M.; Vinardell, M. P.; Solans, C.; Vauthier, C., 2015. Interactions of PLGA nanoparticles with blood components: protein adsorption, coagulation, activation of the complement system and hemolysis studies. *Nanoscale*, 7(14), pp.6045–6058.

Freeman, J.B. et al., 2012. Evaluation of a multi-marker immunomagnetic enrichment assay for the quantification of circulating melanoma cells. *Journal of Translational Medicine*, 10(1), p.192. Available at: Journal of Translational Medicine.

Friedmann-Morvinski, D. & Verma, I.M., 2014. Dedifferentiation and reprogramming: Origins of cancer stem cells. *EMBO Reports*, 15(3), pp.244–253.

Gabizon, A., & Papahadjopoulos, D., 1992. The role of surface charge and hydrophilic groups on liposome clearance in vivo. *Biochimica et Biophysica Acta (BBA)-Biomembranes*, 1103(1), pp.94–100.

Gacche, R.N. & Meshram, R.J., 2014. Angiogenic factors as potential drug target: Efficacy and limitations of anti-angiogenic therapy. *Biochimica et Biophysica Acta - Reviews on Cancer*, 1846(1), pp.161–179. Available at: http://dx.doi.org/10.1016/j.bbcan.2014.05.002.

Gao, Y. et al., 2014. Nanotechnology-based intelligent drug design for cancer metastasis treatment. *Biotechnology Advances*, 32, pp.761–777.

Garcia-Mazas, C., Csaba, N. & Garcia-Fuentes, M., 2016. Biomaterials to suppress cancer stem cells and disrupt their tumoral niche. *International Journal of Pharmaceutics*. Available at: http://linkinghub.elsevier.com/retrieve/pii/S0378517316311449.

Gay, L., Baker, A.-M. & Graham, T.A., 2016. Tumour Cell Heterogeneity. *F1000Research*, 5, p.238. Available at: http://f1000research.com/articles/5-238/v1.

Gee, M.S. et al., 2016. Point of care assessment of melanoma tumor signaling and metastatic burden from µNMR analysis of tumor fine needle aspirates and peripheral blood. *Nanomedicine: Nanotechnology, Biology, and Medicine*, pp.1–8. Available at: http://dx.doi.org/10.1016/j.nano.2016.12.006.

Ghiorzo, P. et al., 2009. CDKN2A and MC1R analysis in amelanotic and pigmented melanoma. *Melanoma Research*, 19(3). Available at: http://journals.lww.com/melanomaresearch/Fulltext/2009/06000/CDKN2A_and_MC1R_analysis_in_amelanotic_and.3.aspx.

Gibney, G.T. et al., 2015. Safety, correlative markers, and clinical results of adjuvant nivolumab in combination with vaccine in resected high-risk metastatic melanoma. *Clinical Cancer Research*, 21(4), pp.712–720.

Gratton, S.E.A. et al., 2008. The effect of particle design on cellular internalization pathways. *Proceedings of the National Academy of Sciences of the United States of America*, 105(33), pp.11613–11618.

Gray, E.S. et al., 2015. Circulating Melanoma Cell Subpopulations: Their Heterogeneity and Differential Responses to Treatment. *Journal of Investigative Dermatology*, 135(8).

Grundy, M., Coussios, C. & Carlisle, R., 2016. Advances in systemic delivery of anti-cancer agents for the treatment of metastatic cancer. *Expert opinion on drug delivery*, 13(7), pp.1–15. Available at: http://www.tandfonline.com/doi/abs/10.1517/17425247.2016.1167036.

Guan, Y.Y. et al., 2014a. Selective eradication of tumor vascular pericytes by peptide-conjugated nanoparticles for antiangiogenic therapy of melanoma lung metastasis. *Biomaterials*, 35(9), pp.3060–3070. Available at: http://dx.doi.org/10.1016/j.biomaterials.2013.12.027.

Guan, J. et al., 2014b. Photodynamic action of methylene blue in osteosarcoma cells in vitro.

Photodiagnosis and photodynamic therapy, 11(1), pp.13–9. Available at: http://www.ncbi.nlm.nih.gov/pubmed/24629696 [Accessed March 25, 2014].

Guan, X. et al., 2014c. Cyclic RGD targeting nanoparticles with pH sensitive polymer–drug conjugates for effective treatment of melanoma. *RSC Adv.*, 4(98), pp.55187–55194. Available at: http://xlink.rsc.org/?DOI=C4RA08537J.

Guezguez, B. et al., 2007. Dual Role of Melanoma Cell Adhesion Molecule (MCAM)/CD146 in Lymphocyte Endothelium Interaction: MCAM/CD146 Promotes Rolling via Microvilli Induction in Lymphocyte and Is an Endothelial Adhesion Receptor. *The Journal of Immunology*, 179, pp.6673–6685.

Guo, R. et al., 2013. Case Report Micropthalmia Transcription Factor (MITF) as a diagnostic marker for metastatic melanomas negative for other melanoma markers. *Int J Clin Exp Pathol*, 6(8), pp.1658–1664.

Haase, O. et al., 2016. High Response Rate to Second-Line Combination Antiangiogenic Chemotherapy in Patients with Metastatic Melanoma. *Journal of Cancer Therapy*, 7(12), pp.908–918. Available at: http://www.scirp.org/journal/PaperDownload.aspx?DOI=10.4236/jct.2016.712088.

Handgretinger, R. et al., 1995. A Phase I Study of Human / Mouse Chimeric Anti-ganglioside GD2 Antibody ch14 . 18 in Patients with Neuroblastoma. *European Journal of Cancer*, 2, pp.261–267.

Harfouche, R. et al., 2009. Nanoparticle-mediated targeting of phosphatidylinositol-3-kinase signaling inhibits angiogenesis. *Angiogenesis*, 12(4), pp.325–338.

Hartman, M.L., Czyz, M. & Mitf, Á.M.Á., 2014. MITF in melanoma : mechanisms behind its expression and activity. *Cell. Mol. Life Sci*, pp.24–27.

Hayes, D.F. & Paoletti, C., 2013. Circulating tumour cells: Insights into tumour heterogeneity. *Journal of Internal Medicine*, 274(2), pp.137–143.

He, X. et al., 2015. RGD peptide-modified multifunctional dendrimer platform for drug encapsulation and targeted inhibition of cancer cells. *Colloids and Surfaces B: Biointerfaces*, 125, pp.82–89. Available at: http://dx.doi.org/10.1016/j.colsurfb.2014.11.004.

Henry, N.L. & Hayes, D.F., 2012. Cancer biomarkers. *Molecular Oncology*, 6(2), pp.140–146. Available at: http://dx.doi.org/10.1016/j.molonc.2012.01.010.

Herreros-Villanueva, M. et al., 2013. SOX2 promotes dedifferentiation and imparts stem cell-like features to pancreatic cancer cells. *Oncogenesis*, 2(8), p.e61. Available at: http://dx.doi.org/10.1038/oncsis.2013.23.

Hou, S. et al., 2013. Polymer Nanofiber-Embedded Microchips for Detection , Isolation , and Molecular Analysis of Single Circulating Melanoma Cells ** Angewandte. *Angewandte Chemie (International ed. in English)*, 52, pp.3379–3383.

Hou, X. et al., 2016. Multifunctional near-infrared dye-magnetic nanoparticles for bioimaging and cancer therapy. *Cancer Letters*, 383(2), p.N.PAG-N.PAG. Available at: http://myaccess.library.utoronto.ca/login?url=http://search.ebscohost.com/login.aspx?direct=true&db=rzh&AN=120534318&site=ehost-live.

Huang, S.K. & Hoon, D.S.B., 2016. Liquid biopsy utility for the surveillance of cutaneous malignant melanoma patients. *Molecular Oncology*, 10(3), pp.450–463. Available at: http://dx.doi.org/10.1016/j.molonc.2015.12.008.

Huang, X. et al., 2010. The effect of the shape of mesoporous silica nanoparticles on cellular uptake and cell function. *Biomaterials*, 31(3), pp.438–448.

Jandl, T. et al., 2013. Melanoma stem cells in experimental melanoma are killed by radioimmunotherapy. *Nuclear Medicine and Biology*, 40(2), pp.177–181. Available at: http://dx.doi.org/10.1016/j.nucmedbio.2012.10.006.

Jayson, G.C. et al., 2016. Antiangiogenic therapy in oncology: current status and future directions. *Lancet (London, England)*, 388(10043), pp.518–529. Available at: http://dx.doi.org/10.1016/S0140-6736(15)01088-0.

Jeannot, V. et al., 2016. Targeting CD44 receptor-positive lung tumors using polysaccharide-based nanocarriers: Influence of nanoparticle size and administration route. *Nanomedicine: Nanotechnology, Biology, and Medicine*, 12(4), pp.921–932.

Jin, Y.J. et al., 2012. Hyaluronic acid derivative-based self-assembled nanoparticles for the treatment of melanoma. *Pharmaceutical Research*, 29(12), pp.3443–3454.

Jopling, C., Boue, S. & Izpisua Belmonte, J.C., 2011. Dedifferentiation, transdifferentiation and reprogramming: three routes to regeneration. *Nature reviews. Molecular cell biology*, 12(2), pp.79–89. Available at: http://www.ncbi.nlm.nih.gov/pubmed/21252997.

Jour, G., Ivan, D. & Aung, P.P., 2016. Angiogenesis in melanoma: an update with a focus on current targeted therapies. *Journal of clinical pathology*, 0, pp.1–12. Available at: http://www.ncbi.nlm.nih.gov/pubmed/26865640.

Kakavand, H. et al., 2016. Targeted therapies and immune checkpoint inhibitors in the treatment of metastatic melanoma patients : a guide and update for pathologists. *pathology*, 48(February), pp.194–202.

Kamaly, N. et al., 2016. Degradable Controlled-Release Polymers and Polymeric Nanoparticles: Mechanisms of Controlling Drug Release. *Chemical Reviews*, 116(4), pp.2602–2663. Available at: http://pubs.acs.org/doi/abs/10.1021/acs.chemrev.5b00346.

Kelly, P.N. et al., 2007. Tumor growth need not be driven by rare cancer stem cells. *Science*, 317(5836), p.337. Available at: http://www.ncbi.nlm.nih.gov/entrez/query.fcgi?cmd=Retrieve&db=PubMed&dopt=Citation&list_uids=17641192.

Kennedy, C. et al., 2001. Melanocortin 1 receptor (MC1R) gene variants are associated with an increased risk for cutaneous melanoma which is largely independent of skin type and hair color. *Journal of Investigative Dermatology*, 117(2), pp.294–300. Available at: http://dx.doi.org/10.1046/j.0022-202x.2001.01421.x.

Kim, J. et al., 2012. Herceptin conjugated PCL-PEG-PCL triblock copolymer for cancer targeting and imaging. *Macromolecular Research*, 20(8), pp.875–882.

King, D.M. et al., 2004. Phase I clinical trial of the immunocytokine EMD 273063 in melanoma patients. *Journal of Clinical Oncology*, 22(22), pp.4463–4473.

Koch, M.B. et al., 2001. Microphthalmia Transcription Factor and Melanoma Cell Adhesion Molecule Expression Distinguish Desmoplastic / Spindle Cell Melanoma From Morphologic Mimics. *The American journal of surgical pathology*, 25(1), pp.58–64.

Kolev, V.N. et al., 2014. PI3K / mTOR Inhibitor VS - 5584 Targets Cancer Stem Cells and Prevents Tumor Regrowth After Chemotherapy in Preclinical Models of Small Cell Lung Cancer. , 12(2), p.33342.

Kowalczyk, A. et al., 2009. The GD2-specific 14G2a monoclonal antibody induces apoptosis and enhances cytotoxicity of chemotherapeutic drugs in IMR-32 human neuroblastoma cells. , 281, pp.171–182.

Kruger, G.M. et al., 2002. Neural Crest Stem Cells Persist in the Adult Gut but Undergo Changes in Self-Renewal , Neuronal Subtype Potential , and Factor Responsiveness. , 35, pp.657–669.

Kumari, S. & Kondapi, A.K., 2016. Lactoferrin nanoparticle mediated targeted delivery of 5-fluorouracil for enhanced therapeutic efficacy. *International Journal of Biological Macromolecules*, 95, pp.232–237. Available at: http://dx.doi.org/10.1016/j.ijbiomac.2016.10.110.

Kunjachan, S. et al., 2014. Passive versus active tumor targeting using RGD- and NGR-modified polymeric nanomedicines. *Nano Letters*, 14(2), pp.972–981.

Landow, S.M., Gjelsvik, A. & Weinstock, M.A., 2016. Mortality burden and prognosis of thin melanomas overall and by subcategory of thickness, SEER registry data, 1992-2013. *Journal of the American Academy of Dermatology*, pp.1–6. Available at: http://www.ncbi.nlm.nih.gov/pubmed/27887797%0Ahttp://linkinghub.elsevier.com/retrieve/pii/S0190962216309100.

Legha, S.S. et al., 1998. Development of a biochemotherapy regimen with concurrent administration of cisplatin, vinblastine, dacarbazine, interferon alfa, and interleukin-2 for patients with metastatic melanoma. *Journal of Clinical Oncology*, 16(5), pp.1752–1759.

Li, H. et al., 2015. Rational Design of Polymeric Hybrid Micelles with Highly Tunable Properties to Co-Deliver MicroRNA-34a and Vismodegib for Melanoma Therapy. *Advanced Functional Materials*, 25(48), pp.7457–7469.

Li, J. et al., 2015. Nanobiotechnology for the Therapeutic Targeting of Cancer Cells in Blood. *Cellular and Molecular Bioengineering*, 8(1), pp.137–150.

Li, L. et al., 2016. Multifunctional "core-shell" nanoparticles-based gene delivery for treatment of aggressive melanoma. *Biomaterials*, 111, pp.124–137. Available at: http://www.ncbi.nlm.nih.gov/pubmed/27728812.

Li, Z. et al., 2010. Arginine-glycine-aspartic acid-conjugated dendrimer-modified quantum dots for targeting and imaging melanoma. *Journal of Nanoscience and Nanotechnology*, 10(8), pp.4859–4867. Available at: http://www.ncbi.nlm.nih.gov/entrez/query.fcgi?cmd=Retrieve&db=PubMed&dopt=Citation&list_uids=21125820.

Lianidou, E.S., Markou, A. & Strati, A., 2015. The Role of CTCs as Tumor Biomarkers. In R. Scatena, ed. *Advances in Cancer Biomarkers: From biochemistry to clinic for a critical revision*. Dordrecht: Springer Netherlands, pp. 341–367. Available at: http://dx.doi.org/10.1007/978-94-017-7215-0_21.

Lienard, D. et al., 2009. Vaccination of Melanoma Patients With Melan-A / Mart-1 Peptide and Klebsiella Outer Membrane Protein P40 as an Adjuvant. , 32(8).

Liu, J. et al., 2014. PH-Sensitive nano-systems for drug delivery in cancer therapy. *Biotechnology Advances*, 32(4), pp.693–710. Available at: http://dx.doi.org/10.1016/j.biotechadv.2013.11.009.

Liu, Y. et al., 2014. Multifunctional pH-sensitive polymeric nanoparticles for theranostics evaluated experimentally in cancer. *Nanoscale*, 6(6), pp.3231–42. Available at: http://www.ncbi.nlm.nih.gov/pubmed/24500240.

Liu, Z. et al., 2011. Negative enrichment by immunomagnetic nanobeads for unbiased characterization of circulating tumor cells from peripheral blood of cancer patients. , pp.1–8.

Lobo, N. a et al., 2007. The biology of cancer stem cells. *Annual review of cell and developmental biology*, 23, pp.675–699. Available at: papers://4a2a0975-c75d-46d6-a805-07ce5ecc7f39/Paper/p569.

Longee, D.C. et al., 1991. Disialoganglioside GD2 in human neuroectodermal tumor cell lines and gliomas. *acta neuropathologica*, 82, pp.45–54.

López, M.N. et al., 2007. Melanocortin 1 receptor is expressed by uveal malignant melanoma and can be considered a new target for diagnosis and immunotherapy. *Investigative Ophthalmology and Visual Science*, 48(3), pp.1219–1227.

Luke, J.J. & Hodi, F.S., 2013. Ipilimumab, vemurafenib, dabrafenib, and trametinib: synergistic competitors in the clinical management of BRAF mutant malignant melanoma. *The oncologist*, 18(6), pp.717–25. Available at: http://apps.webofknowledge.com.ezproxy1.lib.asu.edu/full_record.do?product=WOS&search_mode=AdvancedSearch&qid=1&SID=1E8g9GHnEoxNPVnKNE4&page=2&doc=16.

Luo, W. et al., 2016. Molecular cloning, expression analysis and miRNA prediction of vascular endothelial growth factor A (VEGFAa and VEGFAb) in pond loach Misgurnus anguillicaudatus, an air-breathing fish. *Comparative Biochemistry and Physiology Part - B: Biochemistry and Molecular Biology*, 202, pp.39–47.

Lv, R. et al., 2015. Multifunctional anticancer platform for multimodal imaging and visible light driven photodynamic/photothermal therapy. *Chemistry of Materials*, 27(5), pp.1751–1763.

Ma, C. & Armstrong, A.W., 2014. Severe adverse events from the treatment of advanced melanoma: a systematic review of severe side effects associated with ipilimumab, vemurafenib, interferon alfa-2b, dacarbazine and interleukin-2. *Journal of Dermatological Treatment*, 25(5), pp.401–408. Available at: http://informahealthcare.com/doi/abs/10.3109/09546634.2013.813897.

Maeda, H., 2012. Macromolecular therapeutics in cancer treatment: The EPR effect and beyond. *Journal of Controlled Release*, 164(2), pp.138–144.

Maio, M. et al., 2015. Five-year survival rates for treatment-naive patients with advanced melanoma who received ipilimumab plus dacarbazine in a phase III trial. *Journal of Clinical Oncology*, 33(10), pp.1191–1196.

Major, A.G., Pitty, L.P. & Farah, C.S., 2013. Cancer Stem Cell Markers in Head and Neck Squamous Cell Carcinoma. , 2013.

Mak, A.B. et al., 2014. Post-translational regulation of CD133 by ATase1/ATase2-mediated lysine acetylation. *Journal of Molecular Biology*, 426(11), pp.2175–2182.

Marconi, A. et al., 2015. Hypoxia-Inducible Factor-1α and CD271 inversely correlate with melanoma invasiveness. *Experimental Dermatology*, 24(5), pp.396–398.

Matsumura, Y.; Oda, T.; Maeda, H., 1987. General mechanism of intratumor accumulation of macromolecules: advantage of macromolecular therapeutics. *Cancer & chemotherapy*, 14((3 Pt 2)), pp.821–829.

Maynard, A.D., 2006. Safe handling of nanotechnology. *Nature*, 444(7117), p.267.

De Mazière, A.M. et al., 2002. The Melanocytic Protein Melan-A/MART-1 Has a Subcellular Localization Distinct from Typical Melanosomal Proteins. *Traffic*, 3(April), pp.678–693.

Meacham, C.E. & Morrison, S.J., 2013. Tumour heterogeneity and cancer cell plasticity. *Nature*, 501(7467), pp.328–37. Available at: http://www.ncbi.nlm.nih.gov/pubmed/24048065.

Mei, L. et al., 2016. Polymer–Drug Nanoparticles Combine Doxorubicin Carrier and Heparin Bioactivity Functionalities for Primary and Metastatic Cancer Treatment. *Molecular Pharmaceutics*, pp.1–21. Available at: http://pubs.acs.org/doi/abs/10.1021/acs.molpharmaceut.6b00979.

Meng, Z. et al., 2015. Identification of an HLA-DPB1*0501 Restricted Melan-A/MART-1 Epitope Recognized by CD4+ T Lymphocytes: Prevalence for Immunotherapy in Asian Populations. *J Immunother*, 34(7), pp.525–534.

Miyabayashi, T. et al., 2011. Vaccination with CD133 + melanoma induces specific Th17 and Th1 cell-mediated antitumor reactivity against parental tumor. *Cancer Immunology, Immunotherapy*, 60(11), pp.1597–1608.

Mockey, M. et al., 2007. mRNA-based cancer vaccine: prevention of B16 melanoma progression and metastasis by systemic injection of MART1 mRNA histidylated lipopolyplexes. *Cancer gene therapy*, 14(9), pp.802–814.

Monopoli, M.P. et al., 2011. Physical-Chemical aspects of protein corona: Relevance to in vitro and in vivo biological impacts of nanoparticles. *Journal of the American Chemical Society*, 133(8), pp.2525–2534.

Monzani, E. et al., 2007. Melanoma contains CD133 and ABCG2 positive cells with enhanced tumourigenic potential. *European Journal of Cancer*, 43(5), pp.935–946.

Morath, I., Hartmann, T.N. & Orian-Rousseau, V., 2016. CD44: More than a mere stem cell marker. *International Journal of Biochemistry and Cell Biology*, 81, pp.166–173. Available at: http://dx.doi.org/10.1016/j.biocel.2016.09.009.

Mukherjee, N. et al., 2015. Alternative Treatments For Melanoma: Targeting BCL-2 Family Members to De-Bulk and Kill Cancer Stem Cells. *The Journal of investigative dermatology*, 135(9), pp.2155–61. Available at: http://www.sciencedirect.com/science/article/pii/S0022202X15389971.

Navarro, J.R.G. et al., 2013. Nanocarriers with ultrahigh chromophore loading for fluorescence bio-imaging and photodynamic therapy. *Biomaterials*, 34(33), pp.8344–8351. Available at: http://dx.doi.org/10.1016/j.biomaterials.2013.07.032.

Navid, F. et al., 2014. Phase I Trial of a Novel Anti-GD2 Monoclonal Antibody , Hu14 . 18K322A , Designed to Decrease Toxicity in Children With Refractory or Recurrent Neuroblastoma. *Journal of Clinical Oncology*, 32(14), pp.1445–1452.

Negi, L.M. et al., 2012. Role of CD44 in tumour progression and strategies for targeting. *Journal of Drug Targeting*, 20(7), pp.561–573.

Nevala, W.K. et al., 2016. Antibody-targeted chemotherapy for the treatment of melanoma. *Cancer Research*, 76(13), pp.3954–3964.

Notani, K. et al., 2002. Amelanotic malignant melanomas of the oral mucosa. , (April 1982), pp.195–200.

Ogawara, K.I. et al., 2016. Efficient anti-tumor effect of photodynamic treatment with polymeric nanoparticles composed of polyethylene glycol and polylactic acid block copolymer encapsulating hydrophobic porphyrin derivative. *European Journal of Pharmaceutical Sciences*, 82, pp.154–160. Available at: http://dx.doi.org/10.1016/j.ejps.2015.11.016.

Ordóñez, N.G., 2014. Value of melanocytic-associated immunohistochemical markers in the diagnosis of malignant melanoma: A review and update. *Human Pathology*, 45(2), pp.191–205. Available at: http://dx.doi.org/10.1016/j.humpath.2013.02.007.

Otrock, Z.K. et al., 2007. Understanding the biology of angiogenesis: Review of the most important molecular mechanisms. *Blood Cells, Molecules, and Diseases*, 39(2), pp.212–220.

Ott, P.A. et al., 2013. Inhibition of both BRAF and MEK in BRAF V600E mutant melanoma restores compromised dendritic cell (DC) function while having differential direct effects on DC properties. , pp.811–822.

Pàez-Ribes, M. et al., 2009. Antiangiogenic Therapy Elicits Malignant Progression of Tumors to Increased Local Invasion and Distant Metastasis. *Cancer Cell*, 15(3), pp.220–231.

Paget, S., 1889. Distribution of secondary growths in cancer of the breast. *Lancet, I*, pp.571–573.

Paluncic, J. et al., 2016. Roads to melanoma: Key pathways and emerging players in melanoma progression and oncogenic signaling. *Biochimica et Biophysica Acta - Molecular Cell Research*, 1863(4), pp.770–784. Available at: http://dx.doi.org/10.1016/j.bbamcr.2016.01.025.

Park, J.H. et al., 2004. Self-assembled nanoparticles based on glycol chitosan bearing 5??-cholanic acid for RGD peptide delivery. *Journal of Controlled Release*, 95(3), pp.579–588.

Parvanian, S., Mostafavi, S.M. & Aghashiri, M., 2016. Multifunctional nanoparticle developments in cancer diagnosis and treatment. *Sensing and Bio-Sensing Research*, pp.1–7. Available at: http://dx.doi.org/10.1016/j.sbsr.2016.08.002.

Pasut, G. & Veronese, F.M., 2007. Polymer-drug conjugation, recent achievements and general strategies. *Progress in Polymer Science (Oxford)*, 32(8–9), pp.933–961.

Pietila, M., Ivaska, J. & Mani, S.A., 2016. Whom to blame for metastasis, the epithelial-

mesenchymal transition or the tumor microenvironment? *Cancer Letters*, 380(1), pp.359–368. Available at: http://dx.doi.org/10.1016/j.canlet.2015.12.033.

Piktel, E. et al., 2016. Recent insights in nanotechnology-based drugs and formulations designed for effective anti-cancer therapy. *Journal of nanobiotechnology*, 14(1), p.39. Available at: http://www.ncbi.nlm.nih.gov/pubmed/27229857%5Cnhttp://www.pubmedcentral.nih.gov/articlerender.fcgi?artid=PMC4881065.

Pinc, A. et al., 2012. Targeting CD20 in Melanoma Patients at High Risk of Disease Recurrence. *Molecular Therapy*, 20(5), pp.1056–1062. Available at: http://dx.doi.org/10.1038/mt.2012.27.

Pittella, F. et al., 2012. Pancreatic cancer therapy by systemic administration of VEGF siRNA contained in calcium phosphate/charge-conversional polymer hybrid nanoparticles. *Journal of Controlled Release*, 161(3), pp.868–874. Available at: http://dx.doi.org/10.1016/j.jconrel.2012.05.005.

Ponchel, G. & Cauchois, O., 2016. Shape-Controlled Nanoparticles for Drug Delivery and Targeting Applications. In *Polymer Nanoparticles for Nanomedicines.* Springer International Publishing, pp. 159–184.

Popp, M.K. et al., 2014. Photothermal therapy using gold nanorods and near- infrared light in a murine melanoma model increases survival and decreases tumor volume . *Journal of Nanomaterials*, 80301.

Pore, M. et al., 2016. Cancer Stem Cells, Epithelial to Mesenchymal Markers, and Circulating Tumor Cells in Small Cell Lung Cancer. *Clinical Lung Cancer*, 17(6), pp.535–542. Available at: http://dx.doi.org/10.1016/j.cllc.2016.05.015.

La Porta, C. a M. & Zapperi, S., 2013. Human breast and melanoma cancer stem cells biomarkers. *Cancer Letters*, 338(1), pp.69–73. Available at: http://dx.doi.org/10.1016/j.canlet.2012.03.017.

Prabhu, R.H., Patravale, V.B. & Joshi, M.D., 2015. Polymeric nanoparticles for targeted treatment in oncology: Current insights. *International Journal of Nanomedicine*, 10, pp.1001–1018.

Prieto, V.G. & Shea, C.R., 2011. Immunohistochemistry of Melanocytic Proliferations. *Arch Pathol Lab Med*, 135, pp.853–859.

Pucchio, T. Di et al., 2006. Immunization of Stage IV Melanoma Patients with Melan-A / MART-1 and gp100 Peptides plus IFN-α Results in the Activation of Specific CD8 + T Cells and Monocyte / Dendritic Cell Precursors. *Cancer Research*, 66(9).

Quintana, E. et al., 2008. Efficient tumour formation by single human melanoma cells. *Nature*, 456(7222), pp.593–598. Available at: http://www.ncbi.nlm.nih.gov/entrez/query.fcgi?cmd=Retrieve&db=PubMed&dopt=Citation&list_uids=19052619.

Quintana, E. et al., 2010. Phenotypic heterogeneity among tumorigenic melanoma cells from patients that is reversible and not hierarchically organized. *Cancer Cell*, 18(5), pp.510–523. Available at: http://dx.doi.org/10.1016/j.ccr.2010.10.012.

Ramakrishna, S. et al., 2001. "Biomedical applications of polymer-composite materials: a review." Composites science and technology 61.9 (2001): 1189-1224. *Composites science and technology*, 61, pp.1189–1224.

Rao, S. & Prestidge, C.A., 2016. Polymer-lipid hybrid systems: merging the benefits of polymeric and lipid-based nanocarriers to improve oral drug delivery. *Expert Opinion on Drug Delivery*, 13(5), pp.691–707.

Rapanotti, M.C. et al., 2014. Sequential molecular analysis of circulating MCAM / MUC18 expression : a promising disease biomarker related to clinical outcome in melanoma. *Arch Dermatol Res (2014)*, 306, pp.527–537.

Redko, B. et al., 2016. Toward the development of a novel non-RGD cyclic peptide drug conjugate for treatment of human metastatic melanoma. , 4.

Reed, C.M. et al., 2015. Vaccination with melanoma helper peptides induces antibody responses associated with improved overall survival. *Clinical Cancer Research*, 21(17), pp.3879–3887.

Reynolds, A.R. et al., 2009. Stimulation of tumor growth and angiogenesis by low concentrations of RGD-mimetic integrin inhibitors. *Nature medicine*, 15(4), pp.392–400.

Rhee, Y.-H. et al., 2016. Low-level laser therapy promoted aggressive proliferation and angiogenesis through decreasing of transforming growth factor-β1 and increasing of Akt/hypoxia inducible factor-1α in anaplastic thyroid cancer. *Photomed Laser Surg*, 34(6), pp.229–35. Available at: http://online.liebertpub.com/doi/10.1089/pho.2015.3968.

Robert, C. et al., 2011. Ipilimumab plus Dacarbazine for Previously Untreated Metastatic Melanoma. *The new england journal o f medicine original*, 26, pp.2517–2526.

Roeder, Claudia; Schuler-Thurner, Beatrice; Berchtold, Susanne; Vieth, Gisela; von den Driesch, Peter; Schuler, Gerold; Luftl, M., 2005. MAGE-A3 is a frequent tumor antigen of metastasized melanoma. *Arch Dermatol Res*, 296, pp.314–319.

Romberg, B.; Hennink, W. E.; Storm, G., S., 2008. Coatings for Long-Circulating Nanoparticles. *Pharmaceutical Research*, 25(1), pp.55–71.

Rosenberg, B.S.A. et al., 1999. Prospective Randomized Trial of the Treatment of Patients With Metastatic Melanoma Using Chemotherapy With Cisplatin, Dacarbazine, and Tamoxifen Alone or in Combination With Interleukin-2 and Interferon Alfa-2b. *Journal of Clinical Oncology*, 17(3), pp.968–975.

Ross, A.A. et al., 1993. Detection and viability of tumor cells in peripheral blood stem cell collections from breast cancer patients using immunocytochemical and clonogenic assay techniques. *Blood*, 82(9), pp.2605–10. Available at: http://www.ncbi.nlm.nih.gov/pubmed/8219214.

Roth, M. et al., 2014. Ganglioside GD2 as a Therapeutic Target for Antibody-Mediated Therapy in Patients With Osteosarcoma. *cancer*, pp.548–554.

Russell, K.C. et al., 2013. Cell-surface expression of neuron-glial antigen 2 (NG2) and melanoma cell adhesion molecule (CD146) in heterogeneous cultures of marrow-derived mesenchymal stem cells. *Tissue engineering. Part A*, 19(19–20), pp.2253–66. Available at: http://www.pubmedcentral.nih.gov/articlerender.fcgi?artid=3761443&tool=pmcentrez&rendertype=abstract.

Saltari, A. et al., 2016. CD271 downregulation promotes melanoma progression and invasion in 3- dimensional models and in zebrafish. *The Journal of Investigative Dermatology*, 136(10), pp.2049–2058. Available at: http://dx.doi.org/10.1016/j.jid.2016.05.116.

Sang, M. et al., 2011. MAGE-A family : Attractive targets for cancer immunotherapy. *Vaccine*, 29(47), pp.8496–8500. Available at: http://dx.doi.org/10.1016/j.vaccine.2011.09.014.

Sarkar, A. & Sil, P.C., 2014. Iron oxide nanoparticles mediated cytotoxicity via PI3K/AKT pathway: Role of quercetin. *Food and Chemical Toxicology*, 71, pp.106–115. Available at: http://dx.doi.org/10.1016/j.fct.2014.06.003.

Schatton, T. et al., 2008. Identification of cells initiating human melanomas. *Nature*, 451(7176), pp.345–349. Available at: http://www.ncbi.nlm.nih.gov/pubmed/18202660.

Schlaak, M. et al., 2012. Regression of metastatic melanoma by targeting cancer stem cells ABSTRACT : *Oncotarget*, 3(1), pp.22–30.

Schmidt, P. et al., 2011. Eradication of melanomas by targeted elimination of a minor subset of tumor cells.

Schrage, A. et al., 2008. Murine CD146 is widely expressed on endothelial cells and is

recognized by the monoclonal antibody ME-9F1. *Histochem Cell Biol*, 129, pp.441–451.

Schwarzenbach, H., Hoon, D.S.. B. & Pantel, K., 2011. Cell-free nucleic acids as biomarkers in cancer patients. *Nature reviews. Cancer*, 11(6), pp.426–37. Available at: https://login.medscape.com/login/sso/getlogin?urlCache=aHR0cDovL3d3dy5tZWRzY2 FwZS5jb20vdmlld2FydGljbGUvNzQ0MTc4&ac=401%5Cnhttp://www.ncbi.nlm.nih.go v/pubmed/21562580.

Seenivasan, R. et al., 2015. An electrochemical immunosensing method for detecting melanoma cells. *Biosensors and Bioelectronic*, pp.1–28.

Senses, K.M. et al., 2017. Phenotype-based variation as a biomarker of sensitivity to molecularly targeted therapy in melanoma. *Med. Chem. Commun.*, 8, pp.88–95. Available at: http://xlink.rsc.org/?DOI=C6MD00466K.

Sethi, S. et al., 2013. Clinical advances in molecular biomarkers for cancer diagnosis and therapy. *International Journal of Molecular Sciences*, 14(7), pp.14771–14784.

Shakhova, O. & Sommer, L., 2013. Testing the cancer stem cell hypothesis in melanoma: The clinics will tell. *Cancer Letters*, 338(1), pp.74–81.

Sharma, S. et al., 2016. Trends in Analytical Chemistry PLGA-based nanoparticles : A new paradigm in biomedical applications. *Trends in Analytical Chemistry*, 80, pp.30–40.

Shi, J. et al., 2016. Cancer nanomedicine: progress, challenges and opportunities. *Nature Publishing Group*, pp.1–18. Available at: http://dx.doi.org/10.1038/nrc.2016.108.

Shi, S. et al., 2014. Dual drugs (microRNA-34a and paclitaxel)-loaded functional solid lipid nanoparticles for synergistic cancer cell suppression. *Journal of Controlled Release*, 194, pp.228–237. Available at: http://dx.doi.org/10.1016/j.jconrel.2014.09.005.

Shiozawa, Y. et al., 2013. Cancer stem cells and their role in metastasis. *Pharmacology & therapeutics*, 138(2), pp.285–93. Available at: http://www.pubmedcentral.nih.gov/articlerender.fcgi?artid=3602306&tool=pmcentrez&r endertype=abstract [Accessed July 16, 2014].

Shmelkov, S. V. et al., 2008. CD133 expression is not restricted to metastatic colon cancer cells initiate tumors. *The Journal of clinical investigation*, 118(6), pp.2111–2120. Available at: www.jci.org/articles/view/34401.

Shukla, S., Patel, A. & Ambudkar, S. V., ABC Transporters - 40 Years Part II. In -Anthony M., ed. pp. 227–272. Available at: 10.1007/978-3-319-23476-2_10, Doi:

Sigalotti, L. et al., 2002. Cancer testis antigens expression in mesothelioma: role of DNA methylation and bioimmunotherapeutic implications. *British Journal of Cancer*, 86, pp.979–982.

Sigalotti, L. et al., 2008. Cancer testis antigens in human melanoma stem cells: Expression, distribution, and methylation status. *Journal of Cellular Physiology*, 215(2), pp.287–291.

Silva, C.O. et al., 2016. Melanoma Prevention : Challenges and Progresses in Nanotechnology for Melanoma Prevention and Treatment. *CRC Concise Encyclopedia of Nanotechnology*, (May 2016), pp.453–470. Available at: http://dx.doi.org/10.1201/b19457-39.

Silva, J.M. et al., 2015. In vivo delivery of peptides and Toll-like receptor ligands by mannose-functionalized polymeric nanoparticles induces prophylactic and therapeutic anti-tumor immune responses in a melanoma model. *Journal of Controlled Release*, 198, pp.91–103.

Singh, A. & Settleman, J., 2010. EMT, cancer stem cells and drug resistance: an emerging axis of evil in the war on cancer. *Oncogene*, 29(34), pp.4741–4751.

Singh, S.R. et al., 2009. Intravenous transferrin, RGD peptide and dual-targeted nanoparticles enhance anti-VEGF intraceptor gene delivery to laser-induced CNV. *Gene therapy*, 16(5), pp.645–659. Available at: http://www.nature.com/doifinder/10.1038/gt.2008.185%5Cnhttp://dx.doi.org/10.1038/gt.

2008.185.

Slominski, A.T. & Carlson, J.A., 2015. Melanoma resistance: a bright future for academicians and a challenge for patient advocates. *Mayo Clinic Proceedings*, 89(4), pp.429–433.

Smith, F.R., Lattman, E.E. & Carter, C.W., 1991. The Mutation p99 Asp-Tyr Stabilizes Y-A New , Composite Quaternary State of Human Hemoglobin. *Proteins Structure, Function, and Genetics*, 10, pp.81–91.

Spitler, L.E. et al., 2015. Phase II Study of Nab -Paclitaxel and Bevacizumab as First-line Therapy for Patients with Unresectable. *American Journal of Clinical Oncology*, 38(1), pp.61–67.

Staquicini, F.I. et al., 2008. A Subset of Host B Lymphocytes Controls Melanoma Metastasis through a Melanoma Cell Adhesion Molecule / MUC18-Dependent Interaction : Evidence from Mice and Humans. *Cancer Research*, 68(20), pp.8419–8428.

Suh, M.S. et al., 2017. Layer-by-layer nanoparticle platform for cancer active targeting. *International Journal of Pharmaceutics*, 517(1–2), pp.58–66. Available at: http://linkinghub.elsevier.com/retrieve/pii/S0378517316311371.

Sun, X.-X. & Yu, Q., 2015. Intra-tumor heterogeneity of cancer cells and its implications for cancer treatment. *Acta pharmacologica Sinica*, 36(10), pp.1219–27. Available at: http://www.pubmedcentral.nih.gov/articlerender.fcgi?artid=4648179&tool=pmcentrez&rendertype=abstract.

Swart, G.W.M., 2002. Activated leukocyte cell adhesion molecule (CD166/ALCAM): developmental and mechanistic aspects of cell clustering and cell migration. *European Journal of Cell Biology*, 81(6), pp.313–321.

Talelli, M. et al., 2010. Core-crosslinked polymeric micelles with controlled release of covalently entrapped doxorubicin. *Biomaterials*, 31(30), pp.7797–7804. Available at: http://dx.doi.org/10.1016/j.biomaterials.2010.07.005.

Tazzari, M. et al., 2015. Melan-A/MART-1 immunity in a EWS-ATF1 translocated clear cell sarcoma patient treated with sunitinib: a case report. *BMC Cancer*, 15(1), pp.1–8. Available at: http://www.biomedcentral.com/1471-2407/15/58.

Thapa, R. & Wilson, G.D., 2016. The Importance of CD44 as a Stem Cell Biomarker and Therapeutic Target in Cancer. *Stem Cells International*, 2016, pp.1–15.

Toy, R. et al., 2014. Shaping cancer nanomedicine: the effect of particle shape on the in vivo journey of nanoparticles. *Nanomedicine (London, England)*, 9(1), pp.121–34. Available at: http://www.ncbi.nlm.nih.gov/pubmed/24354814%5Cnhttp://www.pubmedcentral.nih.gov/articlerender.fcgi?artid=PMC4057606.

Tran, K.A. et al., 2016. MeK inhibitors and their potential in the treatment of advanced melanoma: the advantages of combination therapy. *Drug Design, Development and Therapy*, 10, pp.43–52. Available at: http://www.dovepress.com/permissions.php.

Upponi, J. R.; Torchilin, V. P., Alonso, M. J.; Garcia-Fuentes, M., 2014. Passive vs. Active Targeting: An Update of the EPR Role in Drug Delivery to Tumors. In M. Alonso, M. J.; Garcia-Fuentes, ed. *Nano-Oncologicals: New Targeting and Delivery Approaches*. pp. 3–45.

Vaidhyanathan, S. et al., 2016. *Factors Influencing the Central Nervous System Distribution of a Novel Phosphoinositide 3-Kinase/Mammalian Target of Rapamycin Inhibitor GSK2126458: Implications for Overcoming Resistance with Combination Therapy for Melanoma Brain Metastases s*, Available at: http://dx.doi.org/10.1124/jpet.115.229393.

Valyi-nagy, K. et al., 2012. Stem cell marker CD271 is expressed by vasculogenic mimicry-forming uveal melanoma cells in three-dimensional cultures. , (February), pp.588–592.

Vansteenkiste, J.F. et al., 2016. Efficacy of the MAGE-A3 cancer immunotherapeutic as adjuvant therapy in patients with resected MAGE-A3-positive non-small-cell lung cancer

(MAGRIT): a randomised, double-blind, placebo-controlled, phase 3 trial. *The Lancet Oncology*, 17(6), pp.822–835.

Vauthier, C. & Ponchel, G., 2016. Polymer Nanoparticles for In Vivo Applications: Progress on Preparation Methods and Future Challenges. In *Polymer Nanoparticles for Nanomedicines*. pp. 3–16.

Van De Ven, A.L. et al., 2012. Rapid tumoritropic accumulation of systemically injected plateloid particles and their biodistribution. *Journal of Controlled Release*, 158(1), pp.148–155. Available at: http://dx.doi.org/10.1016/j.jconrel.2011.10.021.

Veronese, F. M.; Pasut, G., 2005. PEGylation, successful approach to drug delivery. *Drug Discovery Today*, 10(21), pp.1451–1458.

Vinogradov, S. & Wei, X., 2012. Cancer stem cells and drug resistance: the potential of nanomedicine. *Nanomedicine (London, England)*, 7(4), pp.597–615. Available at: http://www.pubmedcentral.nih.gov/articlerender.fcgi?artid=3376090&tool=pmcentrez&rendertype=abstract.

Visvader, J.E. & Lindeman, G.J., 2012. Cancer stem cells: Current status and evolving complexities. *Cell Stem Cell*, 10(6), pp.717–728. Available at: http://dx.doi.org/10.1016/j.stem.2012.05.007.

Wang, A. Qu, L. Wang, L., 2016. At the crossroads of cancer stem cells, radiation biology, and radiation oncology. *Cancer Research*, 76(5), pp.1–10.

Wang, J. et al., 2011. Targeting the NG2/CSPG4 proteoglycan retards tumour growth and angiogenesis in preclinical models of GBM and melanoma. *PLoS ONE*, 6(7), pp.1–13.

Wang, X. et al., 2011. Functional Characterization of an scFv-Fc Antibody that Immunotherapeutically Targets the Common Cancer Cell Surface Proteoglycan CSPG4. *microenvironment and immunology*, 71(24), pp.7410–7422.

Weber, J.S. et al., 2016. Safety Profile of Nivolumab Monotherapy: A Pooled Analysis of Patients With Advanced Melanoma. *J Clin Oncol*, 34, pp.1–7. Available at: http://ascopubs.org/jco/podcasts.

Weidle, U.H., Georges, G.U.Y. & Tiefenthaler, G., 2014. TCR-MHC / Peptide Interaction : Prospects for New Anti-tumoral Agents. *Cancer Genomics & Proteomics*, 278(11), pp.267–277.

Wen, S. et al., 2013. Multifunctional dendrimer-entrapped gold nanoparticles for dual mode CT/MR imaging applications. *Biomaterials*, 34(5), pp.1570–1580. Available at: http://dx.doi.org/10.1016/j.biomaterials.2012.11.010.

Widmer, D.S. et al., 2015. Melanoma' s next top model, it is in the air. *Experimental dermatology*, 24, pp.659–660.

Wilson, B.J. et al., 2014. ABCB5 maintains melanoma-initiating cells through a proinflammatory cytokine signaling circuit. *Cancer Research*, 74(15), pp.4196–4207.

Wouters, J. et al., 2013. The Human Melanoma Side Population Displays Molecular and Functional Characteristics of Enriched Chemoresistance and Tumorigenesis. *PLoS ONE*, 8(10), pp.1–16.

Wu, C. et al., 2017. Colloids and Surfaces B : Biointerfaces Co-delivery of multiple drug resistance inhibitors by polymer / inorganic hybrid nanoparticles to effectively reverse cancer drug resistance. *Colloids and Surfaces B: Biointerfaces*, 149, pp.250–259. Available at: http://dx.doi.org/10.1016/j.colsurfb.2016.10.029.

Wu, X. et al., 2016. Improved SERS-Active Nanoparticles with Various Shapes for CTC Detection without Enrichment Process with Supersensitivity and High Specificity. *acs applied materials and interfaces*, pp.1–34.

Wu, Y. & Wu, P.Y., 2009. CD133 as a Marker for Cancer Stem Cells: Progresses and Concerns. *Stem Cells and Development*, 18(8), pp.1127–1134. Available at: http://www.liebertonline.com/doi/abs/10.1089/scd.2008.0338.

Xiao, Y.F. et al., 2013. microRNA detection in feces, sputum, pleural effusion and urine: Novel tools for cancer screening (Review). *Oncology Reports*, 30(2), pp.535–544.

Xie, J. et al., 2015. Nanotechnology for the delivery of phytochemicals in cancer therapy. *Biotechnology Advances*, 34(4), pp.343–353. Available at: http://dx.doi.org/10.1016/j.biotechadv.2016.04.002.

Xiong, X.B. et al., 2010. The therapeutic response to multifunctional polymeric nano-conjugates in the targeted cellular and subcellular delivery of doxorubicin. *Biomaterials*, 31(4), pp.757–768. Available at: http://dx.doi.org/10.1016/j.biomaterials.2009.09.080.

Xu, Z. et al., 2014. Nanoparticle-delivered transforming growth factor-β siRNA enhances vaccination against advanced melanoma by modifying tumor microenvironment. *ACS Nano*, 8(4), pp.3636–3645.

Yu, A.L. et al., 2016. Alterations of Glycosphingolipids in Embryonic Stem Cell Differentiation and Development of Glycan-targeting Cancer Immunotherapy. *Stem Cells and Development*, (Special Issues: Stem Cells and Gene Therapy), pp.1–58.

Yu, A.L. et al., 2010. Anti-GD2 antibody with GM-CSF, interleukin-2, and isotretinoin for neuroblastoma. *The New England journal of medicine*, 363(14), pp.1324–1334.

Yuan, J. et al., 2013. Immunologic responses to xenogeneic tyrosinase DNA vaccine administered by electroporation in patients with malignant melanoma. , pp.1–11.

Yuan, J. et al., 2016. Novel technologies and emerging biomarkers for personalized cancer immunotherapy. *Journal for immunotherapy of cancer*, 4, p.3. Available at: http://www.pubmedcentral.nih.gov/articlerender.fcgi?artid=4717548&tool=pmcentrez&rendertype=abstract.

Zhang, J., Chen, K. & Fan, Z.H., 2016. *Circulating Tumor Cell Isolation and Analysis* 1st ed., Elsevier Inc. Available at: http://dx.doi.org/10.1016/bs.acc.2016.03.003.

Zhang, Y. & Zhuo, R., 2005. Synthesis and in vitro drug release behavior of amphiphilic triblock copolymer nanoparticles based on poly (ethylene glycol) and polycaprolactone. *Biomaterials*, 26(33), pp.6736–6742.

Zhong, Y. et al., 2010. Cancer stem cells sustaining the growth of mouse melanoma are not rare. *Cancer Letters*, 292(1), pp.17–23. Available at: http://dx.doi.org/10.1016/j.canlet.2009.10.021.

Zhong, Y. et al., 2014. Ligand-Directed Active Tumor-Targeting Polymeric Nanoparticles for Cancer Chemotherapy. *Biomacromolecules*, 15(6), pp.1955–1969.

Zou, Y. et al., 2016. Self-crosslinkable and intracellularly decrosslinkable biodegradable micellar nanoparticles: A robust, simple and multifunctional nanoplatform for high-efficiency targeted cancer chemotherapy. *Journal of Controlled Release*. Available at: http://dx.doi.org/10.1016/j.jconrel.2016.05.060.

Zuckerman, J.E. & Davis, M.E., 2015. Clinical experiences with systemically administered siRNA-based therapeutics in cancer. *Nature Reviews Drug Discovery*, 14(12), pp.843–856. Available at: http://www.nature.com/doifinder/10.1038/nrd4685.

Zuo, Z.-Q. et al., 2016. Promoting tumor penetration of nanoparticles for cancer stem cell therapy by TGF-β signaling pathway inhibition. *Biomaterials*, 82, pp.48–59. Available at: http://linkinghub.elsevier.com/retrieve/pii/S0142961215010029.

Figure 1. Schematic illustration of tumor site derived circulating melanoma cells (CMC) and melanoma cancer stem cells (m-CSCs) in blood flow and representation of the epidermal to mesenchymal transition (EMT) processes. The CMC and m-CSCs possess high metastatic potential and disseminated preferentially to the lung and liver. The main known biomarkers for m-CSCs and CMC are shown in scheme below, highlighting the common markers.
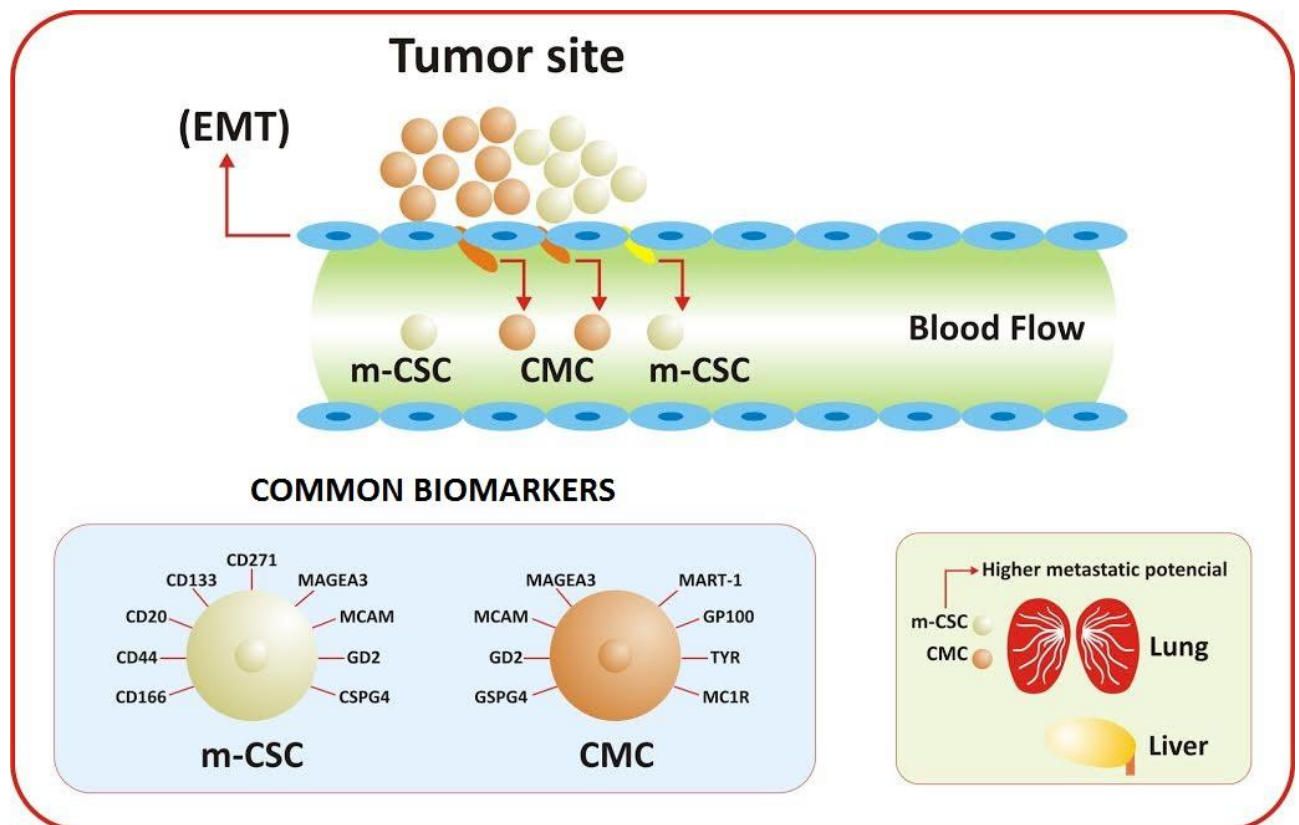
Figure 2. Schematic illustration of passive targeting (a) and active targeting (b) for melanoma treatment and diagnosis. In passive targeting, the enhanced permeation and retention (EPR) effect allows the accumulation of nanoparticles at the heterogeneous tumor niche that contains differentiated melanoma cells (d-mc) and m-CSCs (a). In active targeting, the targeted nanoparticles can recognize surface receptors expressed by m-CSCs, CMC, endothelial cells of tumor vasculature and/or d-mc, and promote a receptor-mediated endocytosis and drug-delivery of antitumoral or diagnosis agents into the melanoma cells.
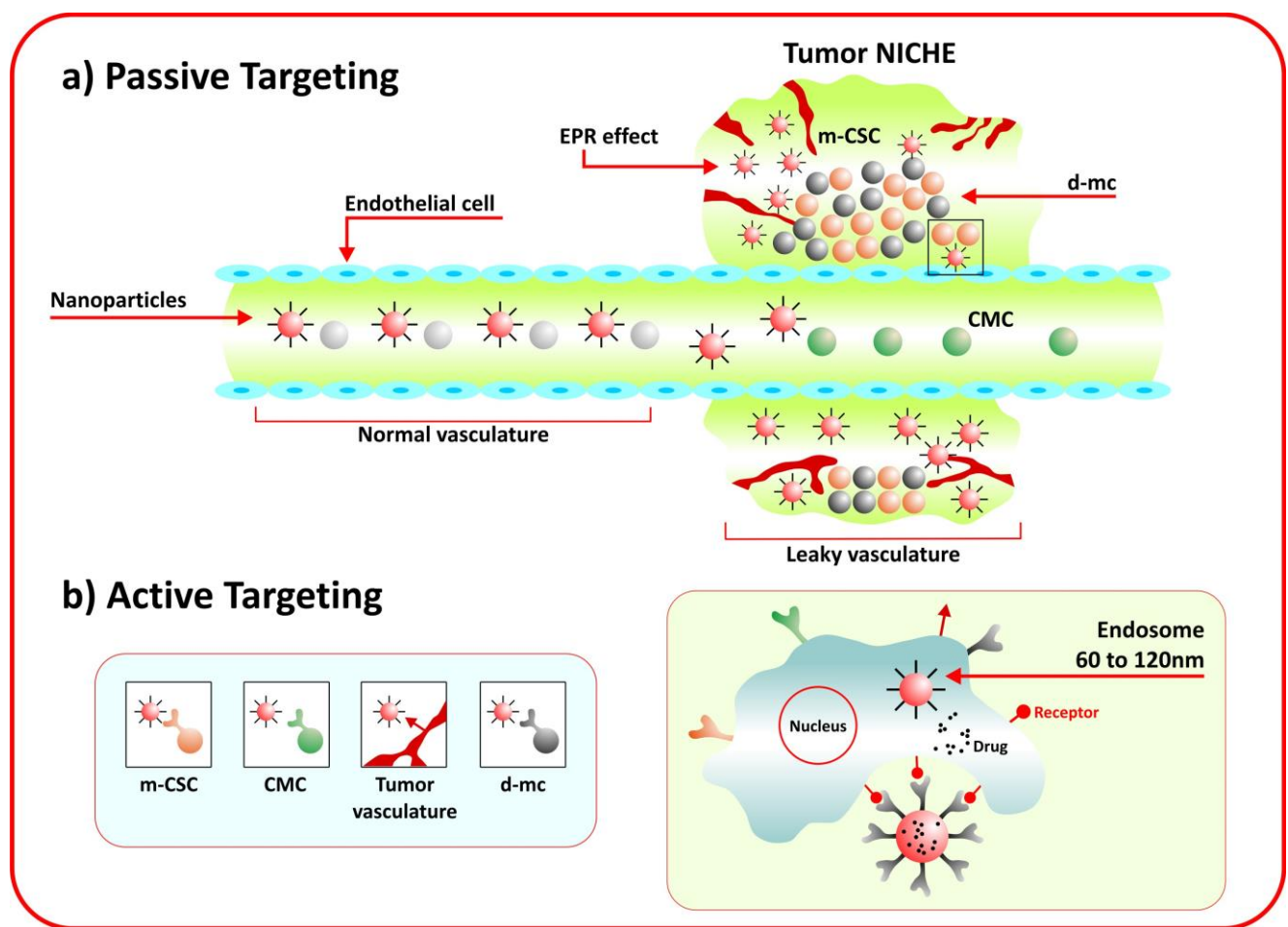
Table 1. Current biomarkers detected in m-CSC and CMC.

Table 1. Current biomarkers detected in m-CSC and CMC

Biomarkers	Type	Cellular localization	Main functions/ Mechanisms	References
(a) Mesenchymal cancer stem cells (m-CSC)				
CD133	TM/IgSF	Plasma membrane	Signaling function/ cell differentiation into tumor endothelium	Mak et al. (2014) Borovski et al. (2011) Wu et al. (2009)
CD271	TM/IgSF/ TNFR	Plasma membrane	Cell survival, apoptosis and adhesion/ regulation of β1-integrin	Valyi-Nagy et al. (2012)
CD166	TM/IgSF/ Alcam	Plasma membrane	Cell growth, migration and adhesion/ heterophilic and homophilic cell-cell interactions	Weidle et al. (2014) Swart (2002)
CD44	TM/IgSF/ HA-R	Plasma membrane	Cell adhesion, migration/ heterophilic and homophilic cell-cell interactions	Ahrens et al. (2001) Faaseen et al. (1992)
CD20	TM/IgSF/B-cell-specific cell-surface molecule	Plasma membrane	Regulates cell-cycle progression of B lymphocytes/ Ca^{+2} channel activity	Cragg et al. (2004) Tedder and Engel (1994)
(b) Circulating Melanoma cells (CMC)				
MART-1	Protein/ MDA	Cytosol (Golgi complex, ER and melanosomes), plasma membrane (HLA- restricted epitope)	Melanocyte differentiation, biosynthesis of melanin and T-cells recognition	Ordóñez (2013) Mazière et al. (2002) Rimoldi et al. (2001)
GP100	Protein/ MDA	Cytosol (melanosomes), plasma membrane (HLA-restricted epitope)	Melanocyte differentiation, biosynthesis of melanin and T-cells recognition	Ordóñez (2013) Mazière et al. (2002)
TYR	Protein/ MDA	Cytosol (melanosomes), plasma membrane (HLA-restricted epitope)	Melanocyte differentiation, biosynthesis of melanin and T-cells recognition	Ordóñez (2013) Mazière et al. (2002)
MC1R	T-GPR	Cytosol, plasma membrane	Regulates the production of melanin (eumelanin and pheomelanin) by melanocytes	Rees (2000) López et al. (2007)
(c) Common Markers (m-CSC and CMC)				
MAGEA3	Protein/ MDA	Cytosol, plasma membrane (HLA-restricted epitope)	Cell cycle progression and apoptosis/ Immune response against cancer	Sigalotti et al. (2002b) Rimoldi et al. (2001)
MCAM/ CD146	TM/IgSF	Plasma membrane	Support endothelial integrity, lymphocyte recruitment/ Cell adhesion, migration, homing, and inflammation /homotypic and heterotypic cell interactions	Duan et al. (2013) Ouhtit et al. (2009) Elshal et al. (2007)
GD2	Ganglioside	Plasma membrane	Cell adhesion/invasion and/or proliferation/ modulate intracellular and intranuclear calcium homeostasis	Yu et al. (2011) Horta et al. (2016)
CSPG4	T-PG	Plasma membrane	Cell adhesion, growth, motility and survival; angiogenesis/ activation of integrins and GTPase family proteins	Wang et al. (2010) Wang et al. (2011b) Price et al. (2011)

Abbreviations: TM- Transmembrane protein/ Alcam- activated leukocyte cell adhesion molecule/ IgSF- immune globulin superfamily/ TNFR- tumor necrosis factor receptor superfamily/ HA-R- hyaluronan receptor/ MDA- melanoma differentiation antigen/ ER- endoplasmic reticulum/ HLA- human leukocyte antigen complex/T-PG- transmembrane proteoglycan/T-GPR- Transmembrane G-protein-couple receptor family.

Table 2. *In vivo* and *in vitro* studies with polymeric nanoparticles loaded with different drugs for passive and active tumor targeting for advanced melanoma treatment.

Polymer(s)	Drug delivered	Systems/Composition	Characteristics	Main results	Reference
PCL	Acetyleugenol (AcE)	AcE-LNCs	Ø ≈210 nm PDI ≈ 0.1 ζ ≈ −10 mV spherical	Oral LNC treatment was more efficient than AcE-LNC treatment B16F10 melanoma tumor model.	Drewes et al., (2016)
PLA	Usnic acid (UA)	NP's-PLA NP's-PLA-UA	Ø ≈246 nm PDI ≈ 0.1 ζ ≈ −25 mV spherical or slightly oval	NP's-PLA-UA reduced the cell viability in 70% over B16F10 melanoma cell line.	Antonio et al., (2016)
PEG-b-PDTC	Doxorubicin (DOX)	SCID-Ms cRGD/SCID-Ms DOX-SCID-Ms cRGD/DOX-SCID-Ms DOX-LPs	Ø ≈ 150 nm PDI ≈ 0.18 ζ- Neutral	DOX-SCID-Ms increased mice survival and decreased systemic toxicity in B16 melanoma tumor model *in vivo* compared to free DOX; cRGD20/DOX-SCID-Ms exhibited better therapeutic efficacy and lower side effects than DOX-LPs *in vivo*.	Zou et al., (2016)
PCL-PEI and PCL-PEG	Hedgehog pathway inhibitor visnodegib (VIS) and microRNA-34a (34a)	VIS/PHM/34a	Ø ≈ 60 nm PDI ≈ 0.3 ζ = +4.3 mV spheres	VIS/PHM/34a showed a synergistic anticancer efficacy in B16F10-CD44+ metastatic melanoma model.	L.Li et al., (2015)
PEG-CMC	Docetaxel (DTX)	DTX-PEGylated-CMC	Ø ≈118 nm PDI ≈ 0.1 ζ ≈ −22 mV	DTX-PEGylated-CMC increasing the tumor accumulation compared to Abraxane® in B16F10 melanoma model.	Ernsting et al., (2012)
PEG-PLA	Hydrophobic porphyrin derivative (Por)	Por-PEG-PLA	Ø ≈ 80 nm ζ ≈ −7.3 mV	Por-PEG-PLA showed *in vitro* phototoxicity in B16BL6 melanoma cells.	Ogawara et al., (2016)
PLGA	PI3K inhibitor (LY)	LY-PLGA	Ø≈ 110 nm spheres	NP-LY demonstrated a higher antiangiogenic response compared to free LY in B16F10 melanoma zebrafish xenograft model.	Harfouche et al., (2009)
mPEG-b-p(HPMAm-Lacn)	DOX	DOX-polymeric micelles	Ø ≈80 nm spheres	pH responsive DOX micelles prolonged survival compared to free DOX group with no adverse effects in B16F10 melanoma tumor model.	Talelli et al., (2010)
LMWH	DOX	LH-DOX-NPs	Ø ≈155 nm PDI≈ 0.2 ζ ≈ −35 mV spheres	pH responsive LH-DOX significantly reduced the tumor growth in B16F10 melanoma tumor model.	Mei et al., (2016)

Aldehyde-PEG-PLA and MPEG-PLA	DTX	TH10-DTX-NPs DTX-NPs	Ø ≈170 nm PDI≈ 0.2 ζ ≈ −22 mV spheres	TH10-DTX-NPs selective targeting the tumor vascular pericytes; promoted an increase in mice survival and low toxicity in B16F10-luc-G5 lung metastasis model *in vivo*.	Y. Y. Guan et al., (2014)
Albumin	Paclitaxel (PTX)	*nab*-PTX (Abraxane®) anti-VEGF conjugated with Abraxane®	Ø ≈160 nm	anti-VEGF conjugated with Abraxane® enhanced tumor regression compared to Abraxane® in human A375 melanoma model.	Nevala et al., (2016)
mPEG-b-PAGE	Epirubicin (EPI)	M(cbm), M(hz), cRGD-M(cbm) and cRGD-M(hz) conjugated with EPI	Ø ≈ 18, 50, 23, and 60 nm, respectively; spheres	pH sensitive cRGD-M presented a significant increasing anti-tumor activity in B16F10 melanoma xenograft model compared with free epirubicin.	X. Guan et al., (2014)
HACE	DOX	DOX-loaded HACE-based NPs	Ø ≈110 nm PDI≈ 0.2 ζ ≈ −24.3 mV spheres	Tumor growth was significantly inhibited by DOX-loaded NPs in the B16F10 melanoma model.	Jin et al., (2012)
Lactoferrin(Lf)	Fluorouracil (5-FU)	5-FU-LfNPs	Ø ≈150 nm PDI≈ 0.3 ζ ≈ −2.5 mV spheres	pH responsive 5-FU-LfNPs prolonged intracellular retention and enhanced cytotoxicity effect (2.7 fold) compared to the free 5-FU in B16F10 cells.	Kumari & Kondapi, (2016)
PLGA, PEG-b-PLGA and PEG-b-PCL	antigens (Melan-A-26, gp100:209 or gp100:44) TLR ligands: Poly(I:C) and CpG	Man-NPs	Ø ≈145 to 190 nm PDI≈ 0.1 to 0.3 ζ ≈ −0.8 to −6.2 mV	Synergistic effect of immunopotentiators and potentiation of the anti-tumor immune response in B16F10 melanoma tumor model.	J. M. Silva et al., (2015)

Abbreviations: LCNs– lipid-core nanocapsules; Ø– size; ζ– zeta potential; PCL– poly(ε-caprolactone); PLA– poly (lactic acid); NPs– nanoparticles; SCID-Ms– self-crosslinkable and intracellularly decrosslinkable micellar nanoparticles; cRGD– cyclic peptide c(RGDfK) for target specificity; DOX-LPs– pegylated liposomal doxorubicin; PCL-PEI– polycaprolactone-polyethylenimine; PCL-PEG– polycaprolactone-polyethyleneglycol; PEG-b-PDTC– polyethyleneglycol)-b-polydithiolane trimethylene carbonate) block copolymer; PHM– polymeric hybrid micelle; PEG-CMC– PEGylated carboxymethylcellulose; CCP– charge-conversional polymer; CaP– calcium phosphate; PLGA– poly(lactic-co-glycolic acid); mPEG-b-p(HPMAm-Lacn)– poly(ethyleneglycol)-b-poly[N-(2-hydroxypropyl) methacrylamide-lactate]; LMWH– biocompatible amphiphilic copolymer of low molecular weight heparin; LH-DOX– low molecular weight heparin- doxorubicin; TH10 peptide– target molecule for NG2 proteoglycan receptors; mPEG-b-PAGE– block copolymer poly(ethylene oxide)-block-(allylglycidyl ether)]; M– micelles; hz– acid-labile hydrazone linkage; cbm– carbamate linkage; *nab*– albumin nanoparticles; HACE-hyaluronic acid-ceramide amphiphilic polymer; CDP– cyclodextrin-based polymer; TF– human transferrin protein; AD– adamantine; Man-NPs– mannose-grafted NPs; TLR– Toll-like receptor.

3   RATIONAL DESIGN OF IMMUNONANOPARTICLES CONCEIVED FOR INTERCEPTING MELANOMA CTCS WITHIN THE BLOOD STREAM

Autores: Sarah Brandão Palácio[a,b]; An Young Taylor Sarahi[b]; Jean Baptiste Coty[b]; Juliette Verganaud[b];Giorgia Egidy[c]; Nereide Stela Santos Magalhães[a]; Christine Vauthier[b]; Gilles Ponchel[b*]

[a]Laboratory of Imunopatology Keizo-Asami, Universidade Federal de Pernambuco, Recife, PE, Brazil

[b]University Paris Sud, Institut Galien Paris-Sud - UMR CNRS 8612, Faculty of   Pharmacy, 92296 Chatenay-Malabry Cedex, France

[c]INRA, UMR955 de Génétique fonctionnelle et médicale, Ecole Nationale Vétérinaire d'Alfort, 7 avenue du Général de Gaulle, Maisons-Alfort, F-94704, France

Correspondent Author*

Gilles Ponchel, Université Paris Sud, Institut Galien Paris-Sud - UMR CNRS 8612

Faculté de Pharmacie, 5 Rue J.B. Clément, 92296 Chatenay-Malabry,France Tel.: +33 01 46 83 59 19 fax: +33 01 46 61 93 34.

E-mail address: gilles.ponchel@u-psud.fr

3.1 Abstract

The aims of this work were developed and characterized nanoparticles and immunonanoparticles conjugated with MART-1 antibody, as well as evaluated their *in vitro* behavior by complement activation, cytotoxicity and cellular uptake assays. Polymeric nanoparticles were developed through the nanoprecipitation method of polymers derived from poly (γ-benzyl-L-glutamate) (PBLG) and the immunonanoparticles conjugated with MART-1 antibody, specific for melanoma cells, were obtained through the streptavidin-biotin binding. The conjugation of this antibody on the nanoparticles surface was evaluated by *western blot*. The nanoparticles were characterized and evaluated *in vitro* in B16-GFP melanoma cells and human umbilical vein endothelial cells (HUVECs) and the complement activation was investigated by bidimensional immunoelectrophoresis. The nanoparticles presented sizes between 20 and 100 nm and negative surface charge (-3 to -30 mV). The conjugation of antibody on the nanoparticle surfaces was detected by the *western blot* technique and confirmed by the changes in particle size and surface charge. The developed nanoparticles were not able to activate the complement system being considered long blood circulation. Regarding the *in vitro* analysis, the particles presented a low cytotoxicity when tested in B16-GFP and HUVECs cells. In the cell capture assays, the immunonanoparticles, containing a specific antibody for the recognition of the overexpressed antigen in melanoma cells, showed an increase of 40 to 50% in the uptake for these cells, indicating a specificity of this nanocarrier. These results suggested a promising application of PBLG-based nanoparticles coupled with MART-1 antibody to be used as systemic drug-delivery systems for melanoma targeting approach and shed light to the optimization of important parameters on the formulation of PBLG immunonanoparticles.

Keywords: Polymeric nanoparticles, PBLG, MART-1, immunonanoparticles, melanoma.

3.2 Introduction

Melanoma, one of the deadly skin cancer, is characterized specially by their high multidrug resistance, high metastatic potential and low survival rates (Slominski and Carlson, 2015). The melanoma incidence increased rapidly over the last 50 years and the 5-year survival rate for patients with advanced cutaneous melanoma was 9 to 28% in Europe (Markovic et al. 2007; Svedman et al., 2016). The high potential of a malignant melanoma to develop a metastatic disease is due to the natural heterogeneity of melanoma cells, leading to a lack of effective chemotherapy administered after surgery (Gray et al., 2015).

Conventional chemotherapy is largely ineffective for the treatment of metastatic melanoma cancer and generally have several limitations as the high toxicity to healthy cells, low target specificity and poor pharmacokinetic properties of the chemotherapeutic agents (Xie et al., 2015). Over the past two decades, the use of nanotechnology has been considered a promising approach to surpass these drawbacks related to conventional chemotherapy and increase the clinical anticancer efficacy (Chowdhury et al., 2016; Silva et al., 2016). Among the nanotechnology-based drug delivery systems, the polymeric nanoparticles offers several advantages for oncology applications, mainly due to their tailoring properties (Kamaly et al., 2016). The chemical surface modification of the polymeric nanoparticles can provide benefits for anticancer therapy, increasing the local concentrations of chemotherapeutic agents, minimizing dose and side effects (Mora-Huertas et al., 2010; Parhi et al., 2012).

Different polymers can be used for nanoparticle formation, but the peptide-based polymers have gained attention in cancer research due to their suitable properties for biomedical applications. These features can include polymer biodegradability, the ability to carrier high drug loading, chemical stability and ability to control their physicochemical and biological characteristics (Duro-Castano et al., 2014). Peptide-based polymers, including poly(γ-benzyl-L-glutamate) (PBLG) has emerged as a promising choice to prepare polymeric nanoparticles

with tailorable structures (Cauchois et al., 2013). The PBLG can adopt rigid α-helices structures and have the ability to form self-assembled nanoparticles by the simple nanoprecipitation method, with different sizes and shapes, depending on the polymer molecular weight (de Miguel et al., 2014; Ponchel & Cauchois, 2016). Besides these attractive chemical properties, the PBLG copolymers can be tailored to allow the attachment of target moieties on the surface of nanoparticles for active drug targeting to cell membranes or intracellular levels. This strategy aim to increase the receptor mediated-endocytosis of nanoparticles by cancer cells and/or direct target to cytoplasmic organelles for gene therapy (Chou et al., 2011; Pan et al., 2012; Zou et al., 2016). Among different classes of molecules used for this purpose, the surface functionalization of nanoparticles with antibody target moieties for specific recognition of biomarkers overexpressed in cancer cells is one of the most well-described strategy (Manjappa et al., 2011;Lammers et al., 2012; Liu et al., 2014).

In the case of melanoma biomarkers, MART-1 is the antigen recognized by T-cells, which is encoded by melanocyte-specific genes involved with the differentiation and production of melanin. MART-1 is overexpressed in the plasma membrane and in the endoplasmic reticulum of melanoma cancer (Chen et al., 1996; Riker et al., 1999). Antibodies against this biomarker are widely used for detection of circulating tumor cells (CTCs) in cutaneous melanoma and their overexpression has been correlated with the metastatic disease (Kawakami et al. 1997, Wang et al., 2001; Rodic et al., 2014). Moreover, MART-1 has been also studied as an immunotherapeutic agent to improve the immune response of patients with melanoma (Mockey et al., 2007; Sioud et al., 2016). However, the use of MART-1 for the development of targeted nanoparticles to melanoma cells as drug delivery systems has not yet been conducted.

Based on these findings, the present study aimed to develop and characterize surface modified PBLG nanoparticles, including those functionalized with MART-1 monoclonal

antibody conceived for intercepting melanoma CTCs within the blood stream, and evaluate their *in vitro* behavior by complement activation, cytotoxicity and cellular uptake assays.

3.3 Materials and methods

3.3.1 Materials

Dry N, N-dimethylformamide (DMF) and dry benzylamine were purchased from Acros Organics (Morris Plains, NJ, USA). Diethyl ether (DEE), methanol and tetrahydrofuran (THF) were purchased from Carlo Erba Reagents (Milan, Italy). Deuterated chloroform (CDCl$_3$), trifluoroacetic acid (TFA), Rhodamine B; 1-Ethyl-3-(3-dimethylaminopropyl) carbodiimide (EDC), trans-2-[3-(4-tert-butylphenyl)-2-methyl-2-propenylidene] malononitrile (DCTB), CF$_3$COOK (Potassium trifluoroacetate), (3-[4,5-dimethylthiazol-2-yl]-2,5 diphenyl tetrazolium bromide) (MTT), Dulbecco's phosphate buffered saline (PBS), Dulbecco's Modified Eagle's Medium - high glucose (DMEM), penicillin (100 U/ml), streptomycin (100 µg/ml), trypsin, glutamine (2µM), HABA avidin reagent and D-biotin-99% (TCL) were purchased from Sigma-Aldrich (Saint Quentin Fallavier, France). N-carboxyanhydride of γ-benzyl-l-glutamate (γ-BLG-NCA) was purchased from ISOCHEM-SNPE (Paris, France). The α-methoxy-ω-amino-poly (ethylene glycol) (MeO-PEG-NH$_2$) Mw = 5000 g.mol^{-1}, α-biotin-ω-amino-poly (ethylene glycol) (Bt-PEG-NH$_2$) Mw = 5000 g.mol^{-1} and α-methoxy-ω-carboxylic acid succinimidyl ester poly (ethylene glycol) (MeO-PEG$_5$-NHS) from IRIS Biotech GMBH (Marktredwitz, DEU). PluronicW F68 (Lutrol F68) was provided by BASF (DEU).

The antibodies Melan-A/MART-1 Antibody (A103) [Alexa Fluor (R) 647] and Mouse IgG1 Kappa Light Chain Isotype Control (P3.6.2.8.1) [Biotin] were purchased from Novus Biologicals Europe (Abingdon, United Kingdom). Polyclonal anti-human C3 antibody raised in goat was purchased from Fitzgerald antibodies (Massachusetts, USA). The Goat anti-mouse IgG-HRP was purchased from Santa Cruz Biotechnology (California, USA). Streptavidin

biotechnology grade was furnished by VWR International (Fontenay-sous-Bois, France). 100 kDa MWCO EMD Millipore Amicon™ Ultra-0.5 centrifugal filters were obtained from Merck Millipore (Darmstadt, DEU). Water was purified by reverse osmosis (MilliQ, Millipore, USA).

B16-GFP melanoma cells were provided by Dr. Giorgia Egidy Maskos (INRA, UMR955, Maisons-Alfort, France). Human umbilical vein endothelial cells (HUVECs) were obtained from the American Type Culture Collection (ATCC).

3.4 Methods

3.4.1 Synthesis of PBLG derivatives

Poly (γ-benzyl-L-glutamate)-benzylamine (PBLG-Bz), Poly (γ-benzyl-L-glutamate)-poly (ethylene glycol) (PBLG-PEG) and poly(γ-benzyl-L-glutamate)-poly (ethylene glycol)-biotin (PBLG-PEG-Bt) were synthesized by anionic ring opening polymerization (ROP) as previously described (Martínez-Barbosa et al., 2007). Briefly, the PBLG-Bz, PBLG-PEG and PBLG-PEG-Bt were prepared by the ROP of γ-benzyl-L-glutamate N-carboxyanhydride (γ-BLG-NCA) initiated by benzylamine (Bz), MeO-PEG-NH$_2$ and Bt-PEG-NH$_2$, respectively, in DMF. Firstly, γ-BLG-NCA (n mM) was weighed under inert atmosphere in an argon-purged three necks round-bottomed flask. The γ-BLG-NCA was dissolved in DMF at a concentration of 0.5 M and it was placed in a cold system, silica gel guard and a bubble detector. After 10 min of mechanical stirring at 30°C the argon flux was stopped. The initiator was added with an argon-purged syringe. Immediately after the addition of the initiator, CO$_2$ bubbles were observed. Absence of γ-BLG-NCA auto-polymerization was confirmed by infrared spectroscopy before addition of the initiator. The reaction evolution was controlled by infrared spectroscopy, by following the disappearance of characteristic NCA bands and the appearance of those of PBLG. Polymers were obtained by precipitation in an excess of cold DEE. The precipitate was filtrated and washed three times with methanol, in order to eliminate the excess

of unreacted PEG. The polymers were finally washed with DEE and dried under vacuum at room temperature for at least 12 h. A second precipitation, purification and drying procedure were performed for all polymers.

3.4.2 Synthesis of PBLG-Rhodamine

PBLG-Rhodamine was synthesized using carbodiimide chemistry approach. Briefly, 2 g of PBLG-Bz and 0.02 g of EDC were weighed in an argon-purged three necks round-bottomed flask and dissolved in DMF. The solution was stirring for 10 min at room temperature with argon flux. Next, a solution of rhodamine B 0.05 M in DMF was added with an argon-purged syringe. The reaction mixture was then left in the darkness for 24 h. The precipitation, purification and drying procedures were carried out as described above. The polymer was washed several times with methanol in order to eliminate the excess of unreacted Rhodamine B.
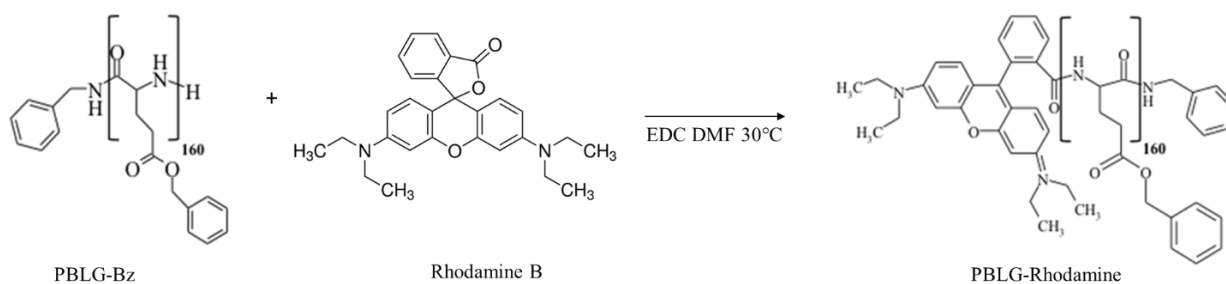
Figure 1. Synthesis scheme of PBLG-Rhodamine.

3.4.3 Characterization of PBLG derivatives

3.4.3.1 Fourier transform infrared spectroscopy

Fourier transform infrared spectroscopy (FT-IR) spectra was carried out to analyze γ-BLG-NCA auto-polymerization and to follow the end of polymerization reaction using a FT-IR spectrophotometer (Perkin Elmer, USA).

3.4.3.2 Proton Nuclear Magnetic Resonance

Proton nuclear magnetic resonance (^{1}H NMR) spectra of the PBLG derivatives were recorded using a B-ACS 60 apparatus (Bruker, DEU) operating at 300 MHz. Samples were measured in CDCl$_3$ and 15% of TFA. For PBLG derivatives containing PEG as initiator, the mass of the polymer could be determined by the integration of the benzyl protons belonging to the PBLG block (7.26 (br, s, 5H, Ph–) or 5.04 (br, s, 2H, –CH$_2$–benzyl)), and the ethylene protons of the PEG block (3.65 (br, s, 4H,–OCH$_2$–CH$_2$O–)) considering the mass of the initiator.

3.4.3.3 Matrix-assisted laser desorption/ionization time-of-flight mass spectrometry

Matrix-assisted laser desorption/ionization time-of-flight mass spectrometry (MALDI-TOF MS) analyses were performed using an UltrafleXtreme mass spectrometer (Bruker Daltonics, Bremen, DEU). Acquisitions were performed in linear positive ion mode. The laser intensity was set just above the ion generation threshold to obtain peaks with the highest possible signal-to-noise (S/N) ratio without significant peak broadening. All data were processed using the program Flex Analysis (Bruker Daltonics, Bremen, DEU). DCTB was used as the matrix for MALDI-TOF MS experiments and CF$_3$COOK was used as a cationizing agent.

3.4.4 Nanoparticles preparation

3.4.4.1 Preparation of self-assembled nanoparticles

Labeled and unlabeled nanoparticles were prepared with PBLG derivatives following a nanoprecipitation method previously described (de Miguel et al., 2014) for morphology and *in vitro* behavior evaluations. Briefly, pure (PBLG, PBLG-Rhod) or mixtures of PBLG derivatives (PBLG/PBLG-Rhod, PBLG-PEG/PBLG, PBLG-PEG/PBLG-Rhod, PBLG-PEG-Bt/PBLG and

PBLG-PEG-Bt/PBLG-Rhod) with a polymer percentage ratio of 90:10 were dissolved in THF at 30°C during 18h. The polymer solution was added dropwise to a 0.125% poloxamer solution under magnetic stirring (700 rpm) for around 5 minutes. Solvents were evaporated under vacuum in the rotavapor at 40ºC. The nanoparticle dispersions were filtered in ultracentrifugal filters (Amicon™100 kDa) and stored at 4 ºC for further use.

The fluorescence of PBLG-Rhod (100%) and PBLG/PBLG-Rhod (10%) nanoparticles was verified in different times (3 and 6 h) in B16-GFP and HUVECs cells (5 x 10^4 cells/well) at the concentration 100 µg/mL by flow cytometry (MoFlo XDP, Beckman Coutler). Data were expressed as fold increase of mean relative fluorescence over negative control (cells without treatment).

The functionality of biotin on the surface of PBLG-PEG-Bt/PBLG nanoparticles was evaluated using the HABA/Avidin colorimetric method (Qi et al., 2004) The HABA dye binds specifically to avidin to produce a yellow-orange colored complex with absorption at 500 nm. Free biotin molecules displace the HABA dye causing an absorbance decrease. The amount of available biotin on the surface of the biotinylated nanoparticles was calculated and data are presented in units of nanomoles of biotin per mL of nanoparticles.

3.4.4.2 Preparation of the immunonanoparticles

Immunonanoparticles (PBLG-PEG-Bt-MART-1) were prepared using PBLG-PEG-Bt nanoparticles and the antibody MART-1 for targeting purpose. First, in order to obtain the theoretical nanoparticles/antibody ratio of 1:5, the approximate number of nanoparticles contained in 50 µL were calculated based on the sphere equivalent diameters in volume from the transmission electronic microscopy (TEM) measurements of 130 nanoparticles (Eq. 1-3).

The theoretical number of biotin molecules per PBLG-PEG-Bt/PBLG-Rhod (90:10) nanoparticles was calculated (Eq. 4) based on the number of PBLG α-helices forming a

nanoparticle, considering that each PBLG-PEG-Bt α-helix corresponds to a single biotin molecule (de Miguel et al., 2014). Nanoparticles were considered to be spherical and PBLG α-helices as rods, whose lengths were calculated by taking into account the projected segment length of a single L-glutamate unit (= 0.15 nm), the number of residues of PBLG-PEG-Bt and PBLG-Rhod equal to 205 and 138, respectively, and the PBLG α-helices diameter of 1.6 nm as reported (Martínez-Barbosa et al., 2008)

$$Mass\ of\ 1\ NP = \text{density of PBLG} \times \left(\frac{4\pi(equivalent\ radius\ of\ NP)^3}{3} \right) \qquad \text{(Eq. 1)}$$

$$Equivalent\ Diameter = \sqrt[3]{Length * width^2} \qquad \text{(Eq. 2)}$$

$$Number\ of\ NP = \frac{Total\ polymer\ mass\ in\ 50\mu L}{mass\ of\ 1\ NP} \qquad \text{(Eq. 3)}$$

$$N_{\alpha helix/np} = \frac{4r_{np}^3}{3(\ 0.9\ h_{\alpha helixA}\ r_{\alpha helixA}^2 + 0.1\ h_{\alpha helixB}\ r_{\alpha helixB}^2\ )} \qquad \text{(Eq. 4)}$$

where NP is nanoparticles, r_{np} is the mean radius of 130 nanoparticles measured by TEM, $r_{\alpha helixA}$ and $h_{\alpha helixA}$ are the radius and the length of PBLG-PEG-Bt helices, and $r_{B\alpha helix}$, $h_{B\alpha helix}$ are those of PBLG-Rhod helices, respectively.

Posteriorly, to insure an efficient antibody coupling and to avoid nanoparticle aggregation, a two-step immunonanoparticle formation was carried out. First, the complex antibodies-streptavidin was obtained using biotinylated antibody associated with an excess of streptavidin solution (1 mg/mL) during 2 h. After unreacted streptavidin was removed by PBS washing three times using ultracentrifugal filters (Amicon™100 kDa). Next, MART-1-

Streptavidin diluted in 50 µL of water was incubated with 50 µL of nanoparticles (1.5 mg/mL) and left overnight on a rotating wheel at 4°C for conjugation reaction. Immunonanoparticles of biotinylated IgG1-streptavidin was obtained as described above and used as nonspecific control.

3.4.5 Physicochemical and biological characterization of nanoparticles

3.4.5.1 Particle size, shape and surface charge

The size and shape of nanoparticles were analyzed by dynamic light scattering (DLS) and transmission electronic microscopy (TEM). The hydrodynamic diameter of nanoparticles was determined at 25 ºC by with a Zetasizer 4 (Malvern, UK), operating at a fixed angle of 173º. For size measurements, 150µL of each sample was diluted in 850 µL of deionized water (MilliQ, Millipore, USA). The temperature was allowed to equilibrate 5 min before measurement. Results are given as mean hydrodynamic diameter of the nanoparticles obtained from at least three measurements on three different preparations of nanoparticles.

TEM images were acquired with a JEM-1400 microscopy (JEOL, Japan), operating under a 120 kV accelerating voltage. The image analysis was carried out using Image J® software. A sample of 3 µL nanoparticles was placed on a copper grill covered with formvar-carbon film (400 mesh) and stained by phosphotungstic acid (1%) for 30 s. The mean size of 130 nanoparticles, from different images, was obtained by TEM. The width (smallest dimension) and the length (longest dimension) of individual nanoparticles taken from a series of microphotographs were measured.

The aspect ratio (Γ) of nanoparticles, which describes the shape of nanoparticles and how elongated they are, was calculated from TEM images using Equation 5.

$$Aspect\ Ratio\ (\Gamma) = \frac{Length}{Width} \qquad (Eq.\ 5)$$

Surface charge of nanoparticles was evaluated by zeta potential measurements (Zetasizer 4, Malvern, UK). For analysis, an aliquot of 500 µL of nanoparticles was diluted in 500 µL of NaCl/1 mM and data of zeta potential were expressed in millivolts.

3.4.5.2 Specific recognition of MART-1-coupled nanoparticles

To assess the MART-1 coupling on the surface of nanoparticles, *Western blotting* technique was used. Aliquots of coupled and uncoupled immunonanoparticles (with or without streptavidin) were centrifuged (16000 g for 40 min) and 10 µL of the supernatant was denatured with 5% β-mercapto-ethanol in Laemmli buffer (20 µL) boiled at 95 ℃ for 5 min. Non-denatured samples of immunonanoparticles (10 µL) were diluted at Laemmil buffer in absence of β-mercapto-ethanol and without heating. Next, samples were loaded to a 4 to 15% gradient Mini-PROTEAN® TGX™ precast protein gels (Bio-Rad) and migrated at 200 V for 40 min. The migrated proteins were then transferred to a nitrocellulose membrane for 45 min at 100 V. The membrane was blocked in 5% nonfat milk in PBS–Tween (0.1%) for 1 h and incubated overnight at 4℃ with a goat anti-mouse IgG-HRP diluted to 1/3000. Proteins were visualized with an enhanced chemoluminescent system (GE Healthcare, Velizy-Villacoublay, France).

3.4.5.3 Complement activation

The method of serial multiple crossed 2D immunoelectrophoresis was used for analyzing the complement C3 activation of nanoparticles (Coty et al., 2016). The analyses were carried out using nanoparticles presenting surface area ranging from 250 to 4000 cm^2/mL or nanoparticles containing the same polymer concentration (1.5 mg/mL), corresponding to different surface areas ranging from 400 to 1875 cm^2/mL. Briefly, nanoparticles samples (50 µL) were incubated with Human serum (25 µL) diluted in Veronal buffer saline (VBS2+) (25 µL) prepared as previous described (Kazatchkine et al., 1985). Samples were incubated for 1 h

at 37°C, cooled at 4°C and analyzed in Agarose gel 1% containing anti-C3 antibody. The gel was prepared in Tricine buffer (Calcium Lactate 1 mM, TRIS 63 mM, Tricine 27 mM, in MilliQ® water, pH 8.6) and then casted on a Gel-Fix™ film. Bands were cutted and then filled with 1% agarose gel prepared in Tricine buffer for the 1st dimension. Wells were formed at the same time using a homemade comb. The gel was placed in Multiphor II electrophoresis system (GE Healthcare, Velizy-Villacoublay, France) and wells were filled with 2.5 µL of samples. The samples were then subjected to the first-dimension electrophoresis (600 V, 16 mA, 100 W), freely migrating in the agarose gel band according to their molecular weight. Then, the gel was turned by 90° for the second dimension corresponding to the rocket immunoelectrophoresis (500 V, 12 mA, 100 W), for 3 h 30 min. Gels were dried, at room temperature, and stained with Coomassie blue to reveal the presence of proteins.

The gels were numerically scanned and area under peaks was integrated using ImageJ® 2.5 software. The first peak on the left side was recognized as native C3, whereas the second peak from the left was attributed to protein fragments derived from C3 cleavage (C3b). The complement activation factor (CAF) was calculated regarding the ratio of peak surface of cleaved protein C3b over the sum of the total peak surface of C3 native and fragments and also removing the natural activation (control) during the performance of the technique, according to the follow equations (Eq. 6-8).

$$\text{Activation}_{sample}(\%) = \left[\left(\frac{C3b_{sample}}{C3_{sample}+C3b_{sample}}\right) \times 100\right] \qquad \text{(Eq. 6)}$$

$$\text{Activation}_{control}(\%) = \left[\left(\frac{C3b_{control}}{C3_{control}+C3b_{control}}\right) \times 100\right] \qquad \text{(Eq. 7)}$$

$$CAF\ (\%) = \left[\left(\frac{Activation_{sample}-Activation_{control}}{100-Activation_{control}}\right) \times 100\right] \qquad \text{(Eq. 8)}$$

3.4.5.4 Receptor expression and cytotoxicity of the nanoparticle

First, the MART-1 expression in B16-GFP cells was verified. Cells were incubated with three different concentrations (8, 16 and 24 µg/mL) of Melan-A/MART-1 Antibody (A103) [Alexa Fluor (R) 647] at 4 ºC on ice in dark, for 1 h. After three PBS washings, MART-1 recognition was revealed using flow cytometry (BD FACSCalibur; BDbiosciences, Le Pont de Claix, France). HUVEC cells, MART-1 receptor-negative, are used as negative control.

The cytotoxicity of nanoparticles was assessed in B16-GFP cells and HUVECs. The cells were cultured in DMEM medium (pH 7.4 = 3.7 g/L $NaHCO_3$) containing 10% of bovine fetal serum, penicillin (100 unit/mL) and streptomycin (100 µg/mL). The HUVECs growth medium was additionally supplemented with 2 mM of L-glutamine. Cells at logarithmic growth phase (3×10^5 cell/mL), between ten and fiftieth passages, were seeded in 96-well culture plates at 10^3 cell/well and incubated at 37°C for 24 h, 5% CO_2 and 95 °C humidity. Next, 100 µL of nanoparticles, with polymer concentrations ranging from 1 to 500 µg/mL, were added to each well and allowed to grow for 24 h. After incubation with 20 µL of MTT (0.5 mg/mL in PBS) for 2 h, the supernatants were removed and 200 µL of DMSO was added to solubilize the formazan crystals formed by viable cells. Viable cells were quantified by recording the UV absorbance at 570 nm using a plate reader multi-well scanning spectrophotometer (MRX II, DYNEX Technologies, Chanilly, USA). Untreated cells were used as control and assays carried out in triplicate. The IC_{50}, concentration that inhibits 50% of cells proliferation, was calculated by non-linear regression analysis with variable Hill slope given by parameter '*p*' using Origin 8.5.

3.4.5.5 Cellular uptake of immunonanoparticles

The specificity of PBLG-PEG-Bt-MART-1 nanoparticles for B16-GFP cells (5×10^4 cells/well) was evaluated at 3 and 6 h in the concentration 100 µg/mL by flow cytometry

(MoFlo XDP, Beckman Coutler). HUVECs cells were used as control, due to the absence of MART-1 receptor. Untreated cells were used as control and assays carried out in duplicate. Data of 10.000 events were analyzed per sample and the results were expressed as fold increase of mean relative fluorescence over negative control (cells without treatment).

3.5 Results and discussion

3.5.1 Synthesis and characterization of PBLG derivatives

PBLG derivatives were obtained and characterized with yield high than 80% (Table 1). The polymerizations were followed by the disappearance of absorption bands in FTIR spectra of the anhydride ring at 1855 cm^{-1} and 1787 cm^{-1} of C_5=O and C_2=O, respectively, which indicated the end of the reaction (Fig. 2).

The amide absorption bands in the FT-IR spectra are used to characterize the polypeptide conformation (Fig. 3). For a polypeptide in an α-helix conformation, the amide I and the amide II bands are located at 1656 cm^{-1} and 1548 cm^{-1}, respectively (Fontaine et al., 2001; Martínez-Barbosa et al., 2007; Segura-Sánchez et al., 2010) and for a β-conformation, the amide I and amide II bands are located at 1630 cm^{-1} and 1536 cm^{-1}, respectively. Furthermore, an absorption band near to 1260 cm^{-1} corresponding to the amide III band is observed in the FT-IR spectrum of a polypeptide in a α-helix conformation as previous reported (Martínez-Barbosa et al., 2007).

Table 1. Characteristics of PBLG derivatives.

Polymers	Dpnt (g mol^{-1})	γ -BLG-NCA (mmol)	[M]o (mol L^{-1})	[I]o (mol L^{-1})	Reaction time (days)	Yield (%)	Mw (g mol^{-1})
PBLG-Bz	160	13.8	0.5	0.009	3	82	45 000[2]
PBLG-PEG	160	15.2	0.025	0.009	6	80	41 000[1]

| PBLG-PEG-Bt	160	15.2	0.025	0.009	6	80	50 000 [1]
PBLG-Rhod	-	-	-	-	1	86	30 193 [2]

[M]o and [I]o are the initial concentration of γ-BLG-NCA and initiator, respectively. Dpnt indicate the theoretical values of each polymerization. Polymers are denominated as follows: PBLG is followed by the name of the initiator (Bz: Benzylamine, PEG: poly (ethylene glycol) Molecular weight was determined by NMR (1) and MALDI-TOF MS (2).

^{1}H NMR and MALDI-TOF MS techniques were used for determining the molecular weight for each polymer (Table 1). The Mw of PEGylated polymers was determined by the ratio between the peak intensities of methylene protons of PEG chain (OCH_2CH_2) and benzyl protons of PBLG chain ($COOCH_2C_6H_5$) (Fig.4). Due to the overlapping of the peaks of polymers without PEG in the NMR spectra, the determination of Mw it was not possible using this technique. Thus, MALDI-TOF MS technique was used to overcome this problematic (Fig. 5a and b). All properties of PGLB derivatives are in agreement in our previous studies (Martínez-Barbosa et al., 2007; Segura-Sánchez et al., 2010).
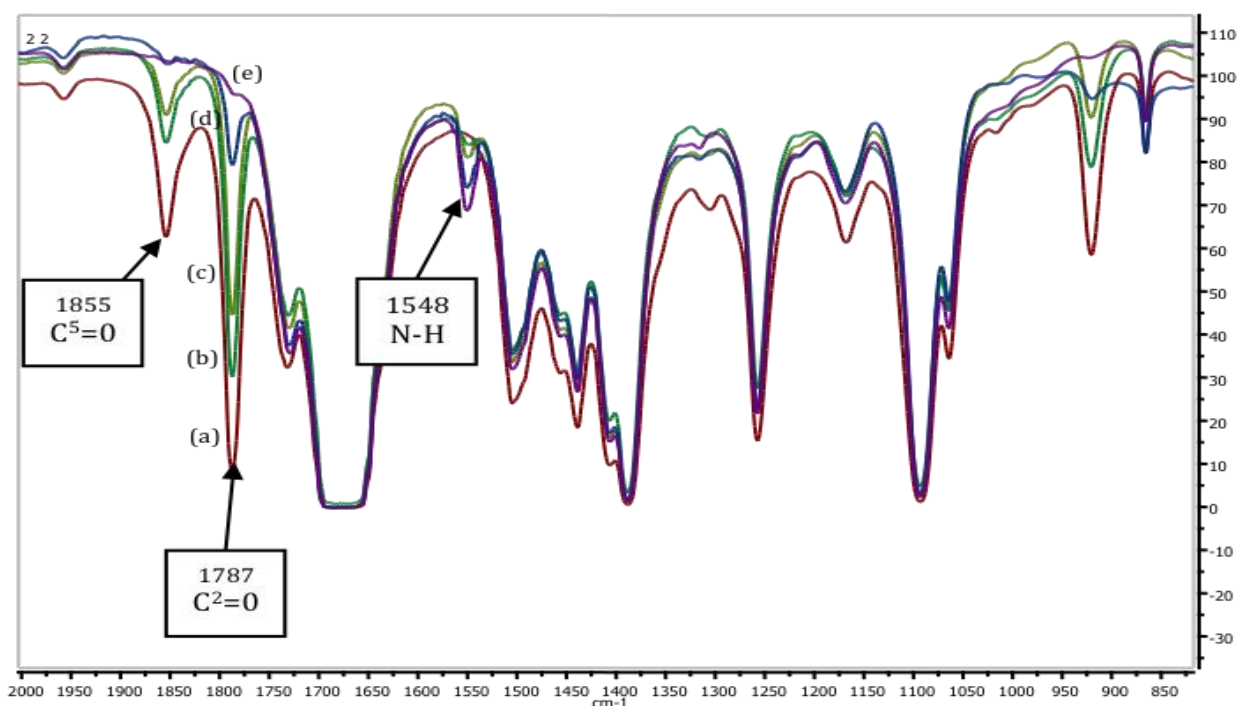
Figure 2. FT-IR spectra of PBLG-Bz polymerization film recorded at 0 min (a), 58 min (b), 139 min (c), 277 min (d) and 570 min (e) of reaction time.
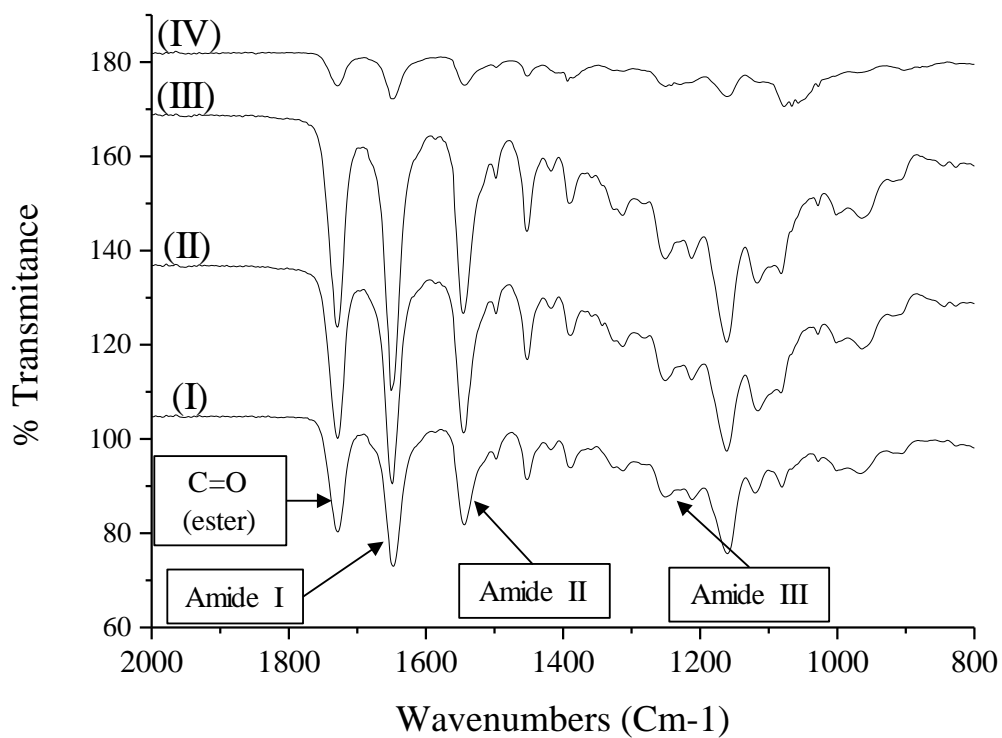
Figure 3. FT-IR spectra of PBLG derivatives: PBLG-Bz (I), PBLG-PEG (II), PBLG-PEG-Bt (III) and PBLG-Rhod (IV).
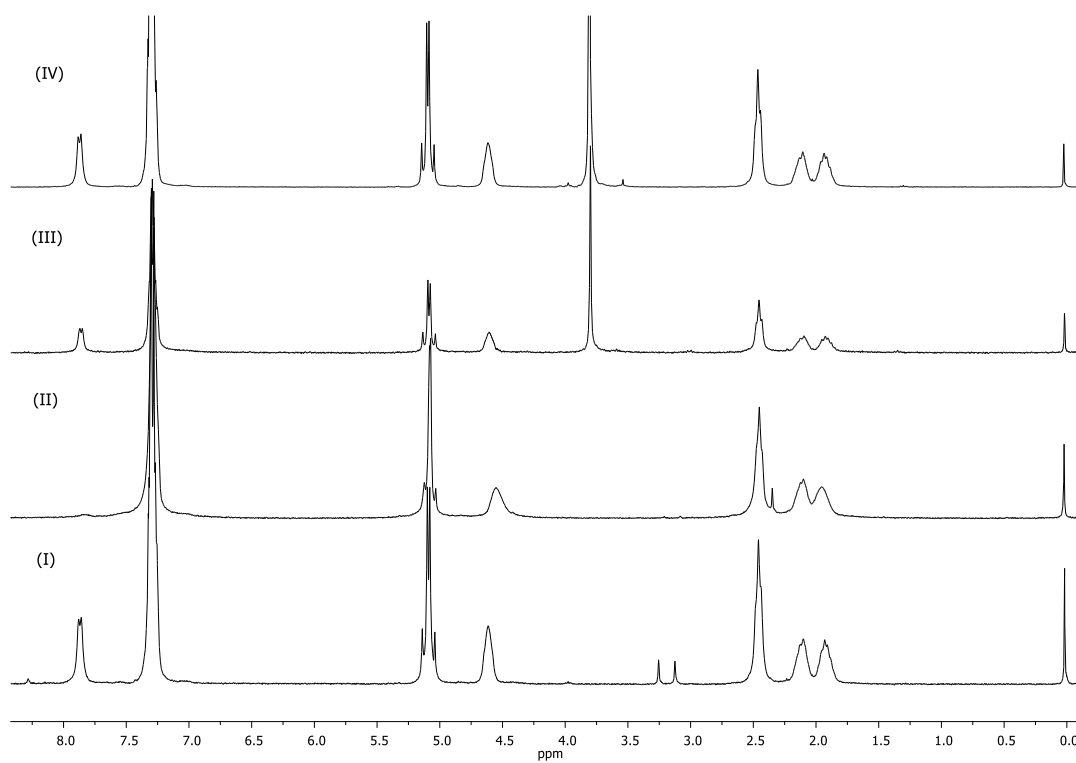
Figure 4. ^{1}H RMN spectra of PBLG derivates: PBLG-Bz (I), PBLG-Rhod (II), PBLG-PEG-Bt (III) and PBLG-PEG (IV).
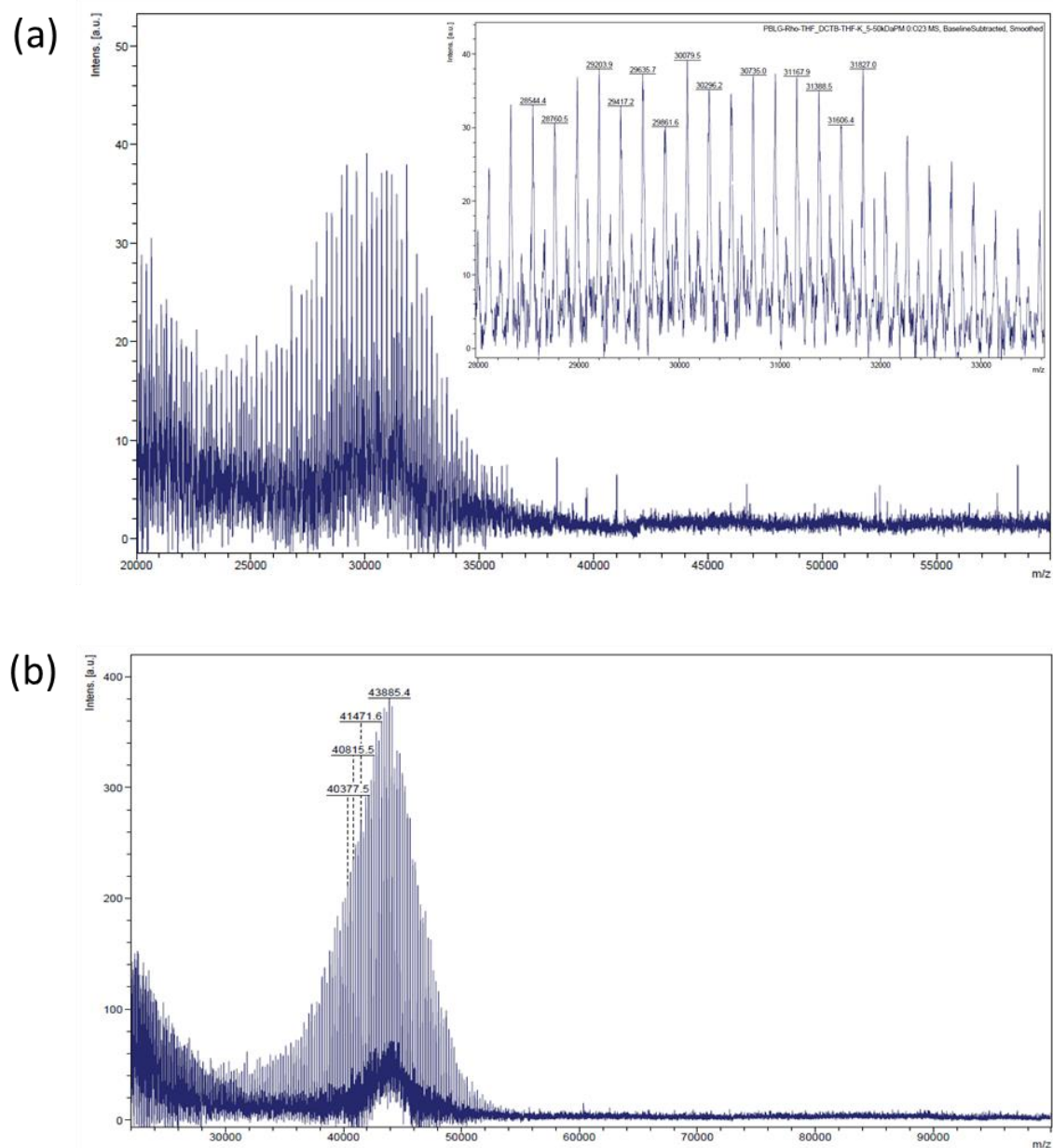
Figure 5. MALDI-TOF MS spectra of PBLG-Rhod (a) and PBLG-Bz (b).

3.5.2 Physicochemical and biological characterization of nanoparticles

3.5.2.1 Particle size, shape and surface charge

The nanoparticles were obtained from one or the mixture of two different PBLG derivatives following the nanoprecipitation method. The nanoparticles size were characterized by DLS and TEM and obtained a particle size between 20 to 100 nm with a narrow size distribution (PDI < 0.2) (Table 2). A 2-fold difference between the size measured by DLS and TEM was verified for all pegylated nanoparticles. These results can be explained by the presence of PEG chains on the nanoparticle surface, which increase the hydrodynamic radius measured by DLS. Saville and coworkers (2013) demonstrated that the hydrodynamic size determined by DLS of nanoparticles is directly proportional to molecular weight of PEG polymers. On the other hand, the nanoparticles size of PBLG-Bz, PBLG-Rhod and PBLG-Bz/PBLG-Rhod measured by TEM presented similar size when compared with those obtained from TEM microphotographs, mainly due to the absence of PEG corona.

Regarding to the nanoparticles conjugated with antibodies (PBLG-PEG-Bt-MART-1/PBLG-Rhod and PBLG-PEG-Bt-IgG/PBLG-Rhod), it was observed an increase of the hydrodynamic size measured by DLS when compared to unmodified PBLG-PEG-Bt nanoparticles. This result indicates the presence of antibody moieties on the surface of nanoparticles, increasing the thickness of hydration layer. In addition, TEM micrograph demonstrated maintenance of the size and morphological aspects of PBLG-PEG-Bt nanoparticles after the antibody conjugation, indicating that particles are stable after surface modification. Equivalent results were observed in other studies with polymeric nanoparticles and antibodies conjugation (Chen et al., 2013; Ramon et al., 2013).

Related to the shape, it was observed that nanoparticles of PBLG-Bz, PBLG-Rhod, PBLG-Bz/PBLG-Rhod and PBLG-PEG/PBLG-Rhod exhibited a slightly higher aspect ratio ($\Gamma \approx 1.4$ to 1.6) with an ellipsoidal shape (Fig. 6 a, b, c and e). On the other hand, all the nanoparticles containing the PBLG-PEG-Bt presented rather spherical morphology ($\Gamma \approx 1.2$) (Fig. 6 d, f, g, h and i). Comparable results were found by Segura-Sanchez and coworkers (2010)

for nanoparticles consisted of PBLG-Bz or PBLG-PEG-Bt. Studies verified that elongated nanoparticles can present a higher non-specific cellular internalization compared with the spherical particles mainly due to the large surface areas that facilitates particle-cell interactions (Gratton et al., 2008; Huang et al., 2010; Toy et al., 2014). However, not only the shape of nanoparticles can influence their cellular internalization rates, but specially their surface characteristics, as the presence of specific ligands that can be modified to improve and drive cellular uptake (Bertrand et al., 2014).

Nanoparticles presented a negative surface charge with zeta potential varying from -30 mV for PBLG to -3 mV for PBLG-PEG-Bt-MART-1 nanoparticles, suggesting a successful coating surface of nanoparticles (Table 2). As expected, the nanoparticles containing the neutral PEG-corona also demonstrated an increase of the zeta potential value (Table 2). The amphiphilic characteristic of the block copolymers PBLG-PEG and PBLG-PEG-Bt would be arrange the hydrophobic PBLG blocks at the core of nanoparticles, while the hydrophilic block containing PEG could be orientate on the surface of nanoparticles, forming a PEG-corona (Martínez-Barbosa et al., 2009; Segura-Sánchez et al., 2010).

In addition, the coupling of antibodies at PBLG-PEG-Bt nanoparticles increased their zeta potential when compared to uncoupled PBLG-PEG-Bt. As observed in another studies related to nanoparticles and antibody conjugation, this result is also an indicative of a successful modification of the surface of nanoparticles, in addition to the increase in particle hydrodynamic radius (Barua et al., 2013; Chen et al., 2013).

Table 2. Morphological characteristics and zeta potential of nanoparticles.

Nanoparticles	DLS mean size ± SD (nm)	PDI	TEM mean size ± SD (nm)	Aspect ratio	ζ potential ± SD (mV)
PBLG	70 ± 1.3	0.17	80 ± 19.0	1.6	-30 ± 0.7
PBLG-Rhod	84 ± 1.6	0.07	97 ± 5.5	1.5	-14 ± 2.5

PBLG/PBLG-Rhod	69 ± 0.3	0.09	54 ± 15.0	1.4	-16 ± 0.2
PBLG-PEG/PBLG	44 ± 0.4	0.12	22 ± 3.2	1.3	-10 ± 1.3
PBLG-PEG/PBLG Rhod	51 ± 0.2	0.19	28 ± 4.0	1.4	-14 ± 1.5
PBLG-PEG-Bt/PBLG	54 ± 0.2	0.17	20 ± 1.5	1.2	-15 ± 0.5
PBLG-PEG-Bt/PBLG Rhod	58 ± 0.2	0.17	34 ± 8.2	1.2	-14 ± 3.8
PBLG-PEG-Bt-MART-1/PBLG Rhod	76 ± 0.6	0.20	34 ± 6.0	1.2	-3.0 ± 0.5
PBLG-PEG-Bt-IgG/PBLG Rhod	74.5 ± 0.6	0.20	33 ± 5.5	1.2	-3.2 ± 0.3

DLS: dynamic light scattering, PDI: polydispersity index, TEM: transmission electronic microscopy, SD: standard deviation, ζ potential: zeta potential.
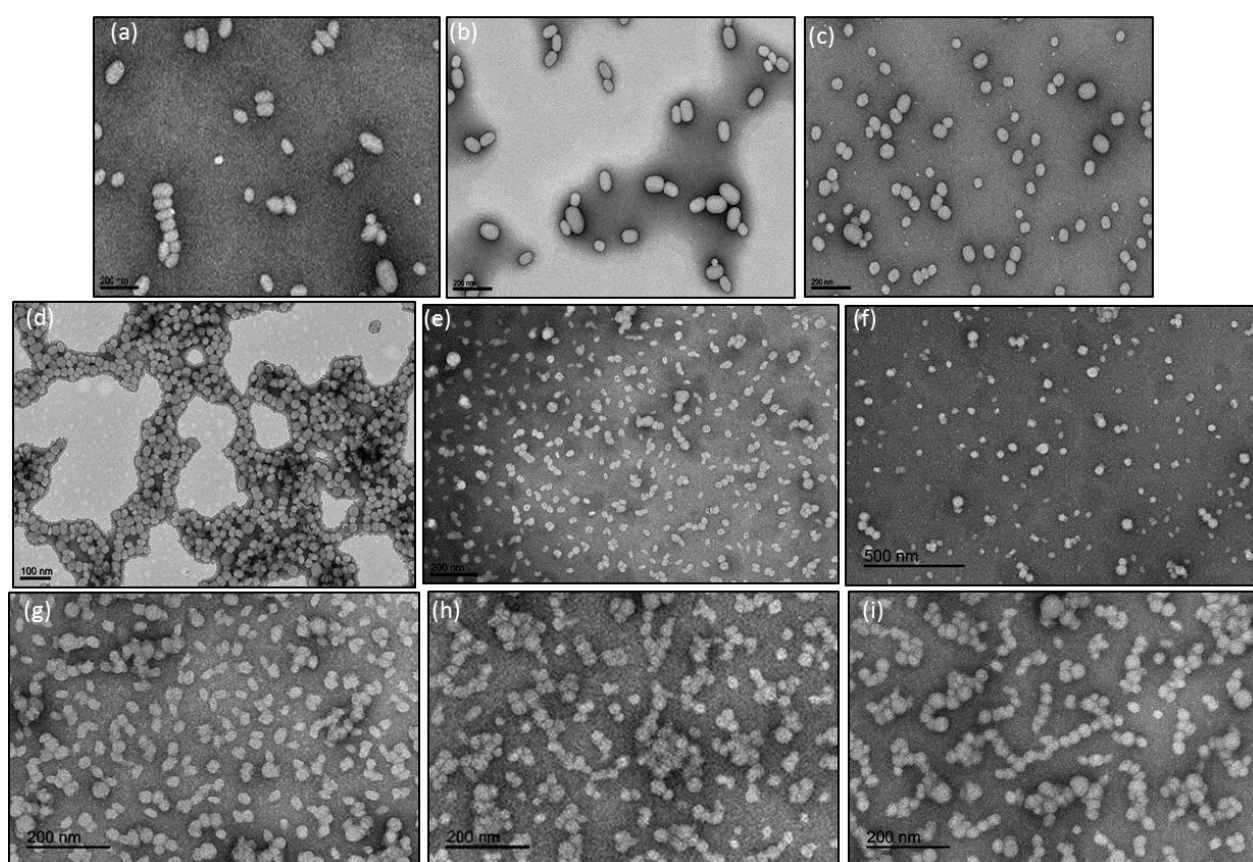
Figure 6. TEM photographs of nanoparticles obtained from the following PBLG derivates. Magnification 20000 ×. PBLG-Bz (a), PBLG-Rhod (b), PBLG/PBLG-Rhod (c), PBLG-PEG/PBLG (d), PBLG-PEG/PBLG-Rhod (e), PBLG-PEG-Bt/PBLG (f), PBLG-PEG-Bt/PBLG-Rhod (g), PBLG-PEG-Bt-MART-1/PBLG-Rhod (h) and PBLG-PEG-Bt-IgG/PBLG-Rhod (i).

The fluorescence of PBLG-Rhod and PBLG/PBLG-Rhod nanoparticles was demonstrated by the cellular uptake assay carried out in B16-GFP and HUVECs cells (Fig. 7). The mean fold changes in fluorescence intensity over control for PBLG-Rhod nanoparticles varying from 1.4 to 1.9 for HUVECs cells and 1.5 to 2.3 for B16-GFP cells. In addition, when the cells were treated with PBLG/PBLG-Rhod the mean fold changes over control approximately 1.2 for HUVECs cells, and 1.1 to 1.4 for B16-GFP cells. These results demonstrated a weak red fluorescence signal detected at cellular uptake experiments, after incubation with PBLG-Rhod and PBLG/PBLG-Rhod nanoparticles, which can be attributed to the low fluorescence intensity of the obtained PBLG-Rhod derivative. Despite of the low fluorescence observed for PBLG-Rhod nanoparticles, these nanosystems can be used on GFP expressing cells as an alternative, especially due to its relatively low cost when compared with other fluorescent labels, such as Alexa Fluor 495. In this way, this remark must be considered for further studies combining fluorescent and targeted nanoparticles, in order to obtain an optimized fluorescent PBLG derivative.
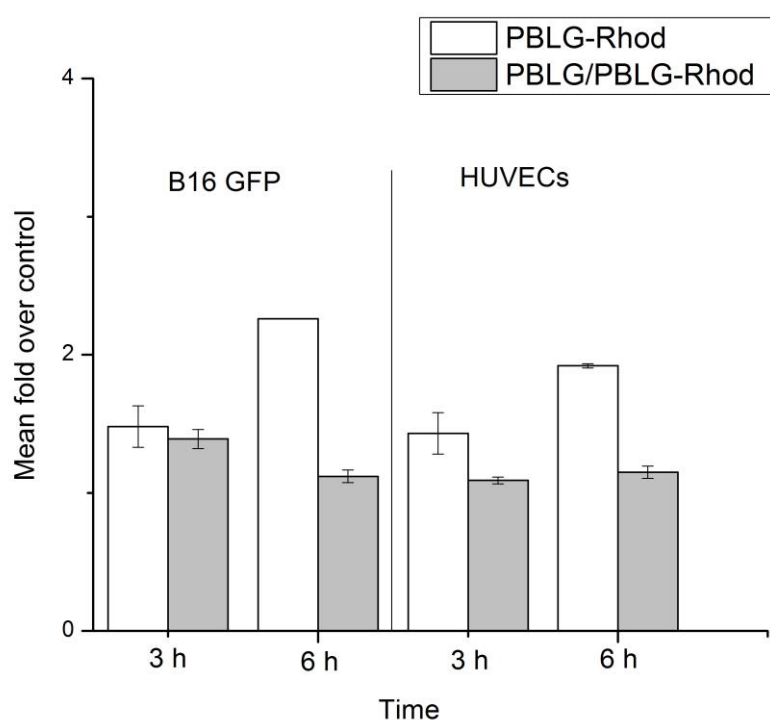
Figure 7. Cellular uptake of PBLG-Rhod (100%) and PBLG/PBLG-Rhod (10%) nanoparticles by B16-GFP and HUVECs cells. Data were expressed as fold increase over control (mean ± SD).

3.5.2.2 Functionality of the biotin grafted onto PBLG-PEG-Bt nanoparticles

The conjugation of the antibody on the surface of PBLG-PEG-Bt nanoparticles via biotin–avidin complexation was first suggested by Segura-Sanchez and coworkers (2010). This methodology to bind antibodies on the surface of nanoparticles is based on the well-described strong affinity of biotin for avidin molecule (Wright et al., 1947). The percentage of biotin available and accessible on the surface of nanoparticles prepared with PBLG-PEG-Bt was approximately 56%, corresponding a theoretical number of 190 accessible biotin molecules per nanoparticle, given that each individual nanoparticle is formed by approximately 340 PBLG-α helix chains. These results can be justified by hydrophilicity, flexibility and length (MW= 5000 g/mol) of the PEG-Bt chains, which favors biotin molecules towards on the surface of nanoparticles and their availability for avidin binding (Segura-Sanchez et al., 2010). As expected, biotin was not detected in PBLG-PEG/PBLG nanoparticles.

3.5.2.3 Specific recognition of MART-1-coupled nanoparticles

The MART-1 was chosen as a biomarker model to improve the receptor-mediated endocytosis and intracellular drug delivery to melanoma cancer cells. As show in the Figure 8, when nanoparticles were incubated with streptavidin-antibody complex, no signal of uncoupled antibodies was detected. These results demonstrated that the binding of the antibody on the surface of nanoparticles occurs mediated by streptavidin, meanwhile in the absence of streptavidin, the remaining free antibodies were observed. Similar results were found by Ramon and coworkers (2013).

The antibody binding on the surface of nanoparticles was also evidenced by the different migration profiles in *western blot* analysis of non-denatured MART-1-nanoparticles in presence or in absence of streptavidin. The broader migration profile detected for antibody conjugated to nanoparticles when compared to uncoupled antibodies. This finding can be attributed to the different morphological and surface characteristics of the MART-1-nanoparticles, which provides a heterogeneous migration profile through the electrophoresis gel. In addition, the *western blot* analysis of the non-denatured antibody-streptavidin complex showed a different migration profile when compared to the antibody conjugated to nanoparticles. As shown in Figure 4 the antibody-streptavidin complex migrates above 220 kDa, corresponding approximately to the molecular mass of streptavidin (55 kDa) plus antibody (150 kDa). These results indicate the ability of PBLG-PEG-Bt nanoparticles to bind with biotinylated antibodies through the formation of biotin-streptavidin complexes, allowing the formation of immunonanoparticles.
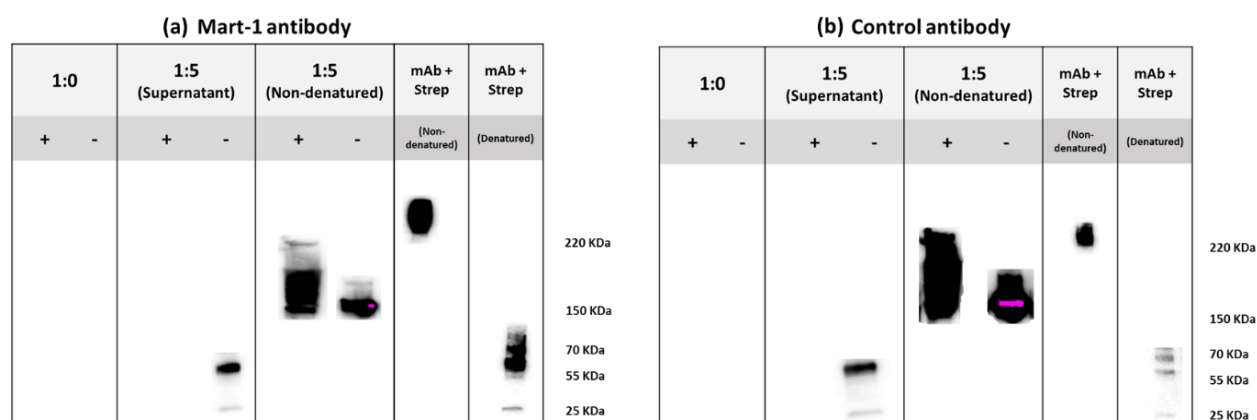
Figure 8. Western blot analysis of the remaining free antibodies found in supernatant of biotinylated nanoparticles and the migration profile of non-denatured nanoparticles containing Mart-1 antibody (a) and control antibody (b) after incubation with (+) or without (-) streptavidin. The Western blot analysis also demonstrated the migration profile of the complex antibody-streptavidin (mAb+Strep) non-denatured and denatured. The theoretical ratios of the number of nanoparticles over the number of antibody molecules were 1:0 and 1:5.
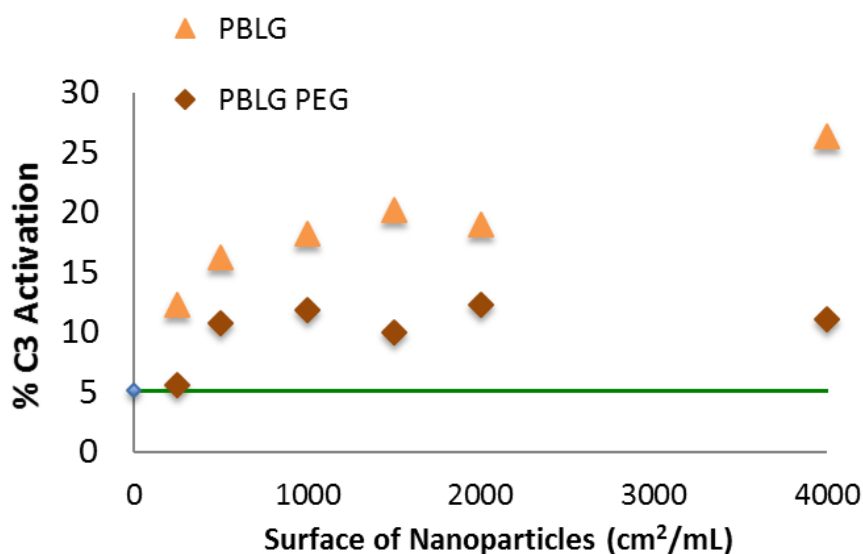
3.5.2.4 Complement activation

The complement system is a major component of the innate immune response against foreign particles and bodies that have the potential to be infectious or pathogenic (Noris & Remuzzi, 2013). A proper biodistribution and long blood lifetime of intravenously administered nanoparticles depends on the extent of their non-specific recognition and opsonization by complement system (Bertholon et al., 2006). It is also well reported that different size and surface properties of nanoparticles can directly influence their interactions with serum proteins and define their clearance from blood circulation (Moghimi & Szebeni, 2003; Lundqvist et al., 2008).

The complement component 3, commonly called C3 protein, is the major component of final pathway of complement cascade and is common to all three complement activation pathways (classical, lectin and alternative). The C3 convertase enzyme cleaves the C3 protein in fragments, C3a and C3b. The C3b is responsible for opsonization of foreign bodies, such as nanoparticles, through the covalent attachment to the particle surface, increasing the antibody response and facilitating foreign bodies clearance through the reticule endothelial system (Nilsson et al., 2007; Noris & Remuzzi, 2013). In this way, the evaluation of complement activation, independently of the pathway, can be measured by the cleavage of C3 protein. The results are represented by eletrophoregrams that generally depicts two peaks, the first related to the native C3 and the second related to the fragment C3b (Coty et al., 2016).

A prior analysis of the ability of PBLG and PBLG-PEG nanoparticles to activate the complement system was performed with samples containing similar surface areas ranging from 250 to 4000 cm^2/mL (Fig. 9). As shown in Figure 3 the complement activation in all tested concentrations were higher for PBLG nanoparticles when compared with PBLG-PEG nanoparticles. At the highest concentration, 4000 cm^2/mL, the % of activation for PBLG was

26% against 11% for PBLG-PEG nanoparticles, which indicated the stealth capability of hydrophilic PEG corona.

In addition, we evaluated nanoparticles with different surface areas, ranging from 400 to 1875 cm^2/mL, which can influence the activation of complement cascade, since the protein interactions depends on the available area of the nanoparticle (Noris & Remuzzi, 2013). The electrophoregrams and respective %CAFs for each tested nanoparticle are depicted in Figure 10. As observed, all the obtained CAF values were below 15%, whereas the positive control showed a CAF of 77%, demonstrating a low ability of these nanoparticles to activate the complement system when they are at the same polymer concentration (1.5 mg/mL) (Coty et al., 2016). In addition, the CAF for immunonanoparticles was lower than PBLG-PEG-Bt nanoparticles, indicate an increase in the furtiveness of this nanocarrier after surface modification. Nevertheless, as expected, the nanoparticles containing only PBLG at a tested surface area (S$_A$) of 470 cm^2/mL or the mixture PBLG/PBLG-Rhod (S$_A$= 700 cm^2/mL) demonstrated a higher %CAF compared to the nanoparticles containing PEG with higher surface areas, ranging from 1100-1875 cm^2/mL. These findings are also consistent with the giving stealth properties of PEG hydrophilic corona (Owens & Peppas, 2006). Besides, nanoparticles did not activate the complement cascade even after their surface modification by coupling antibodies or after the addition of fluorescent PBLG-Rhod.

Figure 9. C3 activation by nanoparticles as a function of the concentration of PBLG and PBLG-PEG. The green line represents the spontaneous activation.

Positive Control	PBLG	PBLG/PBLG-Rhod	PBLG-Rhod	PBLG-PEG/PBLG
CAF= 77%	CAF= 10.4 ± 1.3 %	CAF= 14.7 ± 3.3 %	CAF= 6.7 ± 0.5 %	CAF= 7.1 ± 0.03 %
Negative Control	PBLG-PEG/PBLG-Rhod	PBLG-PEG-Bt/PBLG	PBLG-PEG-Bt/PBLG-Rhod	PBLG-PEG-Bt-MART-1/PBLG-Rod
Spontaneous activation	CAF= 4.5 ± 0.4 %	CAF= 4.2 ± 0.4 %	CAF= 1.6 ± 0.6 %	CAF= -4.9 ± 0.02 %
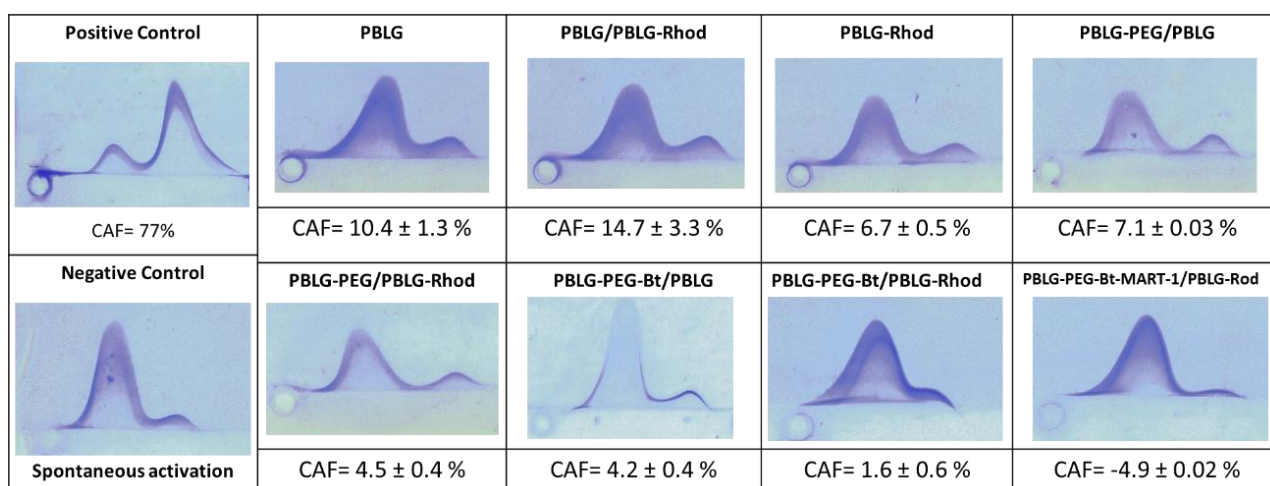
Figure 10. Electrophoregram peaks of complement activation for different PBLG nanoparticles with the respective complement activation factor (% CAF).

3.5.2.5 Receptor Expression and Cytotoxicity of nanoparticles

The evaluation of MART-1 expression on B16-GFP-melanoma and on HUVECs cell lines was performed by flow cytometer analysis after labeling cells with anti-MART-1 antibody coupled with Alexa Fluor (R) 647 at three different concentrations. The results depicted in Figure 11 a and b show an approximately 25-fold shift of the mean fluorescence of B16-GFP

melanoma cells after incubation with all tested antibody concentrations. No differences between the fluorescence mean was observed when the melanoma cells were incubated with 16 or 24 µg/mL of MART-1 antibody, indicating a saturation of the MART-1 binding sites presented on the surface of B16-GFP melanoma cells. It was also demonstrated that approximately 57% of the B16-GFP melanoma cells are positive for MART-1 receptor (Fig. 11a). These results confirm that B16-GFP-melanoma cells present the MART-1 receptors. On the contrary, HUVECs cells did not exhibited a significant fluorescence after MART-1 antibody incubation, thus this lineage was used as a negative control, since they not express MART-1 receptors.
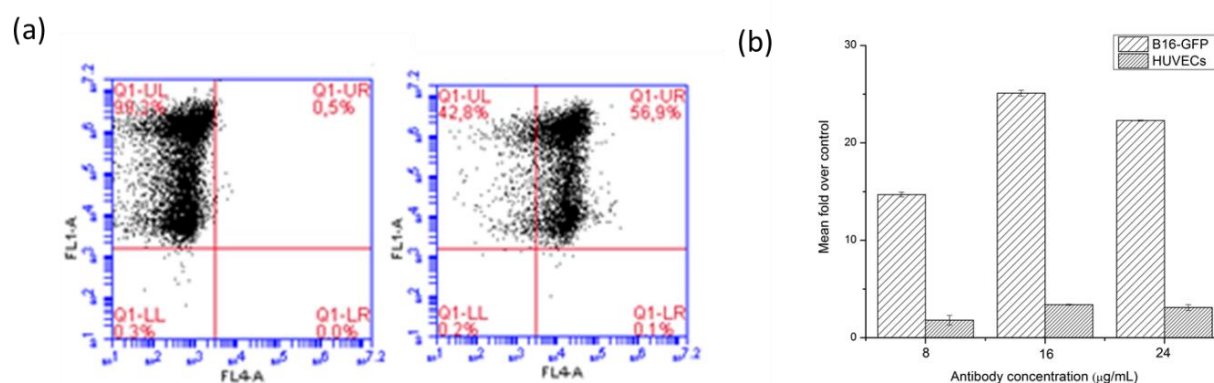
Figure 11. Evaluation of the MART-1 expression on B16-GFP cells and HUVECs cells by flow cytometer. Percentage of B16-GFP cells (MART-1 positive; upper right quadrant) and the number of viable cells shown at each time point (a). Data of fluorescence intensity are shown as mean fold over control as function of the antibody concentration (b).

The cell viability graphs for B16-GFP-melanoma cell line and HUVECs cells are depicted in Figures 12 and 13, respectively. In Fig. 12a the IC_{50} values for PBLG and PBLG/PBLG-Rhod nanoparticles were 306 ± 5.6 and 296 ± 4.2 µg/mL respectively. Regarding the non-fluorescent pegylated nanoparticles, IC_{50} values of 313 ± 4.5 and 320 ± 3.3 µg/mL were verified for PBLG-PEG and PBLG-PEG-Bt, respectively in B16-GFP cells. However, the IC_{50}

values of fluorescent pegylated nanoparticles decreased to 240 ± 2.3 and 184 ± 4.4 µg/mL for PBLG-PEG and PBLG-PEG-Bt, respectively (Fig. 12b). In addition, the nanoparticles coupled with antibody–avidin complexes, PBLG-PEG-Bt-IgG ($IC_{50}= 156 \pm 6$ µg/mL) and PBLG-PEG-Bt-MART-1 ($IC_{50}= 138 \pm 5.1$ µg/mL) demonstrated an enhancement in *in vitro* cytotoxicity against B16-GFP melanoma cells compared to uncoupled PBLG-PEG-Bt nanoparticles (Fig. 12c).

Related to HUVECs, the IC_{50} values for PBLG and PBLG/PBLG-Rhod were 236 ± 8.5 and 162 ± 4.2 µg/mL, respectively (Fig. 13a). In addition, the IC_{50} values of pegylated nanoparticles varied from 138 ± 1.3 µg/mL to 283 ± 4.3 µg/mL. Those finds suggest that the cytotoxicity profile of PBLG based nanoparticles can be affected by their composition and design of their surface. However, a significant decrease of B16-GFP and HUVECs cells viability treated with all nanoparticles formulations was only verified at concentrations above 200 µg/mL. Differently from some polymeric nanocarriers that need to be surface modified to enhancing its tolerance, for example, poly(isobutylcyanoacrylate) (PBICA) nanoparticles coated with polysaccharides (Chauvierre et al., 2007), the obtained PBLG based nanoparticles demonstrated to be well tolerated by cancerigens and normal cells.

Other studies with nanoparticles, polymerosomes and micelles based on different PBLG copolymers, also observed a low cytotoxicity of these nanocarriers when tested in normal and cancerous cells, at polymer concentrations varying from 1 to 500 µg/mL (Du et al., 2010; Upadhyay et al., 2010; Thambi et al., 2011; Goñi-de-Cerio et al., 2013). In this way, the developed PBLG nanoparticles presented a low cytotoxicity in tested cells, suggesting that these nanoparticles can be suitable for anti-cancer drug delivery.

(a)
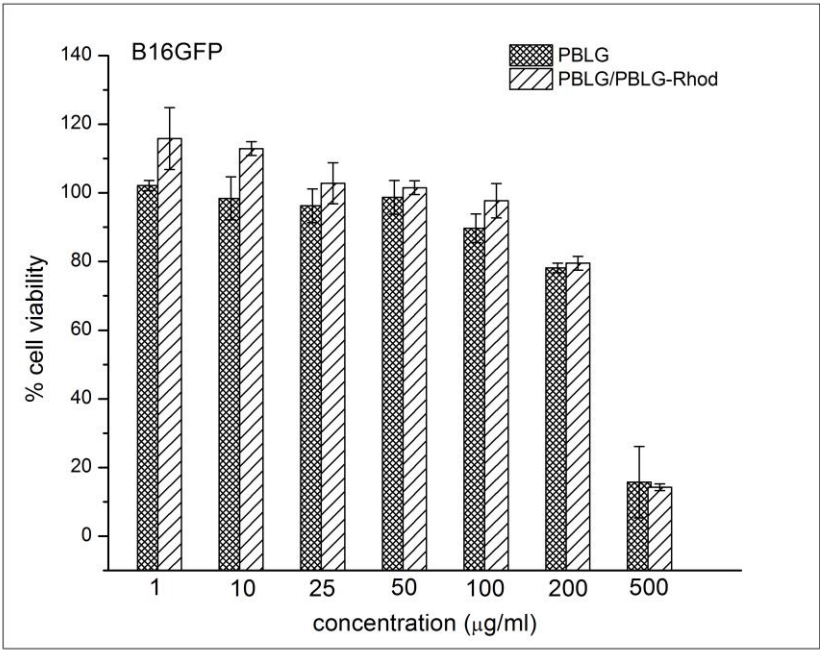
(b)

(
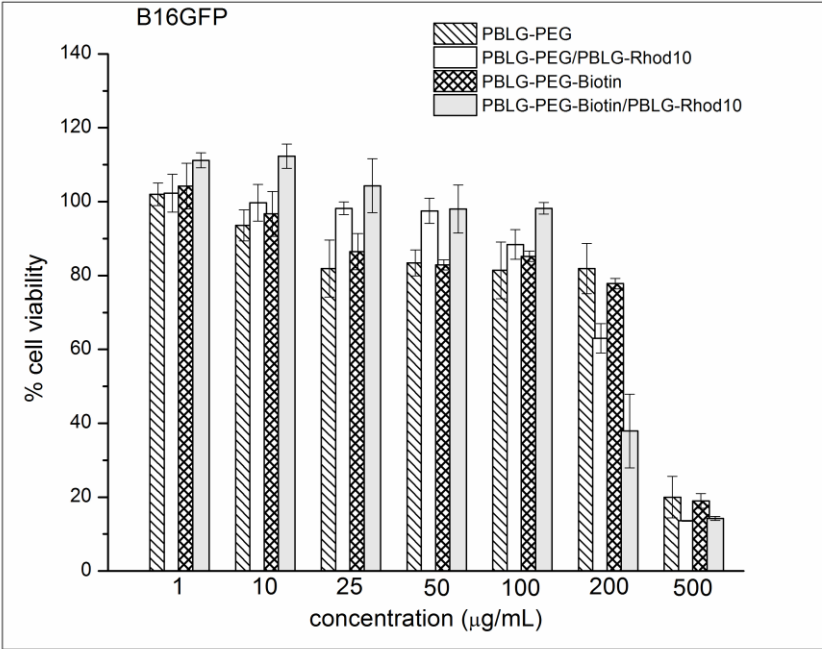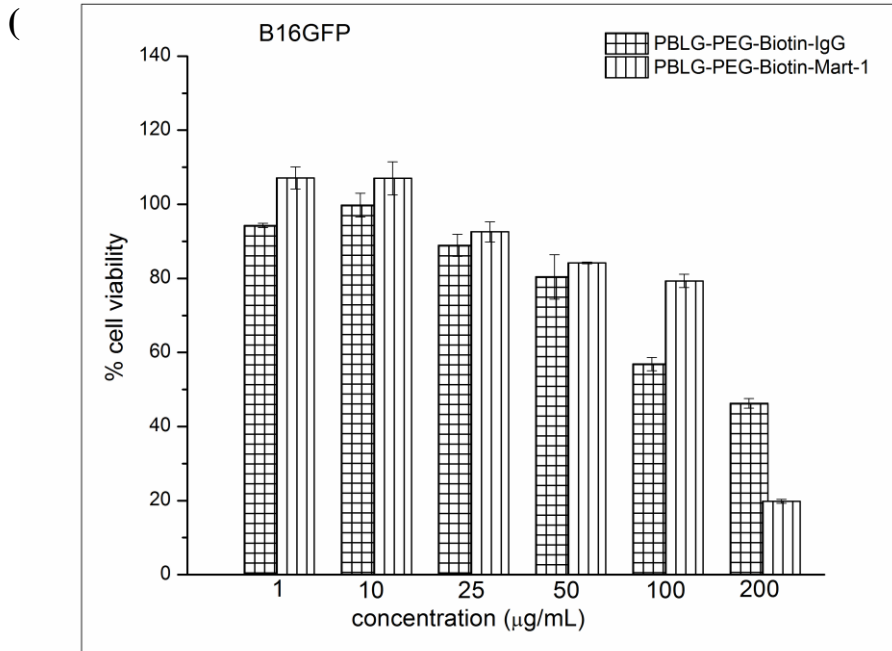
Figure 12. B16-GFP cells viability percentage after treatment with PBLG-derived nanoparticles using the MTT assay. Error bars indicate the standard deviation.

(a)

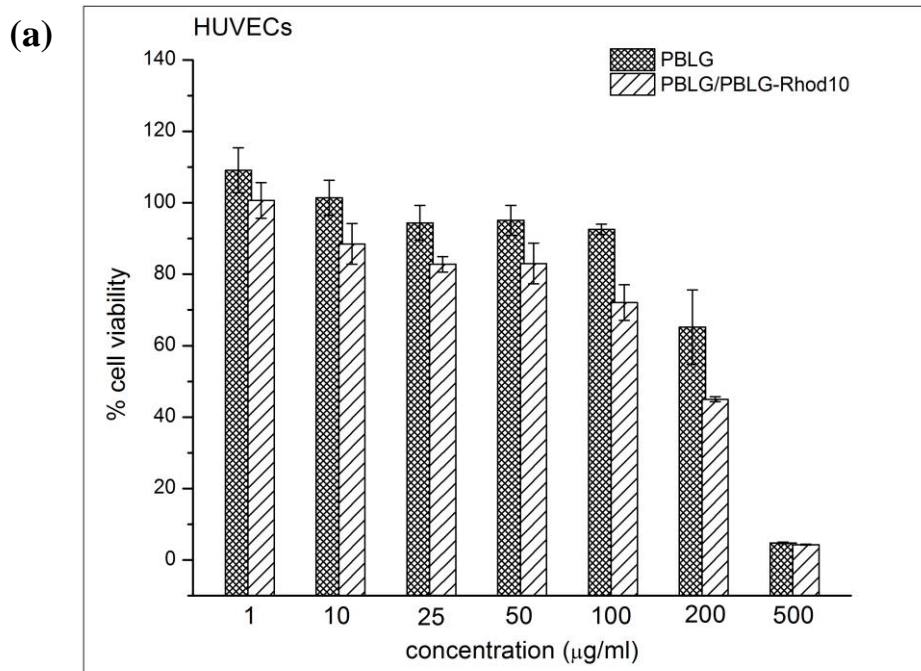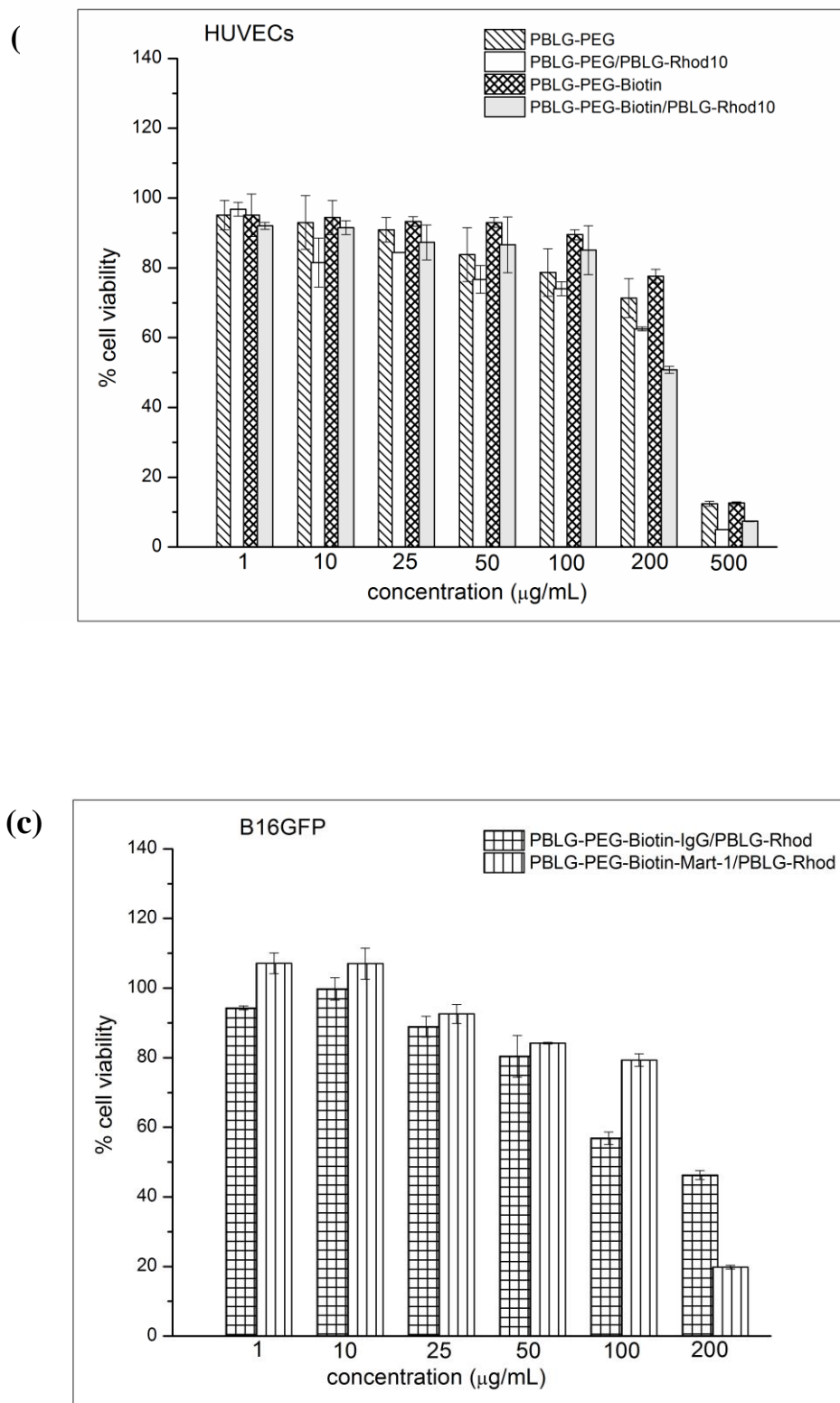**Figure 13.** HUVECs cells viability percentage after treatment with PBLG-derived nanoparticles using the MTT assay. Error bars indicate the standard deviation.
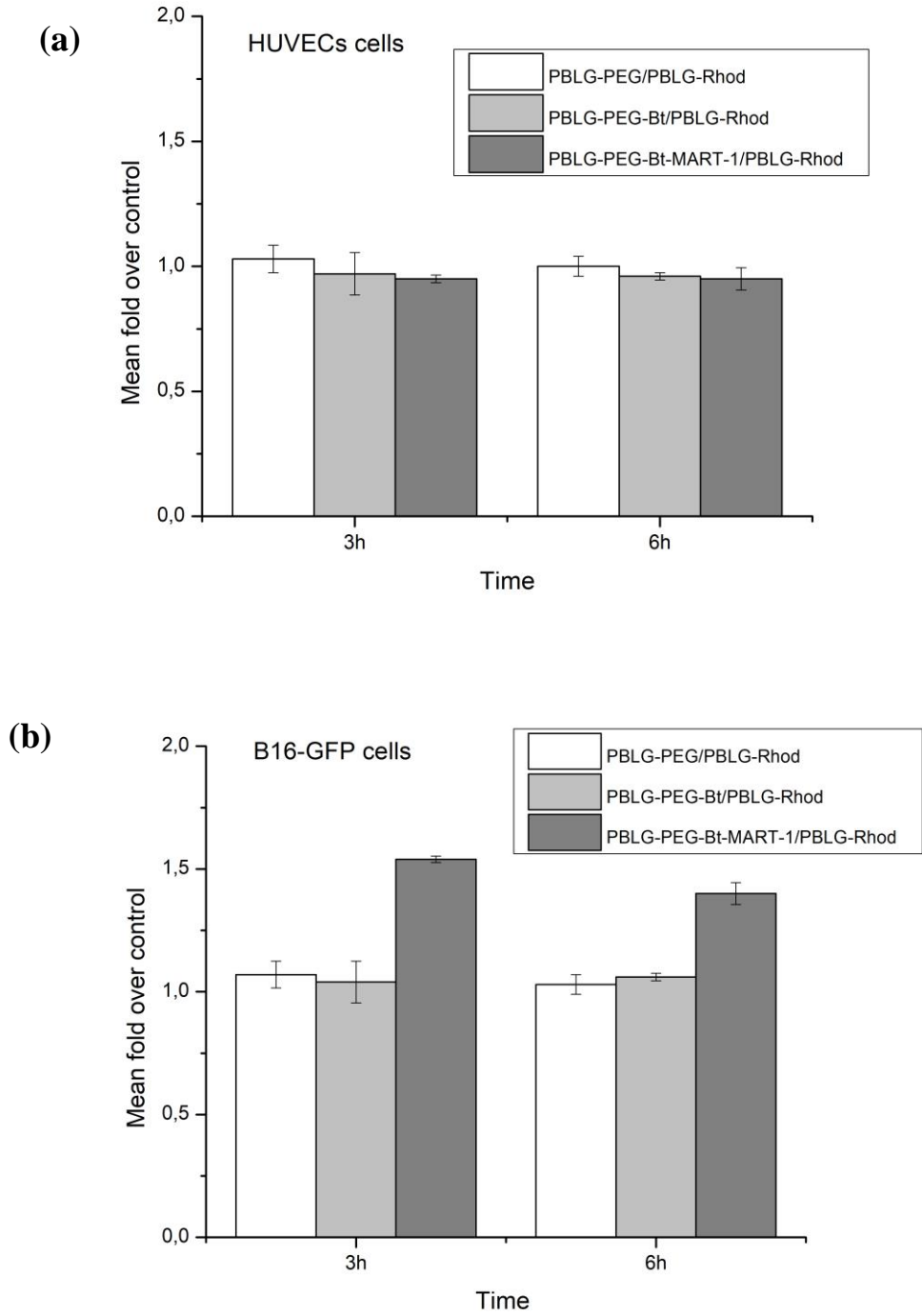
3.5.2.6 Cellular uptake of immunonanoparticles

As observed in Figure 14, the cellular uptake of PBLG-PEG-Bt-MART-1 nanoparticles by B16-GFP when compared to HUVECs cells was increased in 50% and 40% after 3 and 6 h of incubation, respectively. This result indicates a specificity of PBLG-PEG-Bt-MART-1 nanoparticles for the tested melanoma cells due to the presence of MART-1 receptor on the surface of B16-GFP cells. These results show that the B16-GFP cells could be recognized by PBLG-PEG-Bt-MART-1 nanoparticles containing only five molecules of MART-1 antibody coupled at their surface, which indicates a specificity of this target molecule for the tested melanoma cells due to the presence of MART-1 receptor on the surface of B16-GFP cells. Some studies have also shown that immunonanoparticles conjugated with antibodies in a ratio ranging from 2 to 10 antibodies per nanoparticle, can promote an effective cell-particle binding and trigger a receptor-mediated endocytosis (Funovics et al., 2004; Ho et al., 2009; García-Fernández et al., 2017). Similarly, Ramon and coworkers (2013) evaluated three different ratios of nanoparticles per antibody molecules (1:5; 1:10 and 1:20) and demonstrated that the ratio of five molecules of a specific antibody to Ewing's sarcoma, conjugated with PIBCA/chitosan nanoparticles, were sufficient to achieve cell recognition.

Ho and coworkers (2009) analyzed how the number of conjugated Herceptin antibodies per nanoparticle (1.9 to 9.4 antibodies per particle) influence on the cell-particle binding and elucidated if the binding events were monovalent or multivallent. The authors concluded that Herceptin immunonanoparticles (round shape, size of 80 nm) follow the theoretical behaviour of monovalent binding and did not presented a threshold antibody density for binding, but demonstrated that the cell-particle affinity increases linearly with increasing antibody conjugation density. In this way, the increase of the theoretical ratio number of nanoparticles/antibody molecules could also be a strategy to potencialize the specific capture

of PBLG-PEG-Bt-MART-1 nanoparticles by melanoma cells that express MART-1 antigen, but would require an excess of antibody, which significantly increases cost of the formulation.

Figure 14. Cellular uptake of PBLG-PEG/PBLG-Rhod, PBLG-PEG-Bt/PBLG-Rhod and PBLG-PEG-Bt-MART-1/PBLG-Rhod nanoparticles by HUVECs (a) and B16-GFP (b) cells. Data were expressed as fold increase over control (mean ± SD).

The high expression of MART-1 peptide in cytoplasmic organelles, specially in endoplasmic reticulum, makes this biomarker an important target for therapies that aim to delivery exogenous peptides to this organelle and increase the cross-presentation of antigens for the induction of adaptive immunity against tumor cells (Li et al., 2008; Sneh-Edri et al., 2011). Moreover, it has been reported that the treatment of melanoma patients with specific BRAF-inhibitors could increase the expression of MART-1 peptide, which can be used as an opportunity for rational combinations of systemic targeted therapy and immunotherapy for melanoma (Boni et al., 2010). In this way, the next step for this research would be to study the pathways of endocytosis of these nanoparticles and the cytoplasmic distribution of these carriers in melanoma cells for intracellular drug-delivery applications.

3.6 Conclusion

In this work, we obtained stealth, fluorescent label and site-specific nanoparticles based on PBLG derivatives in a nanoscale and homogeneous size. The furtiveness with PEG and targeting with biotin and MART-1 influenced on particle size, shape and surface charge of surface-modified nanoparticles prepared with PBLG derivatives. PBLG nanoparticles were used as a new platform to design targeted immunonanoparticles using MART-1 as a biomarker. The immunonanoparticles containing MART-1 were targeted to B16-GFP cells, not activate the complement system and present low cytotoxicity. In general, this research shed light to the optimization of important parameters on the formulation of PBLG nanoparticles, such as the fluorescence of the PBLG-derivatives and the ratio number of nanoparticles/antibody

molecules, for the development of promising systems to carry anticancer drugs to be used in melanoma therapy.

References

Barua, S. et al., 2013. Particle shape enhances specifity of antibody-displaying nanoparticles. Pnas, 110(9), pp.3270–3275.

Bertholon, I., Vauthier, C. & Labarre, D., 2006. Complement activation by core-shell poly(isobutylcyanoacrylate)- polysaccharide nanoparticles: Influences of surface morphology, length, and type of polysaccharide. Pharmaceutical Research, 23(6), pp.1313–1323.

Bertrand, N. et al., 2014. Cancer nanotechnology: The impact of passive and active targeting in the era of modern cancer biology. Advanced Drug Delivery Reviews, 66, pp.2–25.

Boni, A. et al., 2010. Selective BRAFV600E inhibition enhances T-cell recognition of melanoma without affecting lymphocyte function. Cancer research, 70, (13), pp. 5213-5219.

Cauchois, O., Segura-Sanchez, F. & Ponchel, G., 2013. Molecular weight controls the elongation of oblate-shaped degradable poly(ɤ-benzyl-L-glutamate) nanoparticles. International Journal of Pharmaceutics, 452(1–2), pp.292–299. Available at: http://dx.doi.org/10.1016/j.ijpharm.2013.04.074.

Chen, F. et al., 2013. *In Vivo* Tumor Targeting and Image-Guided Drug Delivery with Antibody-Conjugated, Radiolabeled Mesoporous Silica Nanoparticles Radiolabeled Mesoporous Silica Nanoparticles.

Chen, Y. et al., 1996. Serological analysis of Melan-A (MART-l), a melanocyte-specific. , 93(June), pp.5915–5919.

Chou, L.Y.T., Ming, K. & Chan, W.C.W., 2011. Strategies for the intracellular delivery of nanoparticles. Chemical Society reviews, 40(1), pp.233–245.

Chowdhury, R.M. et al., 2016. Cancer nanotheranostics: Strategies, promises and impediments. Biomedicine & Pharmacotherapy, 84, pp.291–304.

Coty, J.-B. et al., 2016. Serial multiple crossed immunoelectrophoresis at a microscale: A stamp-sized 2D immunoanalysis of protein C3 activation caused by nanoparticles. Electrophoresis, 37(17–18), pp.2401–2409. Available at: http://doi.wiley.com/10.1002/elps.201500572.

de Miguel, L. et al., 2014a. Poly(γ-benzyl-l-glutamate)-PEG-alendronate multivalent nanoparticles for bone targeting. International journal of pharmaceutics, 460(1–2), pp.73–82. Available at: http://www.ncbi.nlm.nih.gov/pubmed/24211357 [Accessed February 6, 2014].

de Miguel, L. et al., 2014b. Poly(γ-benzyl-L-glutamate)-PEG-alendronate multivalent nanoparticles for bone targeting. International journal of pharmaceutics, 460(1–2), pp.73–82. Available at: http://www.ncbi.nlm.nih.gov/pubmed/24211357 [Accessed September 5, 2014].

Duro-castano, A., Conejos-sánchez, I. & Vicent, M.J., 2014. Peptide-Based Polymer Therapeutics. , pp.515–551.

Funovics, M. A., et al. "MR imaging of the her2/neu and 9.2. 27 tumor antigens using immunospecific contrast agents." Magnetic resonance imaging 22.6 (2004): 843-850.

Fontaine, L. et al., 2001. New polyurethanes derived from amino acids. Synthesis and characterization of α,ω-diaminooligopeptides by ring-opening polymerization of glutamate N-carboxyanhydrides. Reactive and Functional Polymers, 47(1), pp.11–21.

García-Fernández, L., et al. "Conserved effects and altered trafficking of Cetuximab antibodies conjugated to gold nanoparticles with precise control of their number and orientation." Nanoscale 9.18 (2017): 6111-6121.

Gratton, S.E.A. et al., 2008. The effect of particle design on cellular internalization pathways. Proceedings of the National Academy of Sciences of the United States of America, 105(33), pp.11613–11618.

Gray, E.S. et al., 2015. Circulating Melanoma Cell Subpopulations: Their Heterogeneity and Differential Responses to Treatment. Journal of Investigative Dermatology, 135(8).

Ho, K., et al. "Tunable immunonanoparticle binding to cancer cells: thermodynamic analysis of targeted drug delivery vehicles." Soft Matter 5.5 (2009): 1074-1080.

Huang, X. et al., 2010. The effect of the shape of mesoporous silica nanoparticles on cellular uptake and cell function. Biomaterials, 31(3), pp.438–448.

Kamaly, N. et al., 2016. Degradable Controlled-Release Polymers and Polymeric Nanoparticles: Mechanisms of Controlling Drug Release. Chemical Reviews, 116(4), pp.2602–2663. Available at: http://pubs.acs.org/doi/abs/10.1021/acs.chemrev.5b00346.

Kawakami, Y. et al., 1997. Production of recombinant MART-1 proteins and specific anti-MART-1 polyclonal and monoclonal antibodies: Use in the characterization of the human melanoma antigen MART-1. Journal of Immunological Methods, 202(1), pp.13–25.

Kazatchkine, M., Nydegger, U., Hauptmann, G., Techniques du Complement, E d. INSERM, Paris, France, 1985.

Lammers, T. et al., 2012. Drug targeting to tumors: Principles, pitfalls and (pre-) clinical progress. Journal of Controlled Release, 161(2), pp.175–187. Available at: http://dx.doi.org/10.1016/j.jconrel.2011.09.063.

Li, Y., Wang, L. X., Yang, G., Hao, F., Urba, W. J., & Hu, H. M. (2008). Efficient cross-presentation depends on autophagy in tumor cells. Cancer research, 68(17), 6889-6895.

Liu, Y. et al., 2014. Multifunctional pH-sensitive polymeric nanoparticles for theranostics evaluated experimentally in cancer. Nanoscale, 6(6), pp.3231–42. Available at: http://www.ncbi.nlm.nih.gov/pubmed/24500240.

Lundqvist, M., Stigler, J., Elia, G., Lynch, I., Cedervall, T., & Dawson, K.A., 2008. Nanoparticle size and surface properties determine the protein corona with possible implications for biological impacts. Proc. Natl. Acad. Sci. U. S. A., 105(38), p.14265.

Manjappa, A.S. et al., 2011. Antibody derivatization and conjugation strategies: Application in preparation of stealth immunoliposome to target chemotherapeutics to tumor. Journal of Controlled Release, 150(1), pp.2–22. Available at: http://dx.doi.org/10.1016/j.jconrel.2010.11.002.

Markovic, S.N. et al., 2007. Malignant Melanoma in the 21st Century, Part 1: Epidemiology, Risk Factors, Screening, Prevention, and Diagnosis. Mayo Clinic Proceedings, 82(3), pp.364–380. Available at: http://www.sciencedirect.com/science/article/pii/S0025619611610331.

Martínez Barbosa, M.E. et al., 2008. Synthesis and ITC characterization of novel nanoparticles constituted by poly(γ-benzyl L-glutamate)-β-cyclodextrin. Journal of Molecular Recognition, 21(3), pp.169–178.

Martínez-Barbosa, M.E. et al., 2007. Synthesis and characterization of novel poly(γ - benzyl-L-glutamate) derivatives tailored for the preparation of nanoparticles of pharmaceutical interest. Polymer international, 57(April), pp.171–180. Available at: http://onlinelibrary.wiley.com/doi/10.1002/pi.2098/full.

Martinez-Barbosa, M.E. et al., 2009. PEGylated Degradable Composite Nanoparticles Based on Mixtures of PEG-b-Poly(gamma-benzyl L-glutamate) and Poly(gamma-benzyl L-glutamate). Bioconjugate Chemistry, 20(8), pp.1490–1496. Available at: http://pubs.acs.org/doi/abs/10.1021/bc900017c%5Cnpapers2://publication/doi/10.1021/bc900 017c.

Mockey, M. et al., 2007. mRNA-based cancer vaccine: prevention of B16 melanoma progression and metastasis by systemic injection of MART1 mRNA histidylated lipopolyplexes. , pp.802–814.

Moghimi, S.M. & Szebeni, J., 2003. Stealth liposomes and long circulating nanoparticles: Critical issues in pharmacokinetics, opsonization and protein-binding properties. Progress in Lipid Research, 42(6), pp.463–478.

Mora-Huertas, C.E., Fessi, H. & Elaissari, A., 2010. Polymer-based nanocapsules for drug delivery. International journal of pharmaceutics, 385(1–2), pp.113–42. Available at: http://www.ncbi.nlm.nih.gov/pubmed/19825408 [Accessed July 10, 2014].

Nilsson, B. et al., 2007. The role of complement in biomaterial-induced inflammation. Molecular Immunology, 44(1–3), pp.82–94.

Noris, M. & Remuzzi, G., 2013. Overview of complement activation and regulation. Seminars in Nephrology, 33(6), pp.479–492. Available at: http://dx.doi.org/10.1016/j.semnephrol.2013.08.001.

Owens, D.E. & Peppas, N.A., 2006. Opsonization, biodistribution, and pharmacokinetics of polymeric nanoparticles. International Journal of Pharmaceutics, 307(1), pp.93–102.

Pan, L. et al., 2012. Nuclear-Targeted Drug Delivery of TAT Peptide-Conjugated Monodisperse Mesoporous Silica Nanoparticles.

Parhi, P., Mohanty, C. & Sahoo, S.K., 2012. Nanotechnology-based combinational drug delivery: An emerging approach for cancer therapy. Drug Discovery Today, 17(17–18), pp.1044–1052. Available at: http://dx.doi.org/10.1016/j.drudis.2012.05.010.

Ponchel, G. & Cauchois, O., 2016. Shape-Controlled Nanoparticles for Drug Delivery and Targeting Applications. In Polymer Nanoparticles for Nanomedicines. Springer International Publishing, pp. 159–184.

Qi, K. et al., 2004. Determination of the bioavailability of biotin conjugated onto shell cross-linked (SCK) nanoparticles. Journal of the American Chemical Society, 126(21), pp.6599–6607.

Ramon, A.L. et al., 2013. siRNA associated with immunonanoparticles directed against cd99 antigen improves gene expression inhibition *in vivo* in Ewing ' s sarcoma. Journal of Molecular Recognition, 26(February), pp.318–329.

Riker, A. et al., 1999. Immune selection after antigen-specific immunotherapy of melanoma. Surgery, 126(2), pp.112–120.

Robert, C. et al., 2011. Ipilimumab plus Dacarbazine for Previously Untreated Metastatic Melanoma. The new england journal o f medicine original, 26, pp.2517–2526.

Rodic, S., Mihalcioiu, C. & Saleh, R.R., 2014. Detection methods of circulating tumor cells in cutaneous melanoma : A systematic review. Critical Reviews in Oncology / Hematology, 91(1), pp.74–92. Available at: http://dx.doi.org/10.1016/j.critrevonc.2014.01.007.

Saville, S.L. et al., 2013. The effect of magnetically induced linear aggregates on proton transverse relaxation rates of aqueous suspensions of polymer coated magnetic nanoparticles. Nanoscale, 5(5), pp.2152–63. Available at: http://www.ncbi.nlm.nih.gov/pubmed/23389324.

Segura-Sánchez, F. et al., 2010. Synthesis and characterization of functionalized poly(γ-benzyl-l-glutamate) derivates and corresponding nanoparticles preparation and characterization. International Journal of Pharmaceutics, 387(1–2), pp.244–252.

Silva, C.O. et al., 2016. Melanoma Prevention : Challenges and Progresses in Nanotechnology for Melanoma Prevention and Treatment. CRC Concise Encyclopedia of Nanotechnology, (May 2016), pp.453–470. Available at: http://dx.doi.org/10.1201/b19457-39.

Sioud, M. et al., 2016. Diversification of Antitumour Immunity in a Patient with Metastatic Melanoma Treated with Ipilimumab and an IDO-Silenced Dendritic Cell Vaccine. Case Reports in Medicine, 2016, pp.1–7. Available at: http://www.hindawi.com/journals/crim/2016/9639585/.

Slominski, A.T. & Carlson, J.A., 2015. Melanoma resistance: a bright future for academicians and a challenge for patient advocates. Mayo Clinic Proceedings, 89(4), pp.429–433.

Sneh-Edri, H., Likhtenshtein, D., & Stepensky, D. (2011). Intracellular targeting of PLGA nanoparticles encapsulating antigenic peptide to the endoplasmic reticulum of dendritic cells and its effect on antigen cross-presentation in vitro. Molecular pharmaceutics, 8(4), 1266-1275.

Svedman, F. C., Pillas, D., Taylor, A., Kaur, M., Linder, R., & Hansson, J., 2016. Stage-specific survival and recurrence in patients with cutaneous malignant melanoma in Europe–a systematic review of the literature., 8, 109. Clinical Epidemiology, 8, p.109.

Toy, R. et al., 2014. Shaping cancer nanomedicine: the effect of particle shape on the *in vivo* journey of nanoparticles. Nanomedicine (London, England), 9(1), pp.121–34. Available at: http://www.ncbi.nlm.nih.gov/pubmed/24354814%5Cnhttp://www.pubmedcentral.nih.gov/articlerender.fcgi?artid=PMC4057606.

Upponi, J. R.; Torchilin, V. P., Alonso, M. J.; Garcia-Fuentes, M., 2014. Passive vs. Active Targeting: An Update of the EPR Role in Drug Delivery to Tumors. In M. Alonso, M. J.; Garcia-Fuentes, ed. Nano-Oncologicals: New Targeting and Delivery Approaches. pp. 3–45.

Walker, J. M., in: Walker, J. M. (Ed.), The Protein Protocols Handbook, Springer, Totowa, NJ, USA, 1996, pp. 757–762.

Wang, R., Dworak, L.J. & Lacy, M.J., 2001. A panel immunoblot using co-incubated monoclonal antibodies for identification of melanoma cells. Journal of Immunological Methods, 249(1–2), pp.167–183.

Wright, L.D., Skeggs, H.R. & Emlen, L.., 1947. Affinity of Avidin for Certain Analogs of Biotin. Experimental Biology and Medicine, 64(2), pp.150–153.

Xie, J. et al., 2015. Nanotechnology for the delivery of phytochemicals in cancer therapy. Biotechnology Advances, 34(4), pp.343–353. Available at: http://dx.doi.org/10.1016/j.biotechadv.2016.04.002.

Zand, S. et al., 2016. Heterogeneity of Metastatic Melanoma. American Journal of Clinical Pathology, 146(3), pp.353–360. Available at: https://academic.oup.com/ajcp/article-lookup/doi/10.1093/ajcp/aqw115.

Zou, Y. et al., 2016. Self-crosslinkable and intracellularly decrosslinkable biodegradable micellar nanoparticles: A robust, simple and multifunctional nanoplatform for high-efficiency targeted cancer chemotherapy. Journal of Controlled Release. Available at: http://dx.doi.org/10.1016/j.jconrel.2016.05.060.

4 TOPICAL LIPOSOMAL-HYDROGELS FOR WOUND CARE APPROACH

4.1 Wound healing properties of β-lapachone-loaded liposomes incorporated in a biopolymer hydrogel

Autores: Sarah Brandão Palácio[a]; Marília Evellyn Dias[a]; Daniel Charles dos Santos Macêdo[a]; Rafaela de Siqueira Ferraz Carvalho[a]; Fábio José Fidélis Almeida[a]; Noemia Pereira da Silva Santos[a,b]; Francisco Carlos de Amanajás Aguiar Junior[b]; Isabella Macário Ferro Cavalcanti[a,b]; Nereide Stela Santos-Magalhães[a*]

[a]Laboratory of Imunopatologia Keizo-Asami (LIKA), Federal University of Pernambuco, Av. Prof. Moraes Rego, 1235, Cidade Universitária, 50670-901, Recife, PE, Brazil

[b]Academic Center of Vitória de Santo Antão, Federal University of Pernambuco, R. Alto do Reservatório, S/n - Bela Vista, 55608-680, Vitória de Santo Antão, PE, Brazil

*Corresponding author:

Prof. Nereide Stela Santos-Magalhães

Universidade Federal de Pernambuco (UFPE)

Laboratório de Imunopatologia Keizo-Asami (LIKA)

Av. Prof. Moraes Rego, 1235, Cidade Universitária,

50670-901, Recife, PE, Brazil

Tel: +55-81-21268587; fax: +55-81-21268485

E-mail: nssm@ufpe.br

4.2 Abstract

The aim of the present study was firstly to develop and characterize a β-lapachone-loaded multilamellar liposomes incorporated in a polymeric blend hydrogel of *Zoogloea* sp. polymer (ZBP) and hydroxyethylcellulose (HEC) (β-lap-Lipo/ZBP/HEC). It also set out to evaluate the *in vitro* kinetics of β-lap from this formulation, as well as its wound healing activity in rats. β-lapachone-loaded multilamellar liposomes were prepared by thin film hydration followed by sonication method. After the preparation, the liposomes were incorporated in a polymeric blend ZBP/HEC. The β-lap-Lipo/ZBP/HEC were characterized by pH, rheological and β-lap content. The *in vitro* release kinetics profile of β-lap from formulations was evaluated using Franz diffusion cells. To investigate the wound healing process, open dermal wounds in male Wistar rats were treated with β-lap-Lipo/ZBP/HEC for 14 days, using ZBP/HEC hydrogel as control. After the sacrifice of the animals, skin samples were processed for histological analysis. With regard to the stability of β-lap-Lipo/ZBP/HEC formulations, no significant changes in pH and rheological behavior were verified during 90 days. The *in vitro* kinetics results showed that β-lap release from β-lap-Lipo/ZBP/HEC was slower compared to β-lap-Lipo and β-lap/ZBP/HEC. In the *in vivo* experiments, ZBP/HEC treatment provided a suitable environment, promoting an increase in fibroblasts, inflammatory cells, vessels and collagen densities during the proliferative phase compared to the untreated animal group. In addition, β-lap-Lipo/ZBP/HEC promoted an increase in local angiogenesis and a decrease of inflammation at the wound site. These results demonstrate that ZBP/HEC itself has a wound healing potential and the incorporation of β-lap-loaded liposomes promoted a synergic effect, specially the β-lap-Lipo/ZBP/HEC60 formulation.

Keywords: β-lapachone; liposomes; *Zoogloea*; biopolymer; hydrogel; wound healing.

4.3 Introduction

Wound healing is a complex and well-organized process in which different cell populations and cytokines are involved. Disturbances in this balanced repair process caused by burn injuries, pressure ulcers and chronic diseases, such as diabetes, can affect wounds that fail to heal in an orderly manner, resulting in chronic or hard-to-heal wounds [1,2]. The current treatment of acute and chronic wounds is generally based on the application of dressings and administration of local drugs. Nowadays, wound dressings are used not just as protective agents, but can also contain bioactive substances, such as drugs, growth factors and peptides that help to stimulate and modulate the physiology of the wound environment, maintain humidity at the wound–dressing interface, promote debridement and control infections [3].

In the global market, modern wound dressings are generally based on synthetic or natural polymers in different forms, such as films, foams and hydrogels [4]. Despite the great flexibility in engineering synthetic polymers, natural polymers have many advantages over them, such as the high moisture content, biocompatibility, non-toxicity, low immunogenicity, ability to integrate with living tissues, biodegradability and low cost [5]. Bacterial cellulose (BC) is a natural polymer with hydrogel characteristics used in the treatment of burns and chronic wounds, specially due to its great mechanical strength, high water-holding capacity and pronounced permeability to gases and liquids, which facilitates the autolytic debridement of necrotic tissue [3]. BCs can be produced by many types of non-pathogenic microorganisms, including *Zoogloea* [6].

The bacteria *Zoogloea* sp. can produce a cellulosic extracellular polysaccharide from sugarcane molasses. This biopolymer is able to form a gelatinous matrix, with hydrogel characteristics [6]. Due to its suitable physicochemical characteristics and biocompatibility *in vitro* and *in vivo* [7,8], *Zoogloea* sp. biopolymer (ZBP) has been used for many applications in the biomedical field, such as a bulking agent in ophthalmology [9], artery angioplasty [10] and

wound healing [11]. Studies have shown that the cellulosic polysaccharide film of *Zoogloea* sp. can reduce healing time and control local infection, representing an effective adjuvant therapy for the treatment of wounds [11,12].

Advanced approaches to wound healing therapies include the use of growth factors [13], endogenous molecules, such as nitric oxide [14] and natural products from medicinal plants [15], such as β-lapachone [16,17]. β-lapachone (β-lap) is a naphthoquinone currently obtained by semi-synthesis derived from lapachol, a molecule isolated from the bark of the *Tabebuia avellanedae* tree. β-lap is considered one of the most promising molecules of the lapachone family and exhibits important biological anti-inflammatory [18], antibacterial [19] and wound healing properties among others [16,17]. The topical application of β-lap for wound healing demonstrated that this molecule at low doses increased the proliferation and migration of cells involved in the healing process, accelerating wound repair [16,17]. Notwithstanding the beneficial biological effects of β-lap, its physicochemical characteristics, such as low solubility in water and low bioavailability, are a drawback for systemic and topical applications [20].

Liposomal formulations have been employed to increase the efficiency of drug release and prolong the action of active substances topically administered for wound healing [21]. Although the topical delivery of drugs loaded in liposomes is very promising, the effectiveness of the system depends greatly on the rheological properties of the liposomal dispersion, and the choice of appropriate vehicles may affect drug performance *in vivo*. Despite the experimental use of liposome dispersions to perform drug permeation studies using skin, clinically, the semisolid dosage form is more suitable than an aqueous dispersion for restricting the application site to a certain area of skin. The aqueous environment of the liposomes favors their incorporation into a hydrogel semisolid vehicle, forming a liposome-loaded-hydrogel formulation. The suggested medical applications for these drug delivery systems have focused on tissue engineering/tissue repair or replacement [22,23].

Drug-loaded liposomes-in-hydrogel formulations have advantages over other conventional formulations such as creams, ointments and gels because they act as a drug reservoir and provide a controlled local drug delivery in the skin, increasing the concentration of drugs in the skin layers and at the same time slow down the systemic absorption of drugs. In addition, the application of this system as a wound dressing can maintaining the moist environment of the wound, necessary for cell activity and migration [15,21,23].

Based on these findings, the aims of the present study were to develop and characterize β-lap-Lipo/ZBP/HEC hydrogel formulation, evaluate the *in vitro* kinetics of β-lap from this formulation, as well as the wound healing property of this system in full-thickness excisional wounds in male Wistar rats. This animal model is useful and suitable for determining rates of healing, the extent of re-epithelization, angiogenesis and histological organization, including collagen distribution in the granulation tissue [24]. Translational animal model studies of wound healing using male rodents of outbred strains are attractive for wound healing studies because of their availability, low cost, ease of handling and less hormonal influence compared to female models [25].

4.4 Materials and Methods

4.4.1 Reagents

β-lap, obtained from lapachol by a semi-synthetic route, was supplied by Dr. Alexandre Goes (Department of Antibiotics, UFPE, Recife, Brazil). Cholesterol (Chol) was purchased from Sigma-Aldrich (St. Louis, USA) and soybean phosphatidylcholine (PC) (98% Epikuron 200) was purchased from Lipoid GMBH (Ludwigshafen, Germany). Solvents and other chemicals were supplied by Merck (Darmstadt, Germany).

Membranes consisted of a glucose exopolysaccharide produced by *Zoogloea* sp. (97.7% purity) were supplied by Polisa (Biopolymers for Health, Carpina, PE, Brazil). The synthetic

hydroxyethylcellulose (HEC), the humectant propylene glycol, methylparaben and propylparaben were purchased from Henrifarma (São Paulo, SP, Brazil).

4.4.2 Preparation of β-lap-loaded liposomes

Multilamellar liposomes (MLV's) containing β-lap (β-lap-Lipo) were prepared using the thin lipid film method [19]. Briefly, lipids at 234 mM (PC:Chol, 8:2) and β-lap (1 mg/ml) were dissolved in a mixture of $CHCl_3$:MeOH (3:1 v/v) under magnetic stirring. The solvents were removed under pressure for 60 min (37 ± 1 °C, 80 rpm) and the thin lipid film were formed. This film was hydrated with 5 ml of pH 7.4 phosphate buffer solution, obtaining β-lap-loaded liposomes at a ratio of 1:57 drug:lipid. The liposomal dispersion was then sonicated (Vibra Cell, Branson, USA) at 200 W and 40 Hz for 10 s to uniform the size of the MLV's.

4.4.3 Preparation of β-lap-Lipo/ZBP/HEC hydrogels

The *Zoogloea* sp. biopolymer (ZBP) hydrogel was prepared by the homogenization of the bacterial cellulose membrane in a laboratory reactor (Ultra-Turrax® T25, Jankel and Kunkel, Staufen, Germany). The final polysaccharide concentration was 0.8% (w/w), calculated by the difference of weight of the gel and the dried material after freeze-drying. The blended ZBP/HEC hydrogel was prepared by adding HEC, propylene glycol, methylparaben and propylparaben in ZBP (0.8%) (w/w). The final concentrations of the components in the blend were as follows: HEC 1% (w/w); propylene glycol 10% (w/w), methylparaben 0.2% (w/w), propylparaben 0.02% (w/w) and water 88.2% (w/w). Next, the mixture was allowed to swell over-night and then homogenized under mechanical stirring (Stirrer 51B, Yamato, Tokyo, Japan) for 15 min in a water bath at 60 °C.

In order to obtain β-lap-Lipo/ZBP/HEC hydrogels, β-lap-loaded liposomes were incorporated into previously prepared ZBP/HEC hydrogel at three different concentrations by

mixing them in the gel, until a homogeneous distribution was attained. Three different β-lap-Lipo/ZBP/HEC were prepared as follows: β-lap-Lipo/ZBP/HEC15 (15 µg/g of β-lap; 2.5 mg/g of lipids); β-lap-Lipo/ZBP/HEC30 (30 µg/g of β-lap; 5.1 mg/g of lipids); β-lap-Lipo/ZBP/HEC60 (60 µg/g of β-lap; 10.2 mg/g of lipids). The β-lap concentrations encapsulated into multilamellar liposomes and incorporated in ZBP/HEC hydrogel was established based on *in vivo* wound healing studies carried out by Kung et al. [16] and Fu et al. [17].

4.4.4 Characterization of β-lap-loaded liposomes

Liposomes were characterized and the parameters analyzed were pH, mean particle size (Ø), polydispersity index (PDI), zeta potential and drug encapsulation efficiency (%EE). Vesicle size and size distribution (PDI) analyses were carried out using photon correlation spectroscopy (Beckman Coulter Delsa™ Nano S Particle analyzer). Zeta potential was measured at 25 °C using the electrophoresis technique (Malvern Zetasizer Nano ZS90, Malvern Instruments Ltd., Worcestershire, UK). In all tests, samples of liposome dispersions were appropriately diluted in purified water and the results represent the mean of three determinations.

β-lap concentration encapsulated into liposomes was determined using a modified HPLC method [26]. The chromatographic analysis was performed on HPLC equipment (Aliance 2695, Waters, Milford Massachusetts, USA) coupled to a photodiode array (PDA) 2998 (Waters, Milford Massachusetts, USA), operated at 256 nm. Reversed phase column C18 (250 mm × 4,6 mm, 5 mm, XBridge™ Waters) was used with a mobile phase consisting of a methanol:aqueous solution of TFA 0.05% (70:30, v/v), at a flow rate of 0.9 ml/min at 37 ºC and injection volume of 50 µl. The β-lap curve was prepared from dilutions of a standard solution (0.4 mg/ml) obtained final concentrations ranged from 0.2 to 2 µg/ml.

For the drug content evaluation, an aliquot of liposomal sample (50 µl) was diluted in methanol (50 ml). The solution was submitted to an ultrasound bath for 15 min, centrifuged at 4.000 rpm for 10 min, filtered (0.22 mm filters, Millex®, Millipore, Massachusetts, USA) and injected into the HPLC system at 256 nm. β-lap content was determined using the Eq. (1):

$$\%\beta - \text{lap content} = \frac{\text{Measured } \beta-\text{lap amount}}{\text{Theoretical } \beta-\text{lap amount}} \times 100 \qquad (1)$$

%EE of β-lap in liposomes was determined by the ultrafiltration/ultracentrifugation technique using Ultrafree® units (Amicon Ultra Centrifugal Filters; Millipore, Billerica, MA). Samples of liposomes were inserted into filtration units and submitted to ultracentrifugation at 14000 rpm for 1h. The concentration of β-lap in the ultrafiltrate (β-lap$_{filtrate}$) was determined by HPLC and the encapsulation efficiency (%) was calculated using Eq. (2) and presented as the percentage of the initial drug content used to prepare the liposomes.

$$\%EE = \frac{\beta-\text{lap content} - \beta-\text{lap filtrate}}{\beta-\text{lap content}} \times 100 \qquad (2)$$

In addition, the pH of liposomal dispersions was measured in undiluted samples with a glass electrode attached to a digital pH meter (Bioblock Scientific 99622, Prolabo, Paris, France) at room temperature.

4.4.5 Characterization and stability of β-lap-Lipo/ZBP/HEC hydrogels

4.4.5.1 Determination of β-lap content in β-lap-Lipo/ZBP/HEC hydrogels

Initially, 0.5 g of β-lap-Lipo/ZBP/HEC hydrogels was transferred to a 50-ml volumetric flask and completed with MeOH. The sample was sonicated in an ultrasound bath (Unique®, Indaiatuba, Brazil) for 15 min. Subsequently, the dispersions were centrifuged (Kubota® KR-20000T, Tokyo, Japan) at 14.000 rpm for 10 min. Finally, supernatant aliquots were filtered

(PVDF Merck-Millipore® Milex-GV, pore size 0.22 μm, Darmstadt, Germany) and the determination of β-lap was performed using the HPLC methodology described above.

4.4.5.2 Rheological behavior and pH

Rheological measurements were performed at 25 °C using a controlled stress rheometer MCR 301 (Anton Paar, Graz, Germany) equipped with a plate-plate geometric cell (diameter = 25 mm and gap = 1 mm). The flow curves were recorded by a steady state rotational flow with shear rate sweep ranging from 10^{-3} to 10^2 s^{-1}. The viscosity data were recorded point by point with 3-sec steps. The samples were analyzed over 90 days.

The shear viscosity of the gels was fitted using the Cross model [27] by the Eq. (3):

$$\eta_{a=}\eta_\infty + \frac{\eta_0-\eta_\infty}{1+(\alpha_c\gamma)^m} \tag{3}$$

where η_a is the apparent viscosity at shear rate, η_∞ is the infinite shear rate viscosity, η_0 is the zero-shear rate viscosity, γ is the critical shear rate, where the slope of the relationship η_a and γ drops (namely the fluid transits from Newtonian to power law behavior), m is the power law index (n−1) and α_c is a constant associated with the rupture of linkages. In order to estimate the parameters η_0, γ, m (η_∞ was set equal to the viscosity of water) of the Cross model, nonlinear regression analysis was carried out using the PDAWREGR V03.40 of RHEOPLUS software package (Antoon Paar, Germany).

The pH of liposomal hydrogels was measured as described above over 90 days.

4.4.5.3 In vitro release kinetics

The release kinetics of β-lap from formulations were performed using an automatic Franz-cell diffusion apparatus (Hanson Vision® MICROETTE™ Plus,

Chatsworth, EUA) with a cross-sectional surface area of 1.86 cm^2 and a receptor compartment volume of 7 ml. Cellulose acetate membranes (MWCO 10000 KDa, Fisher Scientific$^®$ Pittsburgh, USA) were inserted between the donor and receptor compartments. Phosphate buffer solution (0.1 M, pH 7.4) containing 0.5% (m/v) of Tween$^®$ 80 was used as receptor fluid to ensure sink conditions. The system was maintained at 37 ± 0.5 °C with constant magnetic stirring at 350 rpm. An aliquot of β-lap-Lipo (50 µl), β-lap-ZBP/HEC (0.5 g) or β-lap-Lipo/ZBP/HEC (0.5 g) was placed on the surface of the cellulose acetate membrane in the donor compartment. All the samples used for *in vitro* release studies contained the same amount of β-lap (50 µg). At regular time intervals, up to 24 h, 1 ml of the receptor medium was withdrawn and replaced by an equal volume of fresh medium. The withdrawn samples were filtrated (PVDF Merck-Millipore$^®$ Milex-GV, pore size 0.22 µm, Darmstadt, Germany) and β-lap content determined using the HPLC methodology described above. Drug release data were analyzed on the basis of Fickian release kinetics, according to the Higuchi kinetics model [28] using Eq. (4).

$$Q_t = k \times \sqrt{t} \qquad (4)$$

where, Q_t is the mass of β-lap released at a determined time (t), Q_0 is the initial mass of β-lap in the receptor compartment and k is the kinetic rate constant. Release rates were calculated by linear regression analysis using Origin 8.5 software. The correlated determination coefficient (r^2) was used to test the applicability of the release model.

4.4.6 *In vivo* wound healing activity of β-lap-Lipo/ZBP/HEC hydrogels

Healthy adult male Wistar rats (*Rattus norvegicus albinos*) weighing between 200 g and 300 g were furnished by the biotherium of Nutrition Department at Federal University of Pernambuco (Recife, Brazil). This study was approved by the Ethics Committee Animal Experimentation of the Federal University of Pernambuco (UFPE), under Protocol

#23076.017434/2012-11, complied with ARRIVE [29] and national guidelines for biomedical research. Fifty-four animals were randomly divided into six groups of nine animals and were kept in groups of three per cage with free acess to water and food under 12/12 hour dark-light cycles. The rats were anesthetized by the intraperitoneal injection of ketamine hydrochloride at 0.1 ml per 100 g of body weight and xylazine hydrochloride at 0.05 ml per 100 g of body weight for the induction of extended analgesia and immobility. The back of the rat was shaved and then sterilized using an alcohol swab. Full-thickness excisional wounds using a sterile biopsy punch (6 mm diameter) were created on the backs of rats to prevent self-leaking. In the test groups, after wounding, the animals were treated every 2 days with 0.5 g of the gel formulations: ZBP, ZBP/HEC or β-lap-Lipo/ZBP/HEC hydrogels at three different concentrations of β-lap 15, 30 and 60 µg/g. Nine animals were used as a control and did not received any treatment.

Three, seven and fourteen days post-wounding, 3 animals in each group were sacrificed by applying the anesthesic urethame by the intraperitoneal route in a lethal dose of 1.25 g/Kg. Immediately afterwards, a fragment containing the surgical wound, in full extention and depth, was removed using a scalpel for histological examination.

4.4.7 Histological examination

Skin samples (approximately 1 x 1 cm^2) containing the wound areas were collected at 3, 7 and 14 days post-wounding and fixed in 10% formaldehyde for histological analysis. The samples were dehydrated in ethyl alcohol at increasing concentrations, diaphanized by xylene, impregnated and embedded in paraffin. The blocks were cut by a microtome set to deliver 5 µm slices. The resulting slices were placed on slides with albumin and kept in an oven set at 37 °C during 24 h for drying.

The samples were stained with hematoxylin-eosin (HE) for counting inflammatory cells, fibroblasts and vessels. For evaluation of total collagen fibers the slides were stained with

picrosirius-red. Histological images were captured by digital camera (Moticam 3000) coupled to an optical microscope (Nikon E-200) under a fixed field of focus and clarity, yielding 10 fields per slide with a final magnification of 400×. Photomicrographs were evaluated using the ImageJ software version 1:44 (Research Services Branch, US National Institutes of Health, Bethesda, USA.), The plugins "color deconvolution", "cell counter" and "threshould" were used in the cell count and quantification of total collagen fibers in histological sections.

4.4.8 Statistical analysis

Results are expressed as the mean ± standard deviation and the 5% significance level ($p < 0.05$) adopted. Comparisons between means in release kinectics were performed using analysis of variance (ANOVA) followed by Tukey's post-test. The data obtained from histomorphometry were statistically compared using Student's t test.

4.5 Results and discussion

4.5.1 Characterization of β-lap-loaded multilamellar liposomes

The multilamellar vesicles (MLVs) containing β-lapachone (β-lap-Lipo) were prepared with 234 mM of total lipid concentration and β-lap at 1 mg/ml, which correspond to a 1:57 drug/lipid ratio. β-lap-Lipo presented a mean size diameter of 1040 ± 20 nm, PDI < 0.5, a zeta potential of -2.1 ± 0.4 mV and pH 7.4. As expected, the zeta potential showed that the vesicles have neutral surface charge, since the lipids used for their preparation were uncharged lipids. The liposomal dispersion also showed a high β-lap encapsulation efficiency (97 ± 1.65%), which can be explained by the high hydrophobicity of the drug that is embedded in the phospholipid bilayers of MLVs at a drug:phospholipid molar ratio of 1:57.

The characteristics of the liposomes developed in our study are in agreement with those expected for liposomes incorporated into hydrogel systems for wound healing applications such

as multilamellarity and micrometer size [21,23,30]. The micrometer size of MLVs is an important factor in promoting a higher skin deposition of the drugs for an enhanced localized activity with fewer side effects [21].

4.5.2 Characterization and stability of β-lap-Lipo/ZBP/HEC hydrogels

4.5.2.1 Determination of β-lap content

The β-lap content was determined after incorporation of β-lap-Lipo into ZBP/HEC hydrogels to verify a possible drug loss during the process. Three different β-lap-Lipo/ZBP/HEC formulations were evaluated and the β-lap content was as follows: $100.5 \pm 1.06\%$, $100.6 \pm 1.8\%$ and $101.9 \pm 1.4\%$ for β-lap-Lipo/ZBP/HEC15, β-lap-Lipo/ZBP/HEC30 and β-lap-Lipo/ZBP/HEC60, respectively.

4.5.2.2 Rheological behavior and pH

The rheological behavior and stability of β-lap-Lipo/ZBP/HEC during 90 days of storage at 4 ℃ are shown in Fig. 1. The Fig. 1a-e shows the shear viscosity of the formulations as a function of the shear rate. The experiment illustrates the rheological behavior of β-lap-Lipo/ZBP/HEC at three different lipid concentrations (2.5, 5.1 and 10.2 mg/g) in hydrogels. Viscosity/shear rate graphs clearly showed a shear thinning behavior of all formulations and also the effect of lipid content on shear viscosity during storage time (Fig. 1a-c). The liposome-hydrogel formulations at 2.5 and 5.1 mg/g depicted a greater variation in shear rate viscosity values at evaluated times when compared to the liposome-hydrogel formulations at 10.2 mg/g, which could indicate a slightly lower rheological stability at lower lipid concentrations (Fig. 1a-c).

The effect of lipid concentration and storage time on the viscosity of the β-lap-Lipo/ZBP/HEC hydrogels is shown in Fig. 1d,e and even better demonstrated in Fig. 1f, which

represents the zero shear rate viscosity, estimated by the Cross model, as a function of lipid concentration. The presence of liposomes in hydrogels at different lipid concentrations of 2.5, 5.1 and 10.2 mg/g contributed to 4.3, 2.0 and 1.6-fold increases, respectively, in the zero rate viscosity on day 1, when compared to the ZBP/HEC hydrogel (1421 Pa.s). On the other hand, when the zero rate viscosity of liposome-hydrogels was compared between days 1 and 90, a 2.4-fold increase was observed for the formulation with the highest concentration of lipids (10.2 mg/g), whereas for formulations at the low lipid concentrations of 2.5 and 5.1 mg/g, respective decreases of 3.7 and 1.7-fold were found (Fig. 1f). Between days 1 and 90, the increase in zero shear rate viscosity and the low variation in shear viscosity behavior, at the highest lipid concentration (10.2 mg/g), suggest that the increase in lipid content of the liposome-hydrogel system could improve the storage stability of the formulation. In a similar way, Mourtas et al. [22] studied the effects of multilamellar liposomes on rheological properties of a hydrogel and demonstrated that the storage modulus increased with increasing liposome loading.

In summary, the liposomes seemed to stabilize the hydrogel network in the same way that the high viscosity of hydrogel and its polymer network is expected to preserve the original liposomal size and prevent leakage of originally entrapped drug [15]. These findings suggest that the blend containing the thickening agents HEC and ZBP is stable and suitable for incorporating multilamellar liposomal dispersions intended for topical use.

The pH stability of the β-lap-Lipo/ZBP/HEC hydrogels was also monitored over 90 days. As expected, there were no significant changes in the pH values during storage time. The pH values obtained were 6.6 ± 0.04; 7.0 ± 0.02 and 7.2 ± 0.11 for the formulations 2.5, 5.1 and 10.2 mg/g, respectively. The pH of the ZBP and ZBP/HEC hydrogel were 5.5 ± 0.02 and 6.2 ± 0.06, respectively. The pH of liposomal gels was suitable for topical application and compatible with the pH of the wound bed that ranges from neutral to alkaline [31].

4.5.2.3 In vitro release studies

Fig. 2 shows the *in vitro* release profile of β-lap from liposomes (β-lap-Lipo), hydrogel (β-lap/ZBP/HEC) and the liposomal dispersion incorporated into the hydrogel (β-lap-Lipo/ZBP/HEC).

The release profiles of β-lap-Lipo and β-lap-Lipo/ZBP/HEC were different at all evaluated times ($p < 0.05$), while for β-lap-Lipo/ZBP/HEC and β-lap/ZBP/HEC, the release profiles were different from 8 to 24 h ($p < 0.05$). The cumulative amount of β-lap released from the liposome formulation (β-lap-Lipo) over 8 hours was $51.6 \pm 5.64\%$ ($14 \, \mu g/cm^2$). On the other hand, β-lap/ZBP/HEC showed a cumulative amount of β-lap released from the gels of $37.55 \pm 7.05\%$ ($10.19 \, \mu g/cm^2$), whereas liposomal gel, in the same β-lap concentration (β-lap-Lipo/ZBP/HEC), showed a significantly lower cumulative amount of β-lap, namely $19.7 \pm 4.03\%$ ($5.4 \, \mu g/cm^2$). Thus, the amount of drug released from the liposomal gel was 2.6-fold lower than β-lap-Lipo and 1.9-fold lower than β-lap free in hydrogel ($p < 0.05$). The diffusion kinetic coefficients, calculated according to the Higuchi model for β-lap-Lipo, β-lap/ZBP/HEC and β-lap-Lipo/ZBP/HEC were $k = 5.5 \pm 0.48$ ($r^2 = 0.98$); $k = 4.4 \pm 0.26$ ($r^2 = 0.94$); $k = 2.9 \pm 0.29$ ($r^2 = 0.96$), respectively ($p < 0.05$). These results demonstrated that the incorporation of β-lap-Lipo in a ZBP/HEC polymeric blend promotes a delayed but sustained release of the drug for up to 24 h. This observation, plus the fact that the encapsulation into MLV liposomes sustains β-lap release from the gel formulation, suggests that both processes, that is the release of β-lap from the liposomes and its diffusion through the gel, are important determining factors for β-lap release from liposomal gels. This hypothesis is supported by other liposome-in-gel systems previously reported [32,33].

In addition, other studies have demonstrated that the topical use of multilamellar liposomes dispersed in hydrogels for disease states where skin was injured, e.g., full-thickness skin wounds, burns, atopic eczema, could offer several advantages, such as localizing the effect

of the drug delivery system, maintaining a moist environment at the injured skin, prolonging drug retention time on the skin surface and minimizing side effects [15,23,30,34]. Hurler et al. [15] developed drug delivery systems for burn wound healing purposes based on multilamellar liposomes containing a lipophilic drug, mupirocin, incorporated into chitosan hydrogels. Their results demonstrated that liposomal hydrogel could act as a drug reservoir, providing a slower release of mupirocin through the skin than free mupirocin dissolved in hydrogel.

4.5.3 *In vivo* wound healing activity

ZBP hydrogel, a by-product of the sugarcane production process, has been shown to be a promising biopolymer material for multiple biomedical applications [7,8]. The use of bacterial cellulose hydrogel produced by *Zoogloea* sp. at concentrations ranging from 0.8 to 1% has been studied in various biomedical applications, such as a tissue substitute including its use as a bulking agent for the repair of osteochondral defects [35], urinary incontinence [36] or implant cavity in eviscerated rabbit eyes [9]. The biocompatibility and subcutaneous reactivity of ZBP were also evaluated in rabbits [7]. The common conclusions of these studies were that ZBP hydrogel is biocompatible and integrates with the surrounding tissue, inducing tissue repair and remodelling. Also for assuring the safety of ZBP, a recent preliminary toxicity test demonstrated that this biopolymer is not cytotoxic, genotoxic or acutely toxic [8].

The β-lap is a molecule that also presents a potential wound healing activity. Kung et al. [16] and Fu et al. [17] evaluated a topical ointment containing β-lap at 29.8 µg/g in different wound healing models. In wound healing models the healing process was seen to be more rapid in animals treated with β-lap incorporated into the ointment than in those treated only with the ointment [16]. Likewise, this topical ointment containing β-lap induced the proliferation of macrophages and accelerated tissue repair in burn-wound skin models [17].

Based on the promising activities of β-lap and ZBP, we developed a polymeric blend, consisting of ZBP and HEC, with the aim of incorporating β-lap-loaded liposomes for topical applications in wound healing treatment. It should to be emphasized that the incorporation of drug-loaded nanosystems into ZBP hydrogel remained an unexploited approach until the present study.

The histopathological examination showed significant differences between all the tested groups regarding the cell density of fibroblasts, vessels, inflammatory cells and collagen fibers. Fig. 3 depicts the vessel density of the animal groups tested. On day 3 the vessels density in all treated groups decreased significantly as compared to the untreated group. The treatment with ZBP/HEC hydrogel on day 7 promoted increases of 20% in blood vessels (Fig. 3a), 132.5% in fibroblasts (Fig. 3b), 129% in inflammatory cells (Fig. 3c) and 77% in collagen fiber density (Fig. 3d) as compared to the untreated group. These findings can also be observed in histopathological images (Fig. 4b). Together those data may suggest that ZBP/HEC hydrogel provides suitable environment that facilitates cell growth and adhesion at the wound site, producing an occlusive barrier that increases hydration. Lucena et al. [11] likewise demonstrated that a film of ZBP was able to achieve tissue integration, with the presence of newly formed epithelium and vessels, which are indicative of tissue repair and biocompatibility. This result could be also related to the observed increase in inflammatory cells that affect the production of cytokines and growth factors, stimulating the recruitment, activation and proliferation of fibroblasts and endothelial cells with the formation of granulate tissue during the proliferative phase of wound healing [37].

From day 7 post-wounding, the angiogenic activity of β-lap-Lipo/ZBP/HEC was observed, with increases in blood vessel density of 44%, 54% and 74% for groups treated with β-lap-Lipo/ZBP/HEC hydrogels containing 15, 30 and 60 μg/g of β-lap, respectively, compared with ZBP/HEC hydrogel (Fig. 3a and Fig. 4b). On day 14, the animals treated with β-lap-

Lipo/ZBP/HEC60 also exhibited the higher vessels density among all treatments. This finding could be the result of a directly angiogenic activity of β-lap, corroborating the results of Kung et al. [16], who used β-lap in Vaseline at 29.8 µg/g. The pronounced stimulation of wound angiogenesis by β-lap-Lipo/ZBP/HEC offers an advantage over ZBP/HEC hydrogels in improving wound healing efficacy, since the establishment of new blood vessels is critical for a proper granulation tissue formation [37]. Angiogenic agents, such as vascular endothelial growth factor (VEGF), have been used to treat chronic wounds, such as diabetic ulcers, and have been shown to accelerate tissue repair by increasing extracellular matrix deposition and epithelialization [38].

Regarding fibroblasts, in Fig. 3b and Fig. 4a mean increases of 67.5%, 22% and 50% for ZBP, ZBP/HEC hydrogel and β-lap-Lipo-ZBP/HEC hydrogels, respectively, were seen compared to the untreated group on day 3 post-wounding. Nevertheless, all concentrations of β-lap-Lipo/ZBP/HEC showed a decrease in fibroblast density on day 7 when compared to ZBP/HEC hydrogel, but not when compared with the untreated group (Fig. 3b and Fig. 4b). On day 14, the fibroblast density for the group treated with ZBP was 20% higher, whereas the group treated with β-lap-Lipo/ZBP/HEC60 presented a fibroblast density 35% lower than the untreated group (Fig. 3b and Fig. 4c). Compared to the group without treatment, β-lap-Lipo/ZBP/HEC15 and β-lap-Lipo/ZBP/HEC30 did not seem to affect the normal wound healing process, since the differences between the groups were not significant. This result may also account for the influence of different pH values of the tested hydrogels. As mentioned in the literature, the pH of topical formulations may influence the microenvironment of the wound and cellular events. During wound healing the pH moves from neutral to acid, and previous studies have demonstrated that a reduction in the pH of the surface wound can stimulate fibroblast activity and control enzymatic activity at the wound site [31]. Therefore, the lowest pH (5.5) of ZBP compared to the pH of the β-lap-Lipo/ZBP/HEC hydrogels (pH 6.6 to 7.2)

might account for the increase in fibroblast cell density when compared with other treated groups, except for ZBP/HEC hydrogel on day 7.

Moreover, regarding inflammatory cells (Fig. 3c and Fig. 4a), there were mean decreases of 56.2% and 27% on day 3 for all groups treated with β-lap-Lipo/ZBP/HEC and ZBP/HEC hydrogel, respectively, when compared to the untreated group. A significant mean decrease of 38.5% on day 7 was also observed for groups treated with β-lap-Lipo/ZBP/HEC at all concentrations when compared to ZBP/HEC hydrogel (Fig. 3c and Fig. 4a,b). On the other hand, when compared to the untreated group on day 7, the groups treated with ZBP, ZBP/HEC hydrogel and β-lap-Lipo/ZBP/HEC hydrogels (15 and 30 µg/g) presented increases of 64%, 129%, 41%, 64%, respectively, in the density of inflammatory cells (Fig. 3c and Fig. 4b), which is an advantage during the proliferative phase for the formation of granulation tissue [37]. On contrast, on day 14 the group treated with ZBP/HEC hydrogel and β-lap-Lipo/ZBP/HEC60, presented a 32% decrease in inflammatory cell density compared to the untreated group (Fig. 3c and Fig. 4c). These results indicate that the incorporation of β-lap-Lipo into ZBP/HEC hydrogel may drive the process of inflammation in the wound bed at the early stages of the healing.

In the analysis of collagen fibers, mean increases of 38.4% and 77% were observed during the proliferative phase (day 7) for groups treated with β-lap-Lipo/ZBP/HEC and ZBP/HEC hydrogel, respectively, compared to the untreated group (Fig. 3d). The pronounced increase in collagen fibers for the group treated with ZBP/HEC hydrogel, may be explained by the simultaneous increase in inflammatory cells during the proliferative phase. The macrophages encountered at the wound site may release cytokines, such as TGF-β, a potent chemoattractor and activator of fibroblasts, stimulating the formation of collagen fibers as reported previously [39]. Conversely, a decrease in collagen fibers was observed on days 3 and 14 for all treatments when compared to the untreated group (Fig. 3d). As described in the

literature, the prophylaxis of hypertrophic scars and keloid development may be achieved using drugs that inhibit fibroblast proliferation and collagen production [40]. Thus, the observed decrease in collagen synthesis on day 14, specially for groups treated with ZBP/HEC hydrogel, may be a strategy for preventing or attenuating excessive scar formation, thereby avoiding the excessive collagen deposition and formation of hypertrophic scars and keloids in patients more susceptible to this pathological wound healing.

Finally, the ZBP/HEC hydrogel has shown to stimulate the proliferation of the cells involved in the wound repair process, whereas the β-lap-Lipo demonstrated to act in synergism with ZBP/HEC, increasing the wound angiogenesis and controlling of the inflammatory process during the proliferative phase of skin repair.

Overall, results indicate that β-lap-Lipo/ZBP/HEC60 revealed a most stable rheological behavior associated with a higher angiogenic activity compared with β-lap-Lipo/ZBP/HEC15 and β-lap-Lipo/ZBP/HEC30. Together these results suggest that the β-lap-Lipo/ZBP/HEC60 formulation exhibits most suitable properties to be used as a topical product for wound healing applications.

4.6 Conclusions

β-lapachone-loaded multilamellar liposomes were incorporated in a polymeric blend hydrogel of *Zoogloea* sp. polymer and hydroxyethylcellulose exhibiting stable pH, rheological properties and drug release profile suitable for topical applications in wound healing. Results achieved from *in vivo* wound healing process demonstrated that the polymeric blend ZBP/HEC hydrogel increased the proliferation ratio of fibroblasts, collagen, vessels and inflammatory cells during the proliferative phase of wound healing. These results indicate that the ZBP/HEC hydrogel behaves as a conductor in the healing process and produces tissue integration, promoting the tissue repair of the lesion. Other important findings were the proangiogenic and

anti-inflammatory effects of the β-lap-Lipo/ZBP/HEC hydrogel, particularly during the proliferative phase of the skin repair, contributing to the physiological healing process. Moreover, for the groups treated with β-lap-Lipo/ZBP/HEC hydrogels, collagen synthesis decreased during the last phase of wound repair. The *in vivo* analysis suggests that β-lap-Lipo and ZBP/HEC hydrogel act in synergism, enhancing wound healing activity, specially in controlling collagen synthesis, inflammation and the formation of new vessels at the wound site. The overall results, including the physicochemical characteristics of β-lap-Lipo/ZBP/HEC hydrogel, specially β-lap-Lipo/ZBP/HEC60, revealing its potential as a topical product for wound healing treatment.

Acknowledgements

References

[1]   World Health Organization, Burns.

http://www.who.int/mediacentre/factsheets/fs365/en/, 2016 (accessed 20.10.16).

[2]   H. Brem, M. Tomic-Canic, Cellular and molecular basis of wound healing in diabetes, J. Clin Invest. 117 (2007) 1219–1222. doi:10.1172/JCI32169.

[3]   I. Sulaeva, U. Henniges, T. Rosenau, A. Potthast, Bacterial cellulose as a material for wound treatment: Properties and modifications: A review, Biotechnol. Adv. 33 (2015) 1547–1571. doi:10.1016/j.biotechadv.2015.07.009.

[4]   P.S. Murphy, G.R.D. Evans, Advances in wound healing: a review of current wound healing products., Plast. Surg. Int. 2012 (2012) 1–8. doi:10.1155/2012/190436.

[5]   C. Chang, L. Zhang, Cellulose-based hydrogels: Present status and application prospects, Carbohydr. Polym. 84 (2011) 40–53. doi:10.1016/j.carbpol.2010.12.023.

[6]   M. Paterson-Beedle, J.F. Kennedy, F.A.D. Melo, L.L. Lloyd, V. Medeiros, A cellulosic exopolysaccharide produced from sugarcane molasses by a *Zoogloea* sp., Carbohydr. Polym. 42 (2000) 375–383. doi:10.1016/S0144-8617(99)00179-4.

[7]   P.C. de C. Pita, F.C.M. Pinto, M.M. de M. Lira, F. de A. Dutra Melo, L.M. Ferreira, J.L.A. Aguiar, Biocompatibility of the bacterial cellulose hydrogel in subcutaneous tissue of rabbits, Acta Crúrgica Bras. 30 (2015) 296–300. doi:10.1590/S0102-865020150040000009.

[8]   F.C.M. Pinto, A.C.A.X. De-Oliveira, R.R. De-Carvalho, M.R. Gomes-Carneiro, D.R. Coelho, S.V.C. Lima, F.J.R. Paumgartten, J.L.A. Aguiar, Acute toxicity, cytotoxicity, genotoxicity and antigenotoxic effects of a cellulosic exopolysaccharide obtained from sugarcane molasses, Carbohydr. Polym. 137 (2016) 556–560. doi:10.1016/j.carbpol.2015.10.071.

[9]   F.A. Cordeiro-Barbosa, J.L.A. Aguiar, M.M.M. Lira, N.T. Pontes-Filho, S. Bernardino-Araújo, Use of a gel biopolymer for the treatment of eviscerated eyes: Experimental model in rabbits, Arq. Bras. Oftalmol. 75 (2012) 267–272. doi:10.1590/S0004-2749201200040001.

[10]   J.L.A. Aguiar, E.M. Lins, S.R.B. Marques, A.R.B. Coelho, R.D.O. Rossiter, R.J.V. Melo, Surgarcane biopolymer patch in femoral artery angioplasty on dogs, Acta Cirúrgica Bras. 22 (2007) 77–81.

[11]   M.T. Lucena, M.R. Melo-Júnior, M.M.M. Lira, C.M.M.B. Castro, L.A. Cavalcanti, M.A. Menezes, F.C.M. Pinto, J.L.A. Aguiar, Biocompatibility and cutaneous reactivity of

cellulosic polysaccharide film in induced skin wounds in rats, J. Mater. Sci. Mater. Med. 26 (2015) 1–6. doi:10.1007/s10856-015-5410-x.

[12]   A.G.S. Martins, S.V.C. Lima, L.A.P. De Araújo, F.D.O. Vilar, N.T.P. Cavalcante, A wet dressing for hypospadias surgery., Int. Braz. J. Urol. 39 (2013) 408–413. doi:10.1590/S1677-5538.IBJU.2013.03.15.

[13]   G. Gainza, S. Villullas, J.L. Pedraz, R.M. Hernandez, M. Igartua, Advances in drug delivery systems (DDSs) to release growth factors for wound healing and skin regeneration, Nanomedicine:NBM. 11 (2015) 1551–1573. doi:10.1016/j.nano.2015.03.002.

[14]   G. Han, L.N. Nguyen, C. MacHerla, Y. Chi, J.M. Friedman, J.D. Nosanchuk, L.R. Martinez, Nitric oxide-releasing nanoparticles accelerate wound healing by promoting fibroblast migration and collagen deposition, Am. J. Pathol. 180 (2012) 1465–1473. doi:10.1016/j.ajpath.2011.12.013.

[15]   J. Hurler, O.A. Berg, M. Skar, A.H. Conradi, P.J. Johnsen, N. Skalko-Basnet, Improved burns therapy: liposomes-in-hydrogel delivery system for mupirocin, J. Pharm. Sci. 101 (2012) 3906–3915. doi: 10.1002/jps.23260.

[16]   H.-N. Kung, M.-J. Yang, C.-F. Chang, Y.-P. Chau, K.-S. Lu, *In vitro* and *in vivo* wound healing-promoting activities of β-lapachone, Am. J. Physiol. Cell Physiol. 295 (2008) C931-43. doi:10.1152/ajpcell.00266.2008.

[17]   S.C. Fu, Y.P. Chau, K.S. Lu, H.N. Kung, β-lapachone accelerates the recovery of burn-wound skin, Histol. Histopathol. 26 (2011) 905–914.

[18]   C.H. Tseng, C.M. Cheng, C.C. Tzeng, S.I. Peng, C.L. Yang, Y.L. Chen, Synthesis and anti-inflammatory evaluations of β-lapachone derivatives, Bioorganic Med. Chem. 21 (2013) 523–531. doi:10.1016/j.bmc.2012.10.047.

[19]   I.M.F. Cavalcanti, J.G. Pontes-Neto, P.O. Kocerginsky, A.M. Bezerra-Neto, J.L.C. Lima, Antimicrobial activity of β-lapachone encapsulated into liposomes against meticillin-

resistant *Staphylococcus aureus* and *Cryptococcus neoformans* clinical strains, J. Glob. Antimicrob. Resist. 3 (2015) 103–108. doi:10.1016/j.jgar.2015.03.007.

[20]   N. Nasongkla, A.F. Wiedmann, A. Bruening, et al. Enhancement of solubility and bioavailability of β-lapachone using cyclodextrin inclusion complexes. Pharmaceutical Research. 20 (2003) 1626-1633.

[21]   S. Thirumaleshwar, P. K. Kulkarni, D. V. Gowda, Liposomal Hydrogels: A novel drug delivery system for wound dressing, Curr. Drug Ther. 7 (2012) 212–218. doi:10.2174/157488512803988021.

[22]   S. Mourtas, M. Haikou, M. Theodoropoulou, C. Tsakiroglou, S.G. Antimisiaris, The effect of added liposomes on the rheological properties of a hydrogel: a systematic study, J. Colloid Interface Sci. 317 (2008) 611–619. doi:10.1016/j.jcis.2007.09.070.

[23]   B.C. Ciobanu, A.N. Cadinoiu, M. Popa, J. Desbrières, C.A. Peptu, Modulated release from liposomes entrapped in chitosan/gelatin hydrogels, Mater. Sci. Eng. C. 43 (2014) 383–391. doi:10.1016/j.msec.2014.07.036.

[24]   P.V. Peplow, T. Chung, G.D. Baxter, Laser Photobiomodulation of Wound Healing, Photomed. Laser Surg. 28 (2010) 291–325.

[25]   W.A. Dorsett-Martin, A.B. Wysocki, Rat models of skin wound healing, Sourceb. Model. Biomed. Res. (2008) 631–638. doi:10.1007/978-1-59745-285-4.

[26]   M.S.S. Cunha Filho, F.C. Alves, G.M.C. Alves, D.B. Monteiro, F.P.M. de Medeiros, P.J. Rolim Neto, Beta-lapachona: desenvolvimento e validação de metodologia analítica para nova alternativa, Rev. Bras. Farm. 86 (2005) 39–43.

[27]   M.M. Cross, Rheology of non-newtonian fluids: a new flow equation for pseudoplastic systems, J. Colloid Sci. 20 (1965) 417–437.

[28]   T. Higuchi, Mechanism of sustained-action medication. Theoretical analysis of rate of release of solid drugs dispersed in solid matrices, J. Pharm. Sci. 52 (1963) 1145–1149. doi:10.1002/jps.2600521210.

[29]   C. Kilkenny, W.J. Browne, I.C. Cuthill, M. Emerson, D.G. Altman, Improving Bioscience Research Reporting: The ARRIVE Guidelines for Reporting Animal Research, PLoS Biol. 8 (2010) e1000412. doi:10.1371/journal.pbio.1000412.

[30]   J. Hurler, K.K. Sørensen, A. Fallarero, P. Vuorela, N. Škalko-Basnet, Liposomes-in-hydrogel delivery system with mupirocin: *In vitro* antibiofilm studies and *in vivo* evaluation in mice burn model, Biomed Res. Int. 2013 (2013). doi:10.1155/2013/498485.

[31]   S.L. Percival, S. McCarty, J.A. Hunt, E.J. Woods, The effects of pH on wound healing, biofilms, and antimicrobial efficacy, Wound Repair Regen. 22 (2014) 174–186. doi:10.1111/wrr.12125.

[32]   S. Mourtas, S. Fotopoulou, S. Duraj, V. Sfika, C. Tsakiroglou, S.G. Antimisiaris, Liposomal drugs dispersed in hydrogels. Effect of liposome, drug and gel properties on drug release kinetics, Colloids Surfaces B Biointerfaces. 55 (2007) 212–221. doi:10.1016/j.colsurfb.2006.12.005.

[33]   C.H.A. Boakye, K. Patel, M. Singh, Doxorubicin liposomes as an investigative model to study the skin permeation of nanocarriers, Int. J. Pharm. 489 (2015) 106–116. doi:10.1016/j.ijpharm.2015.04.059.

[34]   F. Roesken, E. Uhl, S.B. Curri, M.D. Menger, K. Messmer, Acceleration of wound healing by topical drug delivery via liposomes, Langenbecks. Arch. Surg. 385 (2000) 42–9. doi:03850042.423 [pii].

[35]   P.C.V.C. Albuquerque, S.M. Santos, J.L.A. Aguiar, N. Pontes-Filho, R.J.V.D. Mello, M.L.C.R. Costa, C.M.C. Olbertz, T.M. Almeida, A.H.S. Santos, J.C. Silva, Comparative macroscopic study of osteochondral defects produced in femurs of rabbits repaired with

biopolymer gel cane sugar, Rev. Bras. Ortop. (English Ed. 46 (2011) 577–584. doi:10.1016/S2255-4971(15)30415-8.

[36]   R.G. Lucena, S.V.C. Lima, J.L.D.A. Aguiar, R.T. Andrade, F.C.M. Pinto, F.O. Vilar, Experimental use of a cellulosic biopolymer as a new material for suburethral sling in the treatment of stress urinary incontinence, Int. Braz. J. Urol. 41 (2015) 1148–1153. doi:10.1590/S1677-5538.IBJU.2014.0155.

[37]   T. Velnar, T. Bailey, V. Smrkolj, The Wound Healing Process : an Overview of the Cellular and Molecular Mechanisms, 37 (2009) 1528–1542. doi:10.1177/147323000903700531.

[38]   R.D. Galiano, O.M. Tepper, C.R. Pelo, K.A. Bhatt, M. Callaghan, N. Bastidas, S. Bunting, H.G. Steinmetz, G.C. Gurtner, Topical vascular endothelial growth factor accelerates diabetic wound healing through increased angiogenesis and by mobilizing and recruiting bone marrow-derived cells, Am. J. Pathol. 164 (2004) 1935–1947. doi:10.1016/S0002-9440(10)63754-6.

[39]   S. Schreml, R.-M. Szeimies, L. Prantl, M. Landthaler, P. Babilas, Wound healing in the 21st century, J. Am. Acad. Dermatol. 63 (2010) 866–881. doi:10.1016/j.jaad.2009.10.048.

[40]   G. Gauglitz, H. Korting, T. Pavicic, T. Ruzicka, M. Jeschke, Hypertrophic scarring and keloids: pathomechanisms and current and emerging treatment strategies, Mol. Med. 17 (2011) 113-125. doi:10.2119/molmed.2009.00153.

Figure 1. Viscosity *versus* shear rate graphs of the liposomal gels at different lipid concentrations. The upper graphs correspond to the liposomal gel stability followed for a 90-day period: β-lap-Lipo/ZBP/HEC15 (2.5 mg/g) (a), β-lap-Lipo/ZBP/HEC30 (5.1 mg/g) (b) and β-lap-Lipo/ZBP/HEC60 (10.2 mg/g) (c). The lower graphs depict the liposomal gels in three different lipid concentrations on day 1(d) and day 90(e). The last graph (f) shows the effect of lipid concentration in the gels and the storage time on the zero shear rate viscosity values obtained for the liposomal gels, by fitting the rheological measurement using the Cross model.
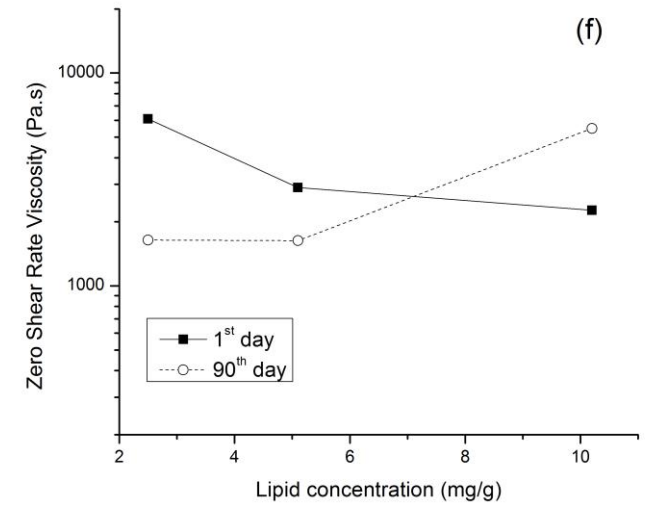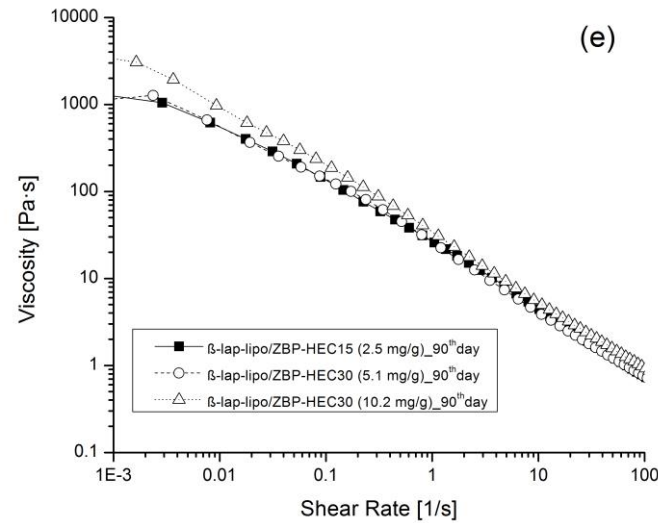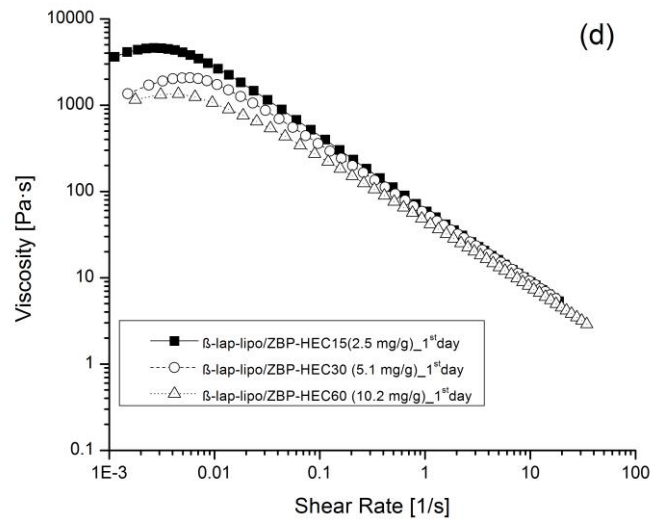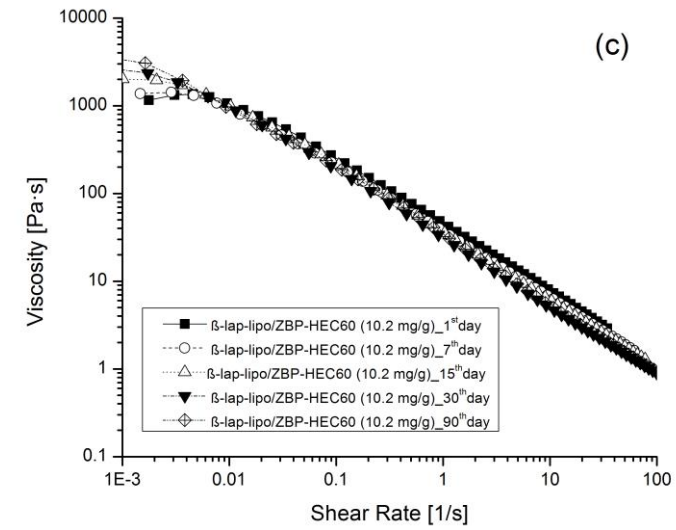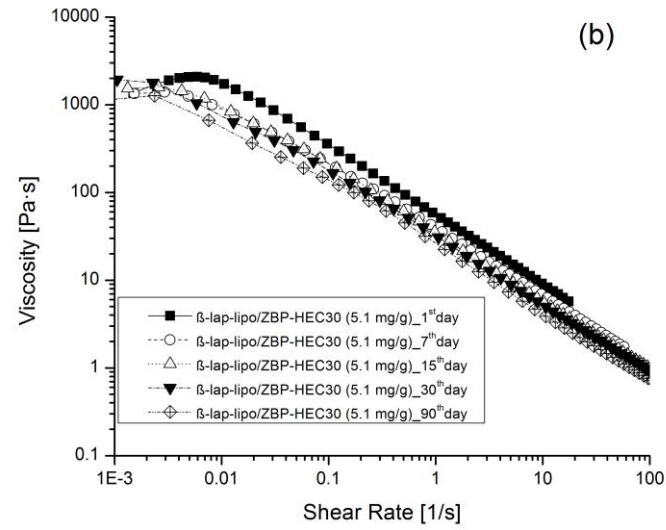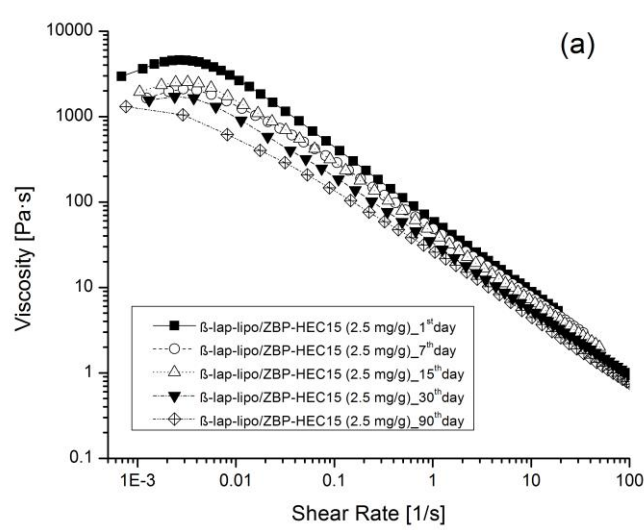
Figure 2. Cumulative amount of β-lap released per time (h) from liposome, control gel and liposomal gel. Each point is the mean from at least three independent experiments and bars represent the standard deviation of means.
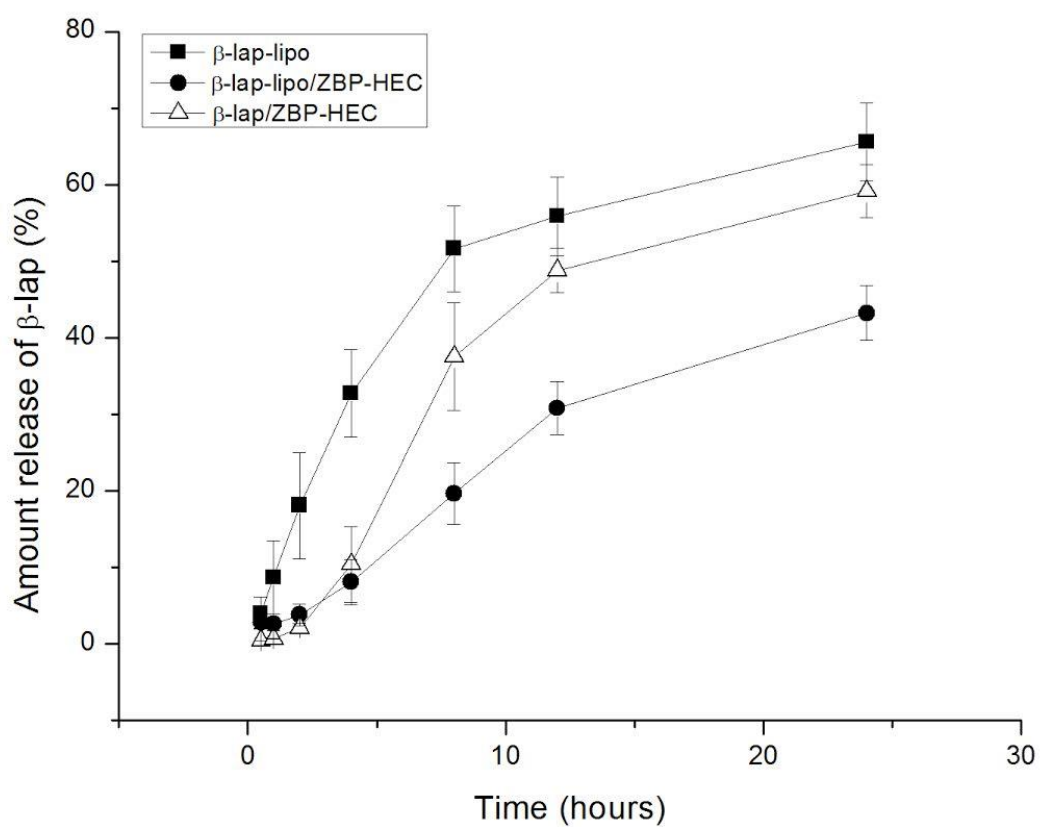
Figure 3. The histograms of cellular densities and collagen fibers on day 3, 7 and 14 post-wounding in the dermis layer of Wistar rats, after treatment with hydrogels or liposomal gels at different concentrations: Vessel density (a); fibroblast density (b); inflammatory cell density (c) and collagen fibers (d). *Significant difference ($p < 0.05$) among all the treated groups as compared with the controls without treatment. **Significant difference ($p < 0.05$) between the analyzed groups treated with hydrogels vehicles and liposomal gels containing β-lap.

(a)

(b)

(c)

(d)
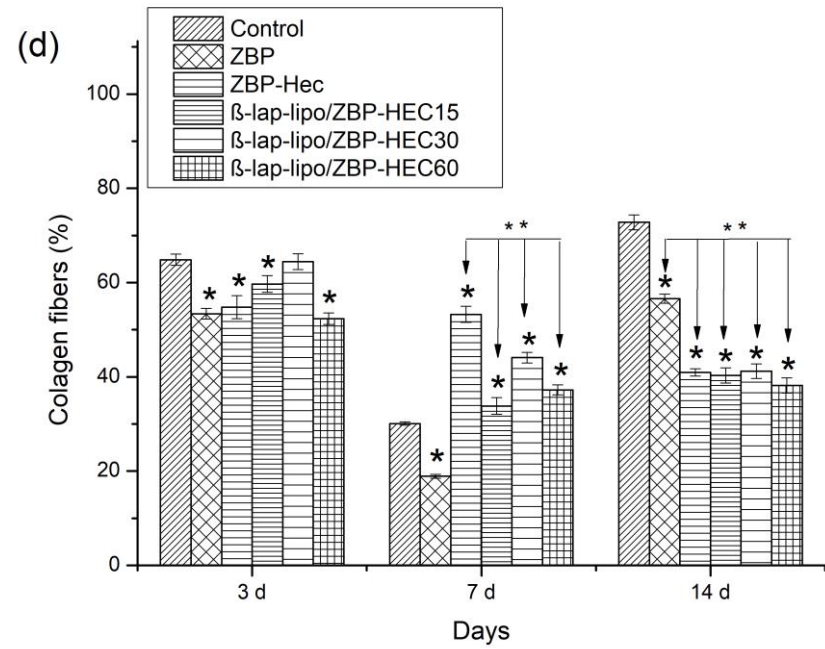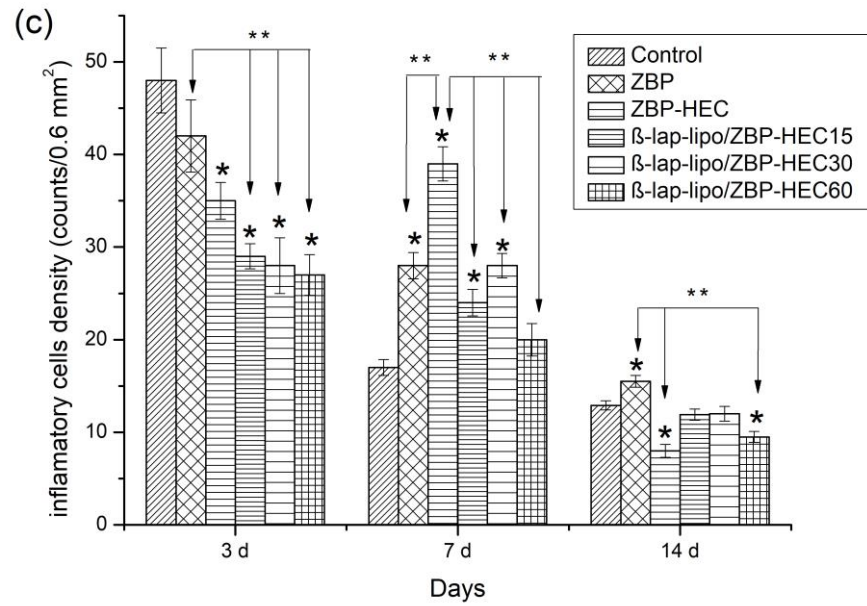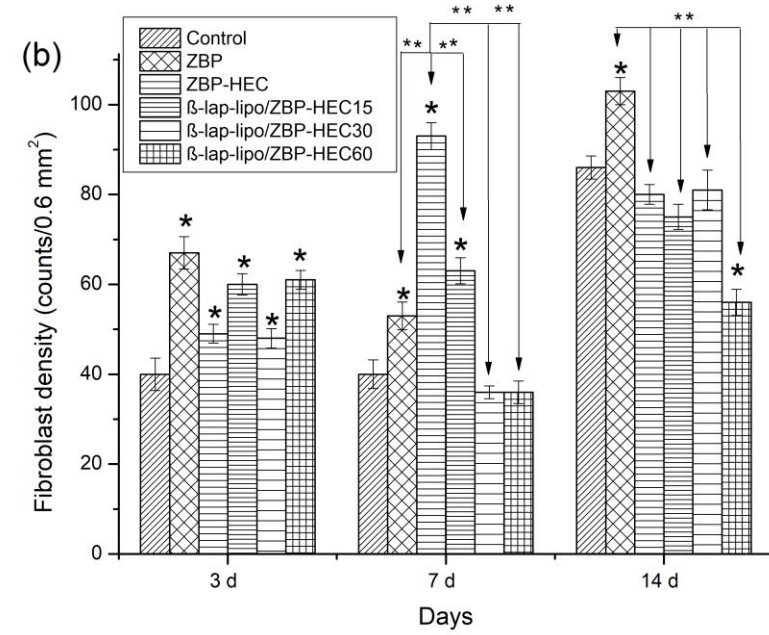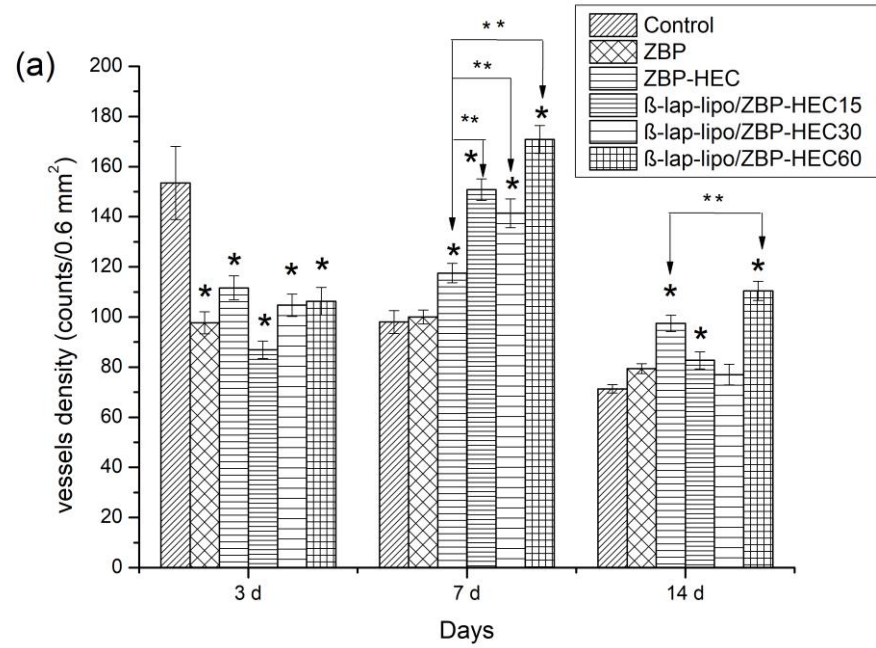
Figure 4. Representative histopathological images of skin in the dermis layer: hematoxylin and eosin-stained sections on day 3, 7 or 14 post-wounding of control (a), ZBP (b), ZBP/HEC (c) and β-lap-Lipo/ZBP/HEC60 (d) groups. Wound area shows fibroblasts (green arrows), inflammatory cells (black arrows) and blood vessels (red arrows). Original magnification: 400 ×.
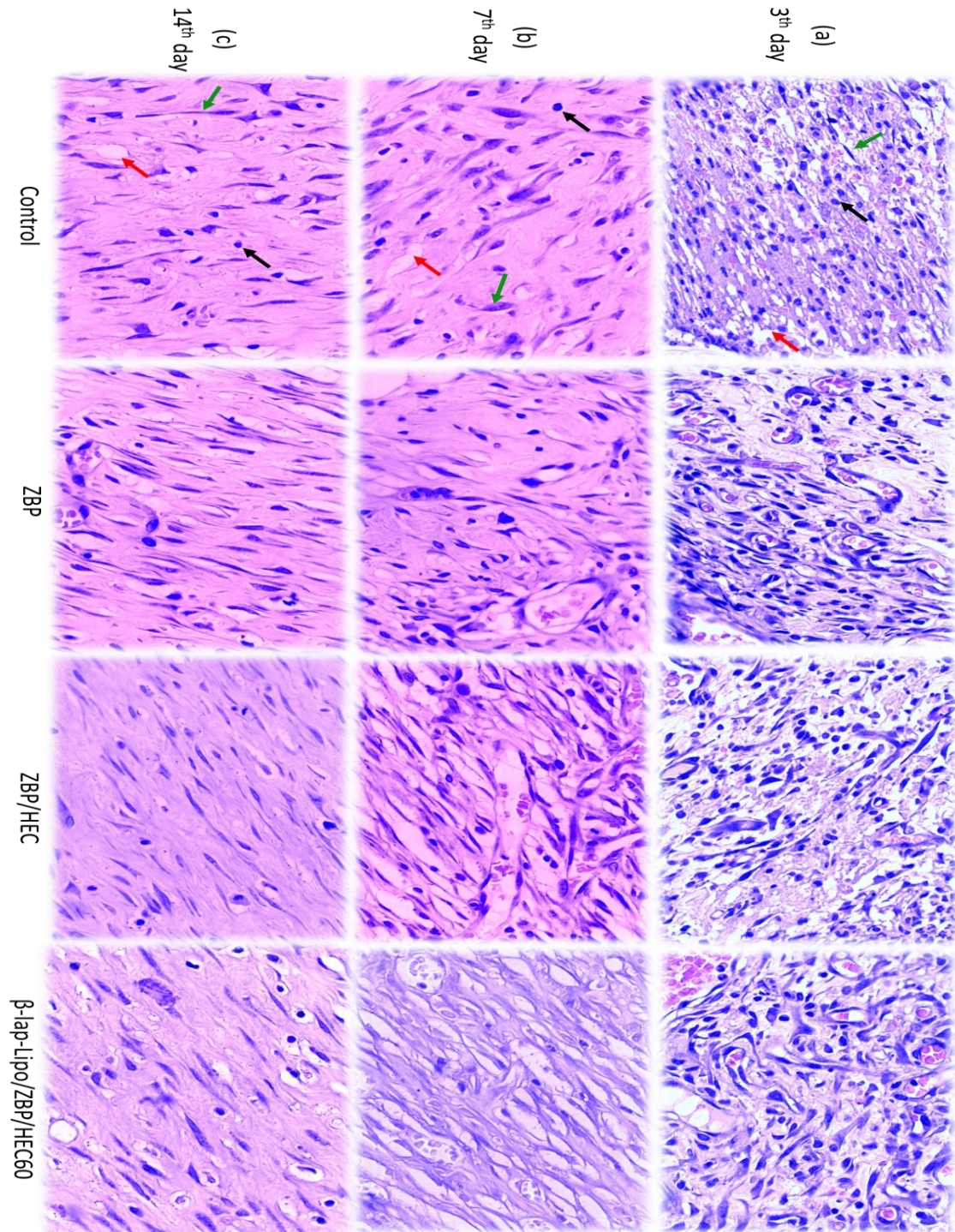
5 CONCLUSIONS AND PERSPECTIVES

The first section of this thesis was dedicated to site-specific polymeric nanoparticles for melanoma treatment. In the first chapter, it was conducted an overview of recent literature about polymeric nanoparticles for the therapeutic targeting of melanoma cells (m-CSCs and CMCs) with high metastatic potential. Based on literature review, it is clear the key role of these cells at the physiopathology of metastasis. The reported biomarkers expressed in m-CSCs and CMCs can be used as potential targets of site-specific theranostic nanoparticles for melanoma. In addition, the optimal design of polymeric nanoparticles for passive and active tumor targeting were also discussed take into account the size, shape and surface properties of the nanoparticles.

In the second chapter, surface modified polymeric nanoparticles (stealth, fluorescent label and site-specific) based on PBLG-derivatives were prepared and characterized. The nanoparticles showed small sizes, homogenous population, slightly elongated shapes and negative surface potential. Besides, the PBLG-based nanoparticles and immunonanoparticles were not recognized by the complement system and were not cytotoxic for normal endothelial or melanoma cells. In addition, the developed immunonanoparticles containing MART-1 antibody (PBLG-PEG-Bt-MART-1) showed a specific cellular uptake by B16-GFP cells, that overexpress the MART-1 receptor. However, further studies should be performed in order to optimize these immunonanoparticles and to enhance their specific recognition by melanoma cells, for example, increasing the antibody ratio conjugated at the surface of nanoparticles, as well as the incorporation of the drugs into these particles to increase the cytotoxicity against melanoma cells. In summary, these studies highlighted the potential of PBLG-based nanoparticles to be used as systemic drug-delivery systems for melanoma targeting approach. As discussed in the literature review, other promising antibodies against CMC and/or m-CSCs biomarkers can be essayed for melanoma therapeutic and diagnosis purposes and the PBLG-based nanoparticles can be used as versatile and modifiable nanoplatforms for this aim.

On the second section of this thesis, a topical polymeric hydrogel containing β-lap-loaded multilamellar liposomes (β-lap-Lipo/ZBP-HEC) was developed for *in vivo* wound healing application. The liposomal-hydrogels showed suitable sizes, pH and rheological characteristics for topical applications. In addition, the release kinetic profile of β-lap from liposomal-hydrogels at the wound site followed the Higuchi model and was 1.9 folds slower than β-lap released from hydrogel. ZBP/HEC hydrogel enhanced the *in vivo* wound healing activity, increasing the density of specific cells involved in the wound repair. In addition, β-lap-Lipo/ZBP-HEC increased around 2-folds the formation of new vessels at wound site and decreased the inflammatory process during the proliferative phase of skin repair. These results suggest that β-lap-Lipo and ZBP/HEC hydrogel had a synergic effect. These promising findings also shed light to future researches using the ZBP/HEC hydrogel as a bioactive vehicle for incorporation of other drugs with topical actions.

Taking into account the overall results, this present work contributed for the development of promising polymeric and lipidic nanocarriers with different biological applications and administration routes: immunonanoparticles containing antibody targeted for MART-1 receptor for systemic treatment of melanoma and β-lapachone encapsulated in multilamellar liposomes and incorporated in a biopolymer hydrogel for topical application in wound healing.

REFERENCES

ALBINO, A. P., SOZZI, G., NANUS, D. M., JHANWAR, S. C., & HOUGHTON, A. N. Malignant transformation of human melanocytes: induction of a complete melanoma phenotype and genotype. Oncogene, v. 7, n. 11, p. 2315–2321, 1992.

ALLEN, T.M; CULLIS, P.R. et al. Drug Delivery Systems: Entering the Mainstream. Science, v. 303, n. 5665, p. 1818-1822, 2004.

ANGELI, E. et al. Nanotechnology applications in medicine. Medical Device Technology, v. 14 (5), p. 29–31, 2008. Disponível em: <http://europepmc.org/abstract/med/12852120>.

ANTÔNIO, E. et al. Poly(lactic acid) nanoparticles loaded with ursolic acid: Characterization and in vitro evaluation of radical scavenging activity and cytotoxicity. Materials Science and Engineering: C, v. 71, p. 156–166, 2017.

BAO, G.; MITRAGOTRI, S.; TONG, S. Multifunctional nanoparticles for drug delivery and molecular imaging. Annual review of biomedical engineering, v. 15, n. 4, p. 253–82, 2013.

BOULAIZ, H. et al. Nanomedicine: Application areas and development prospects. International Journal of Molecular Sciences, v. 12, n. 5, p. 3303–3321, 2011.

BROOKS, M. D.; BURNESS, M. L.; WICHA, M. S. Therapeutic Implications of Cellular Heterogeneity and Plasticity in Breast Cancer. Cell Stem Cell, v. 17, n. 3, p. 260–271, 2015.

BRYS, A. K. et al. Nanotechnology-based strategies for combating toxicity and resistance in melanoma therapy. Biotechnology Advances, v. 34, n. 5, p. 565–577, 2016.

CARNEIRO, G. et al. Topical delivery and in vivo antileishmanial activity of paromomycin-loaded liposomes for treatment of cutaneous leishmaniasis. Journal of liposome research, v. 20, n. 1, p. 16–23, 2010.

CAVALCANTI, I. M. F. et al. Antimicrobial activity of b -lapachone encapsulated into liposomes against meticillin-resistant Staphylococcus aureus and Cryptococcus neoformans clinical strains. Journal of Global Antimicrobial Resistance, v. 3, p. 6–11, 2015.

CHEN, F. et al. In Vivo Tumor Targeting and Image-Guided Drug Delivery with Antibody-Conjugated , Radiolabeled Mesoporous Silica Nanoparticles Radiolabeled Mesoporous Silica Nanoparticles. 2013.

CHOWDHURY, R. M. et al. Cancer nanotheranostics: Strategies, promises and impediments. Biomedicine & Pharmacotherapy. Biomedicine & Pharmacotherapy, v. 84, p. 291-304, 2016.

CIOBANU, B. C. et al. Modulated release from liposomes entrapped in chitosan/gelatin hydrogels. Materials Science and Engineering C, v. 43, p. 383–391, 2014.

CSERMELY, P. et al. Cancer stem cells display extremely large evolvability: alternating plastic and rigid networks as a potential. Seminars in cancer biology, v. 8, p. 1–10, 2014.

DEVALAPALLY, H.; CHAKILAM, A.; AMIJI, M. Role of Nanotechnology in Pharmaceutical Product Development. Journal of Pharmaceutical Sciences, v. 96, n. 10, p. 2548–2564, 2007.

FU, S. C. et al. ß-Lapachone Accelerates the Recovery of Burn-Wound Skin. Histology and Histopathology, v. 26, n. 7, p. 905–914, 2011.

JACKSON, J. E.; KOPECKI, Z.; COWIN, A. J. Nanotechnological advances in cutaneous medicine. Journal of Nanomaterials, v. 2013, p. 1–8, 2013.

JAIN, A. K.; THANKI, K.; JAIN, S. Co-encapsulation of tamoxifen and quercetin in polymeric nanoparticles: Implications on oral bioavailability, antitumor efficacy, and drug-induced toxicity. Molecular Pharmaceutics, v. 10, n. 9, p. 3459–3474, 2013.

KUNG, H.-N. et al. In vitro and in vivo wound healing-promoting activities of beta-lapachone. American journal of physiology. Cell physiology, v. 295, n. 4, p. C931-43, out. 2008. Disponível em: <http://www.ncbi.nlm.nih.gov/pubmed/18650264>. Acesso em: 6 jan. 2013.

LA PORTA, C. A M.; ZAPPERI, S. Human breast and melanoma cancer stem cells biomarkers. Cancer Letters, v. 338, n. 1, p. 69–73, 2013. Disponível em: <http://dx.doi.org/10.1016/j.canlet.2012.03.017>.

LI, J. et al. Nanobiotechnology for the Therapeutic Targeting of Cancer Cells in Blood. Cellular and Molecular Bioengineering, v. 8, n. 1, p. 137–150, 2015.

MORA-HUERTAS, C. E.; FESSI, H.; ELAISSARI, A. Polymer-based nanocapsules for drug delivery. International journal of pharmaceutics, v. 385, n. 1, p. 113-142, 2010.

MOURTAS, S. et al. Liposomal drugs dispersed in hydrogels. Effect of liposome, drug and gel properties on drug release kinetics. Colloids and surfaces. B, Biointerfaces, v. 55, n. 2, p. 212–21, 2007.

MOURTAS, S. et al. The effect of added liposomes on the rheological properties of a hydrogel: a systematic study. Journal of colloid and interface science, v. 317, n. 2, p. 611–9, 2008.

PIKTEL, E. et al. Recent insights in nanotechnology-based drugs and formulations designed for effective anti-cancer therapy. Journal of nanobiotechnology, NULL, v. 14, n. 1, p. 39, 2016.

PORE, M. et al. Cancer Stem Cells, Epithelial to Mesenchymal Markers, and Circulating Tumor Cells in Small Cell Lung Cancer. Clinical Lung Cancer, v. 17, n. 6, p. 535–542, 2016.

REED, C. M. et al. Vaccination with melanoma helper peptides induces antibody responses associated with improved overall survival. Clinical Cancer Research, v. 21, n. 17, p. 3879–3887, 2015.

SUTRADHAR, K. B.; AMIN, L. Nanotechnology in Cancer Drug Delivery and Selective Targeting. Nanotechnology, v. 2014, p. 1–12, 2014.

TAZZARI, M. et al. Melan-A/MART-1 immunity in a EWS-ATF1 translocated clear cell sarcoma patient treated with sunitinib: a case report. BMC Cancer, v. 15, n. 1, p. 1–8, 2015.

TORCHILIN, V. P. Recent advances with liposomes as pharmaceutical carriers. Nature reviews. Drug discovery, v. 4, n. 2, p. 145–160, 2005.

WU, X.; GUY, R. H. Applications of nanoparticles in topical drug delivery and in cosmetics. Journal of Drug Delivery Science and Technology, v. 19, n. 6, p. 371–384, 2009.

XU, X.; ZHONG, J. F. Circulating tumor cells and melanoma progression. The Journal of investigative dermatology, v. 130, n. 10, p. 2349–2351, 20

ANNEXE A- Ethics committee certificate of approval.

Universidade Federal de Pernambuco
Centro de Ciências Biológicas

Av. Prof. Nelson Chaves, s/n
50670-420 / Recife - PE - Brasil
fones: (55 81) 2126 8840 | 2126 8351
fax: (55 81) 2126 8350
www.ccb.ufpe.br

Recife, 02 de maio de 2012.

Ofício nº 427/12

Da Comissão de Ética no Uso de Animais (CEUA) da UFPE
Para: **Profa. Nereide Estela Santos Magalhaes**
Laboratório de Imunologia Keizo Asami-LIKA
Universidade Federal de Pernambuco
Processo nº 23076.017434/2012-11

Os membros da Comissão de Ética no Uso de Animais do Centro de Ciências Biológicas da Universidade Federal de Pernambuco (CEUA-UFPE) avaliaram seu projeto de pesquisa intitulado, **"Estudo in Vivo da Atividade Cicatrizante de Lipossomas Multilamelares Contendo β-Lapachona Veiculado em Biogel Produzido a partir da Zooglea sp.".**
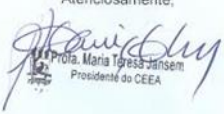
Concluímos que os procedimentos descritos para a utilização experimental dos animais encontram-se de acordo com as normas sugeridas pelo Colégio Brasileiro para Experimentação Animal e com as normas internacionais estabelecidas pelo National Institute of Health Guide for Care and Use of Laboratory Animals as quais são adotadas como critérios de avaliação e julgamento pela CEUA-UFPE.

Encontra-se de acordo com as normas vigentes no Brasil, especialmente a Lei 11.794 de 08 de outubro de 2008, que trata da questão do uso de animais para fins científicos e didáticos.

Diante do exposto, emitimos **parecer favorável** aos protocolos experimentais a serem realizados.

Origem dos animais: Biotério do Departamento de Nutrição-UFPE; Animais: Ratos; Linhagem:Wistar; Sexo: machos; número de animais previsto no protocolo: 48 animais; Peso: 150-250g; Idade:50 a 60 dias.

Atenciosamente,

Profa. Maria Teresa Jansem
Presidente do CEEA

CCB: Integrar para desenvolver